AN ABSTRACT OF THE THESIS OF

Ronald Masao Manabe for the degree of Doctor of Philosophy

in Chemistry presented on December 2, 1976

Title: EFFECTS OF ATMOSPHERIC PRESSURE ON LINE WIDTHS AND SPATIAL DISTRIBUTIONS OF THE TRANSIENT ATOMIC ABSORPTION SIGNALS OF MINOR CONSTITUENTS IN METAL SAMPLE ATOMIZED BY A DYE LASER MICROPROBE

Abstract approved: Redacted for Privacy

Edward H. Piepmeier

Investigations of plasma production by a pulsed dye laser microprobe were made. Comparisons between a Q-switched and a pulsed dye laser system were made on the intensity of the continuum produced by atmospheric breakdown. The dye laser system was found to minimize the production of the continuum which in turn allowed a greater fraction of the energy to be transmitted to the sample surface at atmospheric pressure.

The magnitude of the atmospheric pressure over the sample surface had a significant effect on both the duration and magnitude of the peak absorption of Mn in a reference steel sample. Spatially resolved atomic absorption measurements on the plume indicated that the plume was distributed over a much larger volume at low pressure (1 torr) than at atmospheric pressure. The plume appeared to be

more uniform in composition at low pressure.

Absorption line width measurements of the low pressure plume indicated that the temperature of the plasma had cooled dramatically from an estimated 10, 000-20, 000° K during its formation to 400-1000° K a few microseconds after the termination of the dye laser pulse. Its measured absorption width coupled with the reported values of the emission line widths of high intensity pulsed hollow cathode lamps indicated that a source with a narrower spectral profile was desirable for atomic absorption measurements in the plume.

The duration of the pulsed hollow cathode intensity can be dramatically reduced with the use of a high voltage power supply (800 V) coupled with a high voltage switching transistor. The reduced duration should result in improvement of the line profile and eliminate much of the self-reversal.

The use of a short duration hollow cathode pulse allowed an alternate method of atomic absorption measurements to be carried out. A photoanodic charge integration apparatus was developed to greatly facilitate the atomic absorption measurements.

Effects of Atmospheric Pressure on Line Widths and Spatial Distributions of the Transient Atomic Absorption Signals of Minor Constituents in Metal Samples Atomized by a Dye Laser Microprobe

by

Ronald Masao Manabe

A THESIS

submitted to

Oregon State University

in partial fulfillment of
the requirements for the
degree of

Doctor of Philosophy

June 1977

APPROVED:

Redacted for Privacy

Associate Professor of Chemistry

in charge of major

Redacted for Privacy

Chairman of Department of Chemistry

Redacted for Privacy

Dean of Graduate School

Date thesis is presented December 2, 1976

Typed by Clover Redfern for Ronald Masao Manabe

TABLE OF CONTENTS

LIST OF FIGURES

EFFECTS OF ATMOSPHERIC PRESSURE ON LINE WIDTHS AND SPATIAL DISTRIBUTION OF THE TRANSIENT ATOMIC ABSORPTION SIGNALS OF MINOR CONSTITUENTS IN METAL SAMPLES ATOMIZED BY A DYE LASER MICROPROBE

I. INTRODUCTION

The use of a high intensity pulsed laser for the production of a high temperature plasma for spectrochemical analysis was initiated by the work of Brech (1). The use of a laser microprobe as a sampling tool has many advantages over other microprobe techniques. The laser microprobe can be applied to a wide variety of sample types since the sample does not have to be an electrical conductor. Extremely high vacuum systems are not required. Due to its optical nature, the laser can be visually focused on a small spot allowing the vaporization of a known area on the sample surface.

Several authors have observed extremely high temperatures in the laser produced plasma. Mentall and Nicholls (2) have observed temperatures as high as 24,000°K from calculations using the emission spectra of Ba and Ca. They proposed that the excitation of the spectra resulted from collisions between the analyte atom and the ions and electrons of the plasma superheated by the absorption of the incident laser radiation. Bogershausen and Honle (3) have measured temperatures ranging from 6,000-24,000°K for Fe, W, Zn, and C vaporized by a pulsed laser. The power ranged from 2 kW for

normal-pulse to 1 MW for giant-pulse operation.

Baldwin (4, 5, 6, 7, 8) has compiled a collection of bibliographies dealing with plasma production by pulsed lasers. The underlying theme of the papers was the use of the laser as an initiating force for thermonuclear reactions, but many papers are cited that may be of use to the analytical chemist.

Ready (9, 10) has developed mathematical models to predict the behavior of the interaction of high-power pulsed laser radiation with solid opaque surfaces. In his book (10) many models are proposed for the various phases of the laser interaction with solid samples.

Hora (11) has compiled a collection of papers dealing with the interaction of laser radiation with solid samples.

Bogershausen and Vesper (12) have studied the mechanisms of plasma heating by pulsed laser systems. They have studied the interaction of high powered laser radiation with various samples. They have shown that soon after the plasma has expanded the high temperature plasma has cooled to a non thermal plasma with a high electron density which can absorb laser radiation from subsequent laser spikes.

Klocke (13) has critically studied the physical formation of craters resulting from the vaporization of material from a solid sample surface. He has determined the size and shape of these craters in a variety of sample types. Comparison of the relationship of crater diameter from proposed models of evaporation from various

authors are discussed. Scott and Strasheim (14) have taken high speed photographs to study the nature of the plasma production from various types of lasers. They have found that for a single spike laser system similar to that used in this investigation, plasma emission ceased after a period of 20 μs. They have found that during this time frame the plasma appeared relatively motionless resembling a nebula suspended above the sample surface. They have also found that for multiple-spike laser systems most of the material removed from the sample was ablated in the form of molten metal.

Allemand (15) has time resolved the emission from a Q-switched laser microprobe system. He has found that the emission signals for various analytes from solid samples were very dependent upon the matrices. He has also noted that the presence of the intense continuum causes complication of the emission signal for possible analytical application.

The disadvantages of the laser microprobe system, most of which have been documented by Allemand (15), have prevented application of the technique to a wide variety of sample materials.

The presence of the continuum and the lack of precision has seriously curtailed analytical application of laser microprobes for real chemical analysis. Piepmeier and Osten (16) have developed the concept of a radiation supported shockwave to explain some of the production of the intense continuum above the sample surface. They have

predicted that if the peak power of the laser system can be kept below the threshold breakdown level of the atmosphere, production of the continuum should be minimized. They have also suggested that the continuum production can be further decreased with the use of a short wavelength laser such as the commercially available pulsed dye lasers with operating wavelengths below 600-nm.

To overcome the lack of precision of the analytical method, many authors have proposed the use of atomic absorption, which may not be as dependent as emission is upon the nonuniform excitation conditions present in the plume.

Piepmeier and Malmstadt (17) have observed that the free atom population of aluminum was observable over the sample surface long after atomic emission from the plume has ceased. Mossotti (18) has demonstrated the use of a continuum source in conjunction with a high resolution monochromator for the measurement of atomic absorption signals in the laser plume. Osten (19) and Osten and Piepmeier (20) have used pulsed hollow cathode lamp for the measurement of atomic absorption signals. By using high current pulsed hollow cathode lamps a high resolution monochromator was no longer needed. Krivchikova and Vasil'eva (21) have used atomic absorption to measure the rare earths in a zirconium alloy. The absorption of the analyte atoms was determined by measuring the decrease in the continuum emission from the plasma on a film densitometer. Vul'fson,

Karyakin, and Shidlovskii (22) have discussed the possibility of atomic absorption measurements on the plume by the use of pulsed hollow cathode lamps. In a later paper (23) they demonstrated the utility of pulsed hollow cathode lamps for the determination of Cu in powdered samples.

The emission line profile of the primary source used for laser plume atomic absorption measurements helps to determine the slope and shape of the analytical curve. The nature of the emission line profile of hollow cathodes has undergone critical investigation. de Galan (24) has published a critical review of all sources of broadening mechanisms for atomic spectral lines. Wagenaar and de Galan (25) have used a pressure scanned Fabry Perot interferometer to measure the atomic line profiles emitted by hollow cathode lamps. They have found that the line width was due to Doppler broadening with a Doppler temperature close to that measured for the cathode surface. They have found that increasing the hollow cathode current results in self-absorption and a broadened profile for calcium.

Kirkbright, Troccoli and Vetter (26) have used a Piezoelectric scanning Fabry Perot interferometer to study the line profile of hollow cathode lamps. Bruch and Hannaford (27) have also studied the line profile from a Ca hollow cathode. They have used theoretical

models to predict the nature of the measure profile as a function of self-absorption. Correlations are made between the measured Dopper width of the profile and thermocouple measurements of the cathode surface. Good agreement was found.

DeJong and Piepmeier (28) studied the time resolved emission profile from high intensity pulsed hollow cathode lamps used in laser microprobe atomic absorption measurements. They observed significant self-reversal and line broadening after the initial 21 μs of the hollow cathode pulse The severe self-reversed profile of these pulsed lamps may have significantly influenced the shapes of analytical curves generated by laser microprobe atomic absorption measurements performed by Osten (19). On several occasions the calibration curves obtained were not linear, indicating possible deviation from Beer's law due to a broad spectral bandwidth of the source.

Wagenaar, Pickford and de Galan (29) have measured the absorption profile of Cu in an air-acetylene flame. Their measured half widths of the absorption profile were close to the measured half width of the emission profile of the pulsed hollow cathode (28). Since the flame absorption profiles should be at least as broad or broader than those in the plume (except very early in the plume), this evidence strongly suggests that the pulsed hollow cathode profile may cause non-linear calibration curves.

Piepmeier and de Galan (30) have shown that if the duration of the hollow cathode pulse was kept short (10 μs), self-reversal was not present when the repetition rate was not too high. The use of short duration hollow cathode pulses may enhance the utility of an atomic absorption microprobe for real chemical analysis. Improvements in the spectral profile of the hollow cathode lamp should result in improved sensitivity and linearity of the calibration curves.

This thesis is concerned with the investigation of the physical processes that are occurring during and after the formation of the plasma. Improvement of the analytical precision should result once the optimum operating parameters of the plume production are found.

The first group of experiments done in this investigation dealt with the time and spatial distribution of analyte signals caused by the plume as a function of applied pressure. A pulsed dye laser microprobe system was employed to verify the predictions of Piepmeier and Osten (16). Both emission and absorption measurements were made. The major portion of the work deals with atomic absorption measurements because of its promise of increased precision for the analytical results.

A second group of experiments expanded upon the work of DeJong and Piepmeier (28). These experiments were concerned with the spectral quality of pulsed hollow cathode pulses. Emphasis in this research was placed on the relationship between the emission profile

of the pulsed hollow cathode lamp and the absorption profile of the analyte atoms in the plume. Preliminary measurements were made of the plume absorption spectral profile. The lamp pulsing parameters were adjusted to reduce the amount of self-absorption of the lamp emission profile.

II. INSTRUMENTATION

A. The Laser

The laser used in this project was a Chromabeam 1070 liquid dye laser system (Synergetics Research Incorporated). Figure 1 shows a diagram of the laser cavity. The liquid lasing medium was circulated through the bore of the coaxial flashlamp. The end reflectors were dielectric coated broadband mirrors supplied by the laser manufacturer. The dye solution chosen for this investigation was a 1×10^{-4} M solution of Rhodamine 6G in 95% ethanol. The maximum energy content per pulse was 0.10 Joules. The maximum firing rate was 3 pulses per minute.

Laser Alignment

To insure maximum laser output and efficiency, the optical components of the laser cavity were carefully aligned. This was achieved with the aid of a helium-neon gas laser (University Laboratories Inc. Model 230). A pinhole aperture was placed at the exit of the He-Ne laser to reduce its intensity. The alignment laser beam was then directed down the core of the dye laser cavity. The position of the laser was adjusted so that the beam passed along the bottom edge of the dye tube. Careful adjustment of the alignment beam was necessary to insure that the beam exited at the opposite end at the

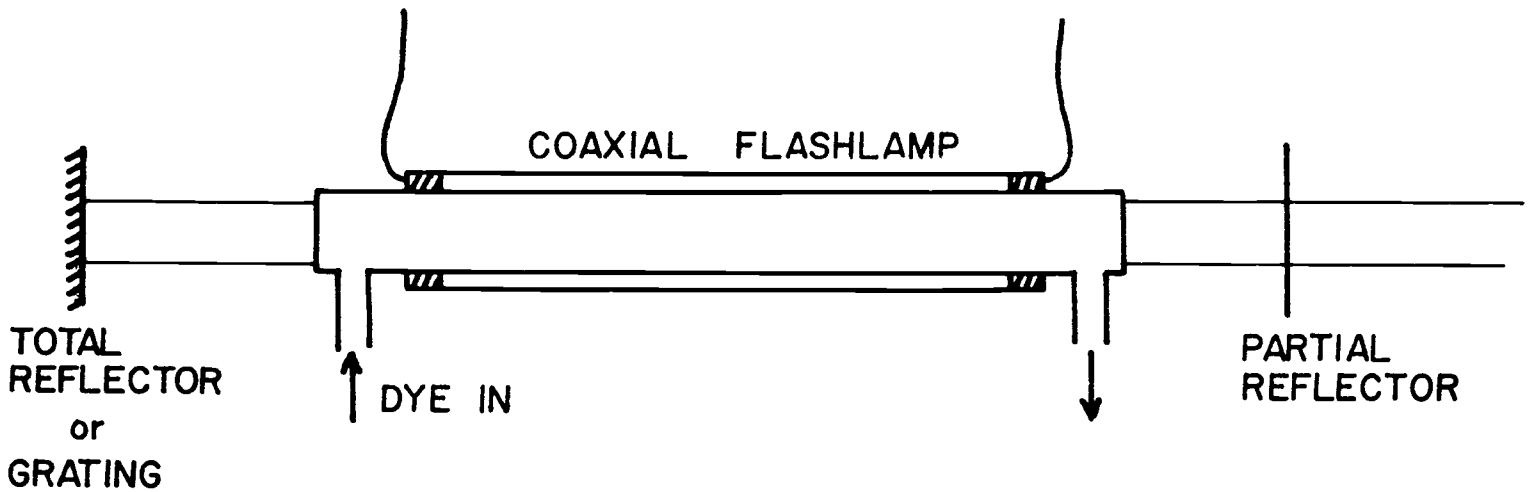

Figure 1. Resonance cavity diagram of a pulsed dye laser.

same position along the dye tube edge as it entered. This assured that the alignment beam was parallel to the walls of the dye tube.

Once the beam was found to transverse the dye tube in a parallel manner, the front and back cavity reflectors were adjusted until the reflection spots were made coincident with the exit aperture on the helium neon laser. This insured that the reflector plates were parallel to one another and that the axis of the dye cavity was perpendicular to the resonance reflectors. Throughout the alignment procedure the dye solution was allowed to pump through the laser cavity.

Laser Triggering Modifications

The original laser trigger used an electromechanical relay in a system similar to that used in conventional automobile ignition systems. The jitter time of the trigger circuit was 1-5 ms. This was due to the mechanical nature of the relay mechanism. For the time resolution required in this investigation the jitter time had to be reduced to a few microseconds.

Figure 2 shows the schematic diagram of an electronic triggering system which eliminated the use of a mechanical relay. The circuit consisted of a high voltage DC power supply and an SCR (silicon controlled rectifier) capacitive discharge ignition circuit. Capacitor C2 was charged to 350 V through the 240 K ohm isolation

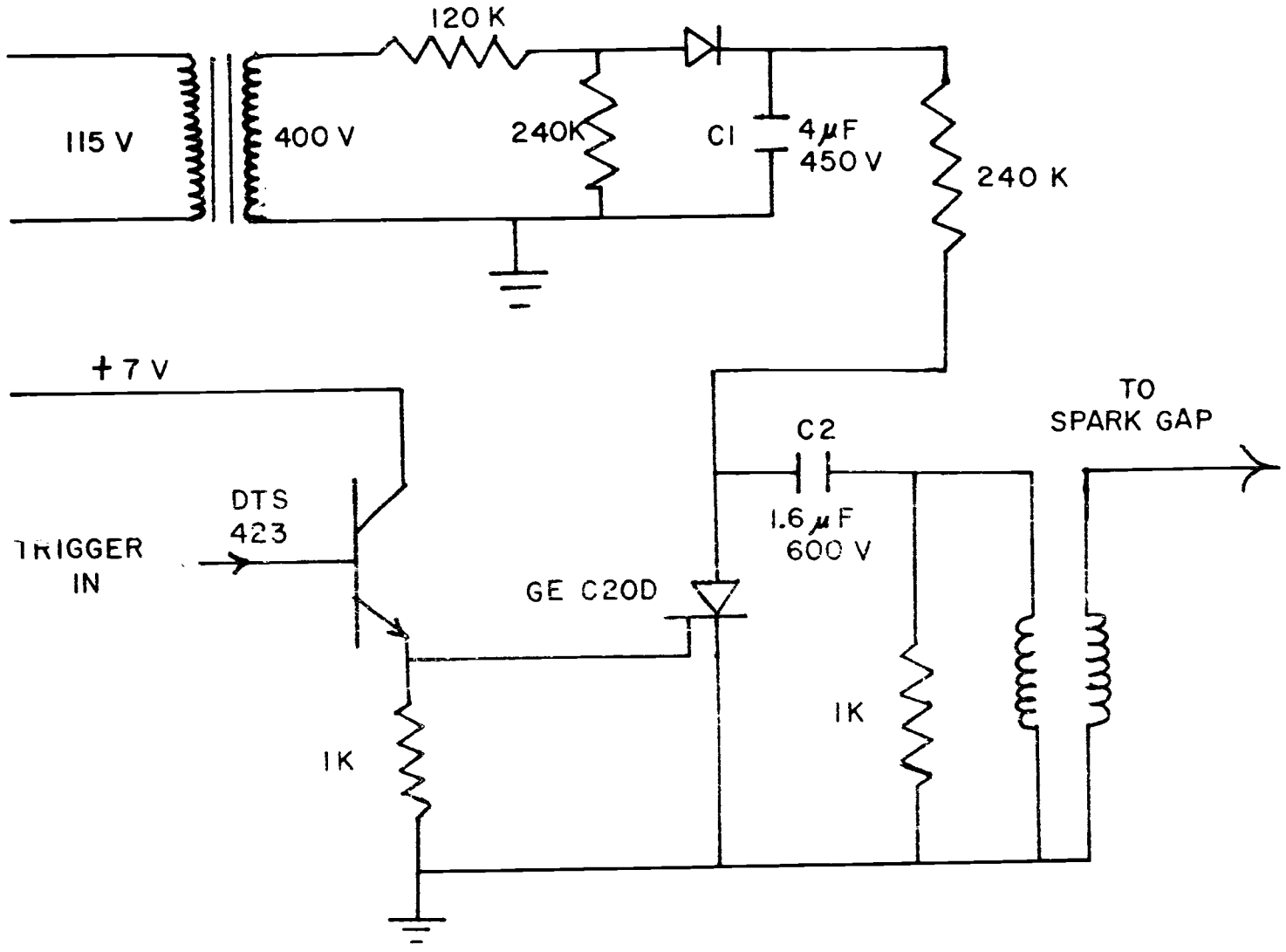

Figure 2. Schematic diagram of the laser sparkgap triggering module.

resistor. When the laser was to be fired, a positive pulse was sent to the gate of the SCR by the emitter follower DTS 423. The SCR shorted the capacitor C2 which sent a voltage transient through the primary of the high voltage transformer. The secondary voltage, in turn, initiated the breakdown of the main spark gap of the flashlamp system.

The use of this electronic system reduced the jitter to approximately 10-20 μs. This was more than adequate for the majority of the measurements. However, during the latter stages of the experimental work, further reduction of the jitter time became necessary.

To eliminate the contribution of electronic jitter from the trigger module the monostable multivibrator of the commercial laser was by-passed. The DTS 423 power transistor was salvaged from the original trigger module and used in a simple emitter follower configuration driven by an external pulse supplied by a Tektronix type 114 pulse generator. The resultant jitter and delay time were not alleviated by this circuit modification.

Attention was turned to the spark gap itself. The original instructions supplied with the laser suggested the use of 1-20 psi positive pressure of nitrogen on the spark gap. Since the delay time appeared to be dependent upon the spark gap pressure, it was felt that by lowering the pressure to atmospheric and allowing a

continuous flow of nitrogen through the spark gap, the delay time would be eliminated and the jitter time reduced. Operation in this way resulted in the reduction of the delay time before firing to 10 μs with a jitter time of 1 μs. The flowrate of nitrogen was found not to be critical provided that the flowrate was sufficient to prevent spontaneous breakdown of the spark gap.

B. Laser Microprobe Optics

The laser microprobe optical system served two functions. The first was the measurement of the energy content of each laser pulse. This was accomplished by use of the laser detection system described by Piepmeier (31). The detection system was basically a photodiode sensor coupled with a peak detection system used to monitor the peak intensity of the laser pulse. The optics consisted of a dual prism deflection system to compensate for polarization effects of the laser beam. The readout of the energy was a Heath model EUW-20A servo recorder.

The second function of the microprobe optics was the direction of the laser beam to the sample chamber. A right angle glass prism was used to direct the horizontal laser beam into a vertical beam toward the sample surface. The laser beam was focused on the sample surface by a 35-mm plano-convex lens. The exact focal point of the laser beam was determined by the introduction of a front

surface mirror into the light path to direct the image formed by the lens into a telescope focused at infinity. The lens was moved until the image of the sample surface was in focus.

The pulsed dye laser beam was aligned through the microprobe optics by the use of unexposed but developed strips of Polaroid film. The beam was directed through the entrance aperture, through the energy monitor optics, and finally through the beam deflection prisms, by noting the image formed on the black Polaroid prints. The laser had sufficient energy to blow off a portion of the emulsion leaving a discoloration where the laser impacted. By monitoring this image produced on the print, the pulsed laser beam was easily tracked through the microprobe optics.

C. Sample Module

A diagram of the sample chamber is shown in Figure 3. The chamber was fashioned from a solid rectangular block of aluminum brackets. O-ring seals were used to allow the chamber to hold a vacuum. The optical windows were plate glass finished synthetic quartz (Suprasil). A 1/4" pipe thread hose connector was attached to the sample chamber to allow connection to the vacuum system. The combined leaks of the sample chamber and vacuum line allowed pressures no lower than 0.1 torr to be obtained.

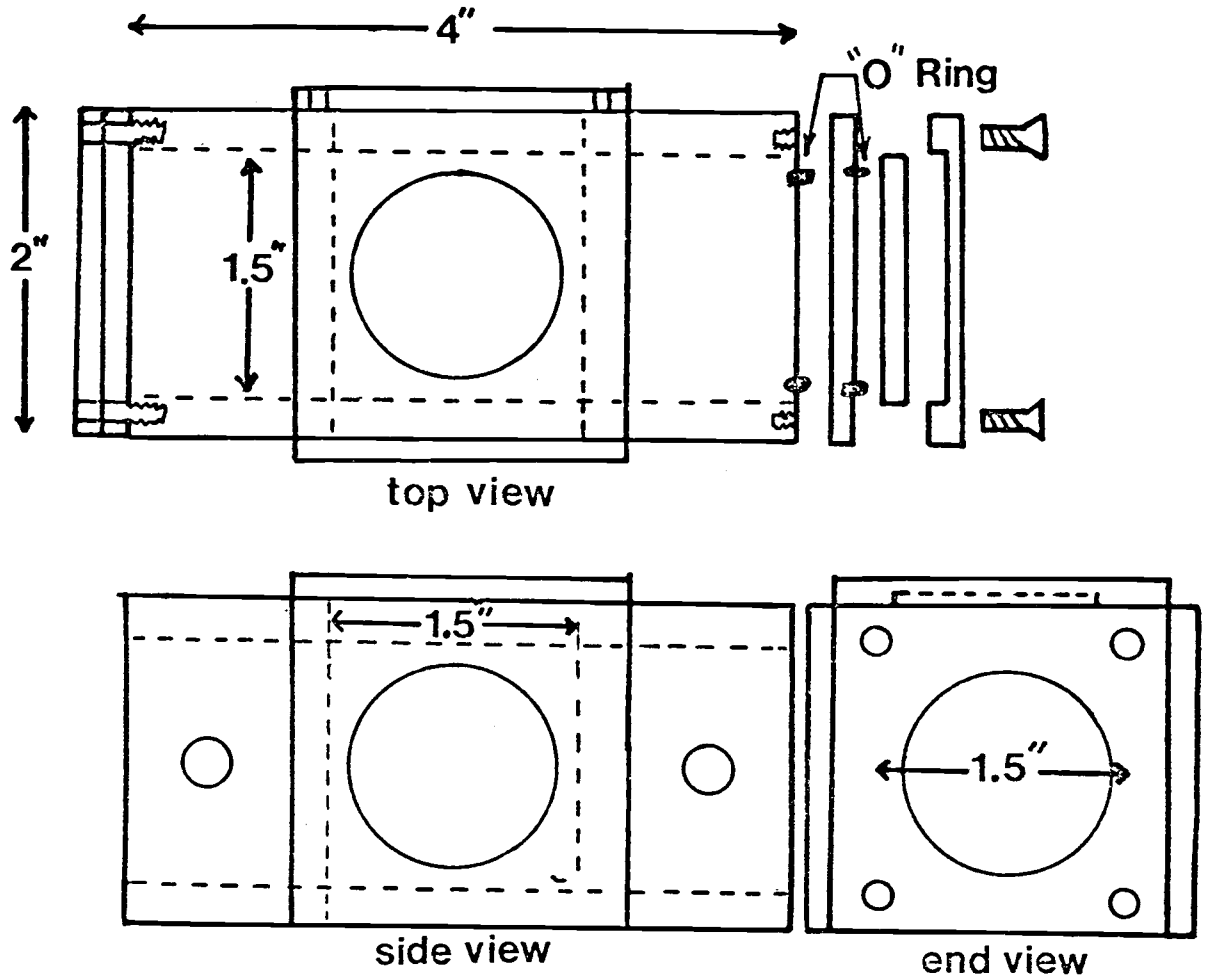

Figure 3. Diagram of the sample chamber.

Figure 4 shows the diagram of the sample positioning system. The sample chamber was mounted on two different sets of translational stages. The stages designated by X and X' moved the sample chamber in a plane perpendicular to the plane of the page. The stages designated Y and Y' moved the sample chamber in a plane that is parallel to the page. The Z axis stages moved the entire sample assembly in a vertical plane allowing different heights above the sample surface to be observed by the monochromator.

The stages designated X and Y moved the sample module and focusing lens as one unit. The Y stage allowed the impact crater area to be moved toward or away from the entrance slit. This stage was used to focus the image of the plume upon the entrance slit. The X stage moved the observation point of the plume in a radial direction outward from the focal spot of the laser. Since the X stage was directly linked to the deflection prism (not shown) and lens of the microprobe optics, the same focal area on the sample was vaporized as the stage was moved.

The stages designated by X' and Y' moved the sample chamber with respect to the other pair X and Y. This set permitted the sample to move in relation to the laser focal spot. This allowed a fresh sample surface to be atomized by the laser without opening the sample chamber. The observation point of the plume by the monochromator was not altered by these stages.

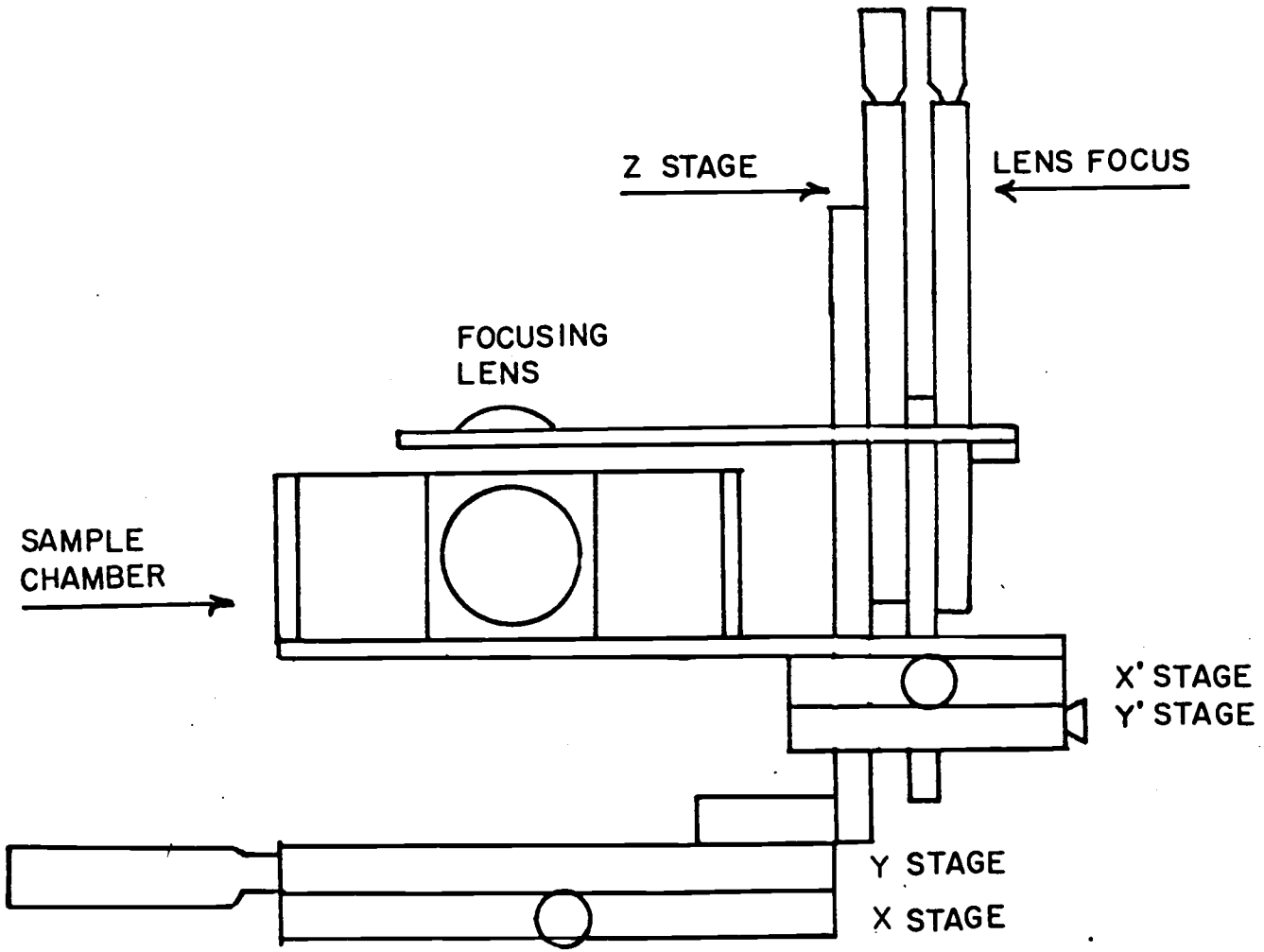

Figure 4. Diagram of sample module positioning system.

The pressure of the atmosphere over the sample in the chamber was controlled by a glass vacuum system described by Osten (19). The pressure of the system was monitored by a RGI swivel Mc-Leod gauge and by a full length mercury manometer.

D. Spectrograph-Spectrometer-Monochromator

Two types of spectrometers were used in this investigation. The first was a research spectrograph-spectrometer described by Osten (19). It was an f/11, 1-meter over-and-under Cznery Turner instrument. The reciprocal linear dispersion in the first order was 0.83 nm/mm. At the focal plane either photographic or photoelectric readout modules were fitted. The photographic module was a Polaroid 4 x 5 inch sheet-film holder modified to be attached at the focal plane. The photoelectric module consisted of two 1P28 photo-multiplier tubes (PMT) to allow dual channel readout. This allowed simultaneous monitoring of the analyte line and the background emission near the spectral line of interest. Power to the PMTs was supplied by a Hewlett Packard model 6516A high voltage power supply. The operating potential of the PMTs was -900 V. The distance between PMT slits was 0.9 mm yielding a wavelength spread of 0.75 nm between channels. The monochromator used in the absorp-tion linewidth studies was a Heath model EU-700 equipped with a Heath Model EU-701 PMT module. This monochromator was

employed as a variable band-pass filter to eliminate interfering lines from the interferometer.

E. Photocurrent Detection Systems

The photoanodic currents from the photomultipliers were monitored by either an oscilloscope or a charge-integration-peak-detection system. Two types of oscilloscopes were used in this investigation. The first was a Tektronic type 555/21A/22A dual beam equipped with Tektronix type 1A1 vertical preamplifiers. The second was a Tektronix Type 7904 equipped with a Textronix type 7B92 time base.

The vertical preamplifiers were either a Tektronix type 7A18 (1-MΩ input impedance) or a Tektronix type 7A19 (50-Ω input impedance). The 7A19 module was used for the observation of signals requiring 50-Ω termination. The rise time of the PMT detection system using this module was 2 ns. For signals that required a higher input impedance with the resultant decrease in the time resolution of the detection system, the 7A18 preamplifier was used. Its bandwidth was 80 MHz.

The oscilloscope tracings were recorded photographically on Polaroid type 410 film. The 7904 oscilloscope was equipped with a type C-50 camera, and the 555 oscilloscope was equipped with a C-19 camera.

A schematic diagram for the photoanodic current integration-peak detection system for the absorption line profile measurements and high temporal resolution atomic absorption measurements is shown in Figure 5. The circuit was very similar to that described by Piepmeier (31). The system was modified to handle the photoanodic currents from photomultipliers rather than the output of photodiode detectors used for the measurement of laser energy.

This was done by reversing the direction of the diodes to accommodate the negative going signals obtained from the output of the photomultiplier tubes. The operational amplifiers used were Mckee Pederson Model MP-1039 instead of the ones used by Piepmeier. The use of a pulse stretching network was eliminated from the circuit. This was possible due to the longer duration of the hollow cathode pulses (1-100 μs) compared to the submicrosecond duration of the Q-switched laser pulses observed by the circuit described by Piepmeier.

Capacitor C1 was the anodic charge integration capacitor. The time constant of the combination of R1 and C1 was chosen to be at least 5 times the half width of the pulse measured. Typical values of C1 and the bypass resistor R1 were chosen to reduce the dc offset caused by dark current of the PMT and yet maintain a relatively long time constant so that the peak detector had time to respond.

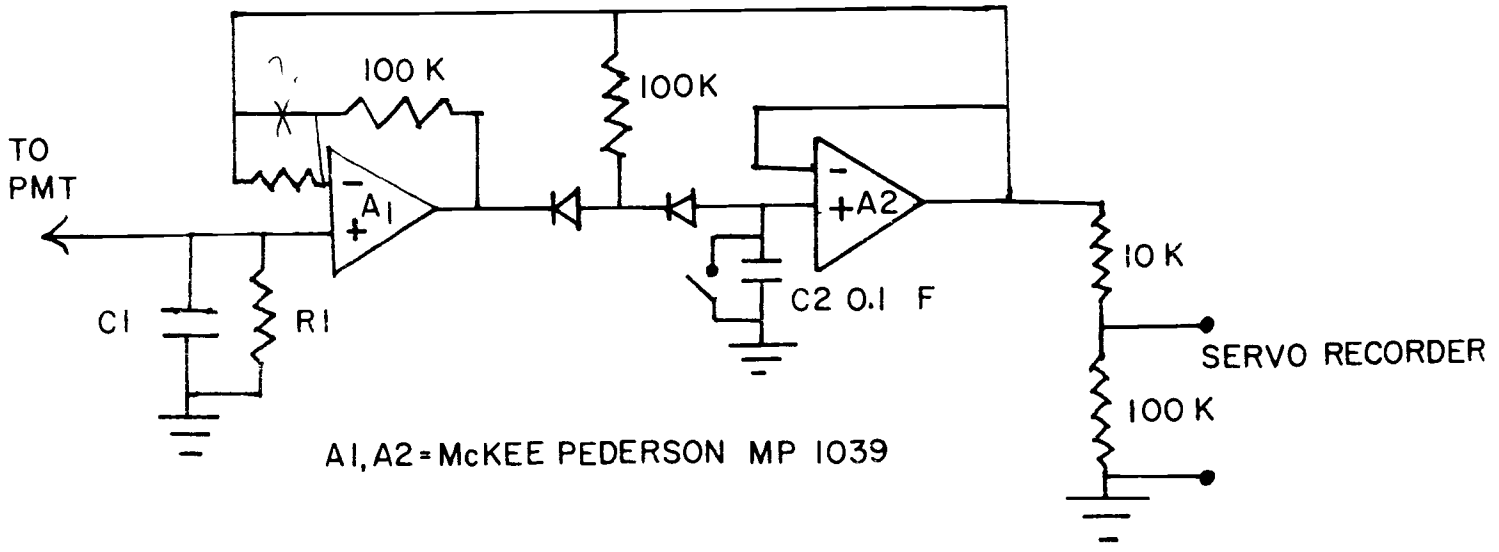

Figure 5. Schematic diagram of photoanodic charge integration and peak detection system.

When a light pulse was observed by the PMT, the voltage on the integration capacitor continually increased until the termination of the light pulse. The peak detection circuitry held this peak value until it was read by either a voltmeter or servo recorder. The value of C1 was chosen such that the peak voltage across the capacitor would be less than 5 volts. In hindsight this value was high. Biasing errors of the dynode chain would not result in little distortion of the signal since most of the current gain occurs during the first few dynodes. The value of resistor R1 was changed to maintain the proper time constant. To reset the peak integrator, C2 was shorted to deplete its charge.

F. Atomic Absorption Apparatus

Hollow Cathode Entrance Optics

Figure 6 shows a block diagram of the instrumentation used to obtain atomic absorption measurements on the plume. Two one-meter focal length spherical mirrors in an over-and-under configuration were used to direct the hollow cathode radiation through the laser plume and monochromator entrance optics. The physical location of the mirrors was determined by backlighting the monochromator. Mirror M1 was moved along the optical path until its aperture was completely filled by the backlight passing through the entrance slit. The second mirror M2 was located so that the image of the entrance

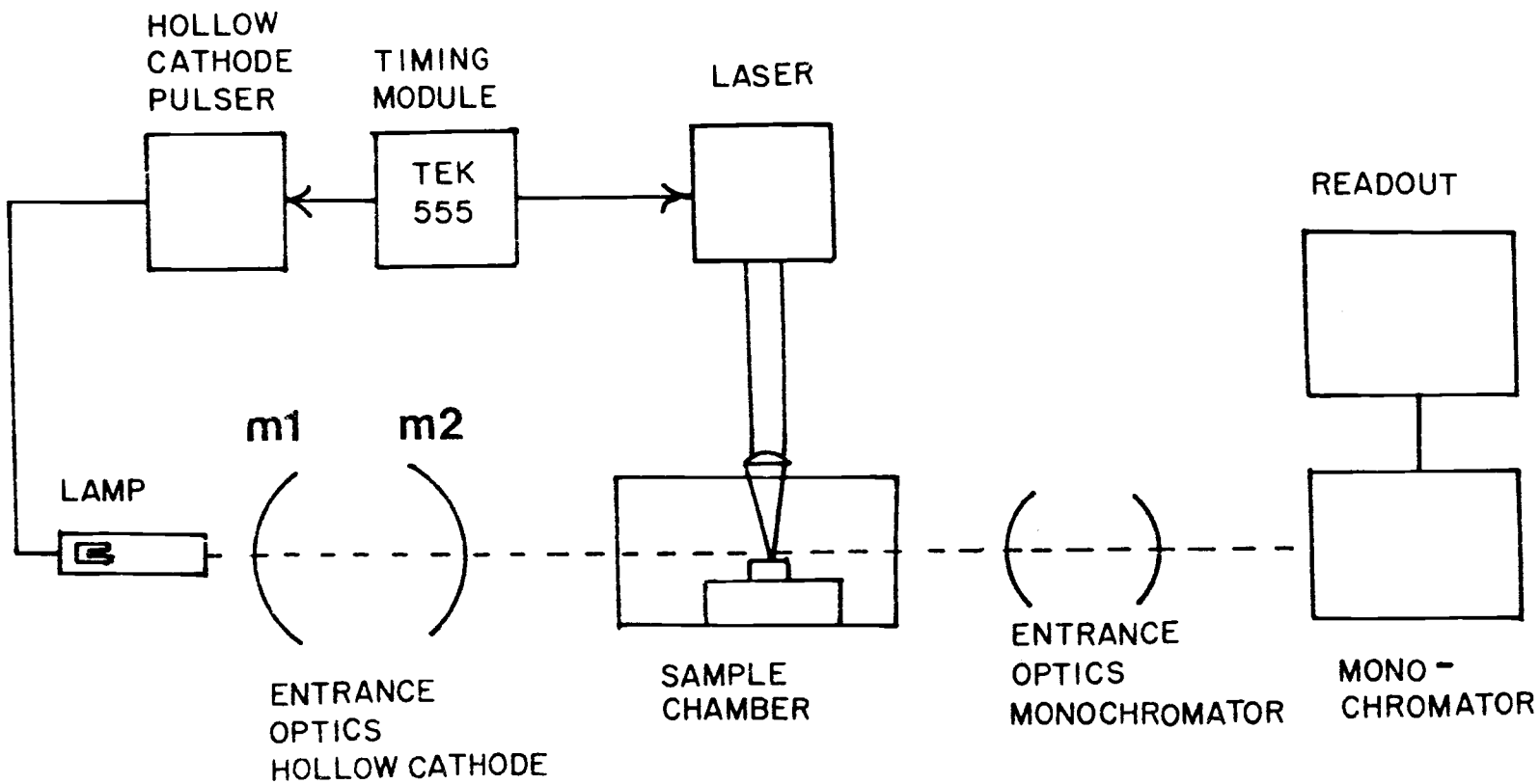

Figure 6. Block diagram of time resolved laser atomic absorption apparatus.

slit was focused approximately 5 cm behind the first mirror. Mirror M1 was tilted so that the aperture of M2 was completely filled. The exact location of the slit image was controlled by the location of M2 along the optical path. The exact location of the hollow cathode was determined by the placement of the slit image exactly in the central region of the hollow cathode cup. The above procedure insured that the image of the hollow cathode would fall at the location of the plume and at the entrance slit of the monochromator.

Hollow Cathode Pulsing Circuit

The schematic diagram of the solid state pulsing circuit is shown in Figure 7. A high voltage switching transistor capable of withstanding 1000 V was required. The circuit was basically a transistor switch with the hollow cathode in series with the collector. R2 allowed an idling bias current of approximately 1 mA to be passed through the lamp. The presence of this current allows more reproducible pulsing characteristics. R1 was a load resistor for protection of the transistor from excess currents. R3 was a current sampling resistor to monitor the pulse currents passing through the collector and base-emitter junction of the transistor.

The pulsing circuit was driven by a Tektronix model 114 pulse generator. The base was connected directly to the output of the pulse generator. This configuration gave the fastest rise time of the

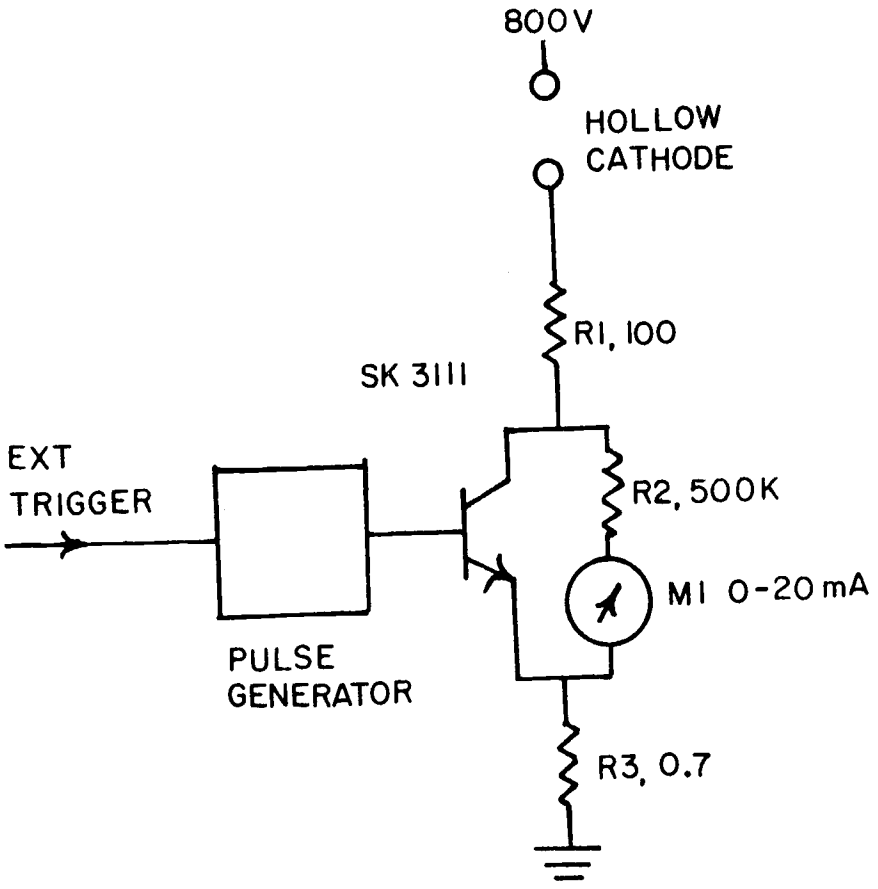

Figure 7. Schematic diagram of hollow cathode pulsing circuit.

current pulses. The magnitude of the current pulses was controlled by the output potential of the pulse generator.

The pulsing circuit was capable of switching 1 A for a duration of 10 ms. The shortest duration pulses observed were 0.5 μs.

III. OVERVIEW OF EXPERIMENTAL DESIGN

The following is an outline of the types of experimental measurements that were made.

A. Atomic Emission

1. Time integrated photographic spectra of continuum emission and analyte emission at various pressures.
2. Time resolved photoelectric measurement of spectral continuum and atomic emission at various pressures.

B. Atomic Absorption

1. Time resolved atomic absorption by use of long duration hollow cathode pulses.
2. Atomic absorption line profile measurements of Cu in lead.
3. Charge-integration atomic absorption measurements of Cu in lead samples using short duration hollow cathode pulses.
4. Continuum absorption measurements to measure non-specific absorption in the plume.

The experimental details for each of these techniques will now be presented.

A. Atomic Emission and Continuum Emission Measurements

Time Integrated Spectra

Photographic readout was used to measure the time integrated spectra of atomic emission. The film that was used was Polaroid ASA 3000 panochromatic film. The film was supplied in 4 x 5 inch sheets. The film was developed in the usual manner as specified by the manufacturer.

Time Resolved Atomic Emission

The temporal behavior of spontaneous emission was observed using photomultipliers. The photocurrent waveforms were displayed on the oscilloscope and photographed. The oscilloscope was triggered either externally by the laser detector or internally with the leading edge of the emission signal from the PMT. In both cases the signal was terminated with a 50-ohm resistor to insure a rapid response time of either the trigger signal or the emission signal from the plume.

B. Atomic Absorption Measurements

Time Resolved Atomic Absorption with Long Duration Hollow Cathode Pulses

The experimental layout of the atomic absorption apparatus was described in Section II-F. The timing module was a Tektronix 555

dual beam oscilloscope. The hollow cathode pulsing circuit was triggered off the positive gate of the upper beam sweep module. The laser was triggered from the delayed trigger output. This arrangement allowed the hollow cathode to reach a constant intensity before the laser was fired. The delay time was approximately 200-400 μs from the initiation of the hollow cathode pulse.

The 555 scope was triggered off the 60 Hz power line frequency. The sweep mode was single sweep. To allow remote triggering of the scope, an air release used for remote tripping of camera shutters was attached to the single sweep start button. This extension allowed the operator to seek shelter during the actual firing of the laser.

The coaxial cable transmitting the photocurrents to the oscilloscope was terminated with a 100-KΩ resistor. This value gave the best compromise between rise time and signal to noise ratio.

Charge Integration Atomic Absorption Measurements

An alternate method of atomic absorption measurements of the laser plume was developed to improve time resolution. The previous method utilized a long duration hollow cathode pulse, and the duration of the atomic absorption signal was short compared to the duration of the hollow cathode pulse. In the charge integration method the hollow cathode pulse was made extremely short compared to the duration of the atomic absorption signal. These short hollow cathode pulses

coupled with a photoanodic charge integration detection system allowed extremely high temporal resolution of the atomic absorption signals. In effect the time constant of the readout system did not limit the time resolution of the atomic absorption signals. The time resolution was entirely dependent upon the duration of the hollow cathode pulse.

The experimental arrangement was similar to that used for the atomic absorption measurements of the previous section. A 7904 oscilloscope was used as the control unit for the sequencing of events. Figure 8 shows the timing signals used to sequence the events. The scope was externally triggered from the laser detector. The sweep of the scope was in the delayed sweep mode. The hollow cathode pulse generator was triggered from the positive gate of the sweep circuitry of the scope. The delay time between the firing of the laser and firing of the hollow cathode was governed by the amount of delay set on the time base of the scope.

A typical experimental procedure is as follows. To determine the value of I_0, the integrated hollow cathode intensity with no laser, the scope was triggered manually to fire the hollow cathode. Eleven firings were made to obtain an average value of I_0.

The peak detection system was reset manually between firings. A sequence of measurements were then made with the laser firing after the preset delay time of the scope. The integrated photoanodic signal was averaged and equated to I, the net signal after

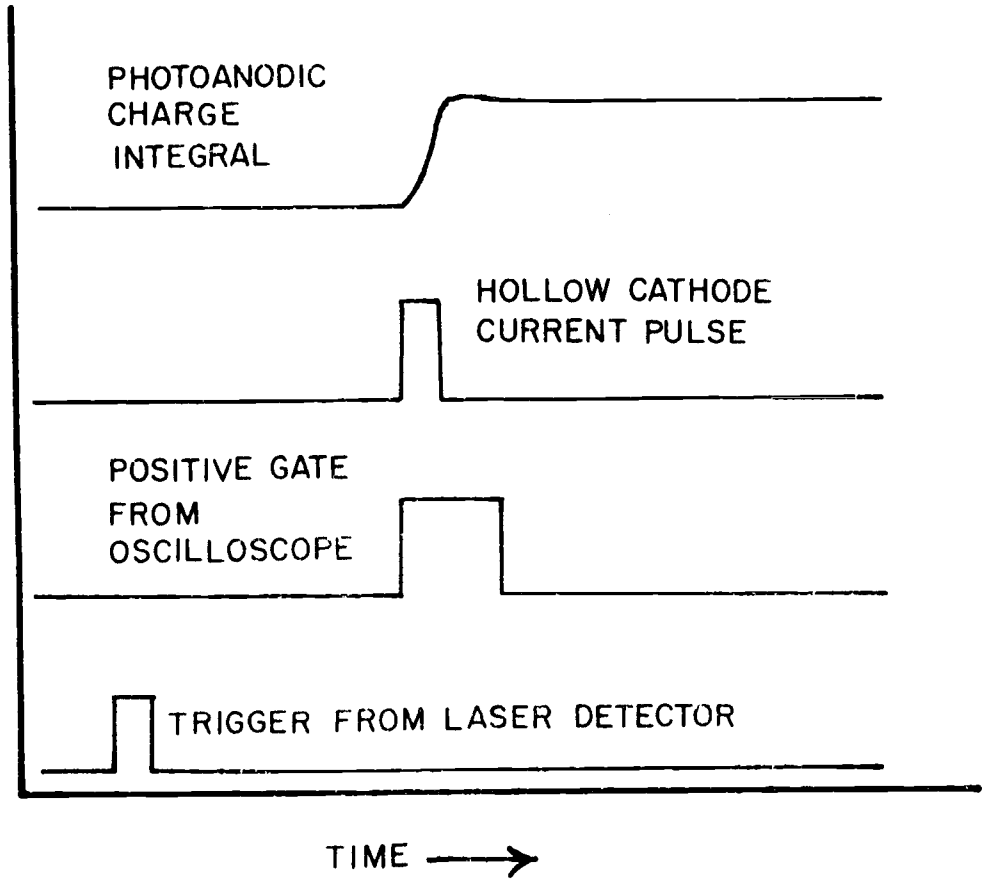

Figure 8. Timing sequence for charge integration atomic absorption measurements.

absorption of the hollow cathode radiation by the plume has occurred.

Continuum Absorption Measurements

A high intensity xenon flash lamp (Xenon Corp.) was substituted for the hollow cathode lamp to measure the non specific absorption in the plume. The flashlamp tube was masked with aluminum foil so that the vertical height of the exposed region of the tube approximated the height of the luminous region of a hollow cathode lamp.

The flashlamp power supply was operated at a potential of 6 KV. The pulse duration was approximately 6 μs. The flashlamp was externally triggered by placing a PNP switching transistor across the remote trigger input. The transistor switch was driven by a Tektronix 114 pulse generator. A trigger pulse duration of 10 μs and a potential of -3 V was used. The pulse generator was externally triggered by the delayed trigger output from the Taktronix 555 scope. The laser was triggered off the positive gate output of Channel A (upper beam).

To determine the delay time to bring the firing of the laser and the firing of the flashlamp into coincidence, the photoelectric signals from the photodetectors were monitored on the oscilloscope. The flashlamp detector was the PMT of the Heath EU700-701 spectrometer and the detector for the laser pulse was a photodiode. The dual beam feature of the 555 allowed simultaneous monitoring of both events.

The delay time was varied until the rise time of the laser and flashlamp were coincident. The delay time from the trigger of the laser firing circuit to the trigger of the flashlamp was approximately 4 μs.

C. Atomic Absorption Line Profile Measurements

General Instrumentation

The experimental apparatus was very similar to that used for the measurement of the time resolved atomic absorption data. The major modification was the introduction of a Fabry Perot interferometer into the optical system. Figure 9 shows a block diagram of the apparatus used. The monochromator was changed to the Heath model EU 700-701 spectrometer. The photoelectric readout system employed was the charge integration peak detection system discussed in Section II-E.

Interferometer Cavity

A piezoelectric scanning (p-z) Fabry-Perot interferometer (Tropel model 242) was employed. Figure 10 shows the optical arrangement of the interferometer cavity. The optical system was the same as that used by DeJong (32). The plates had a maximum reflectivity of 97.5% between 300-330 nm.

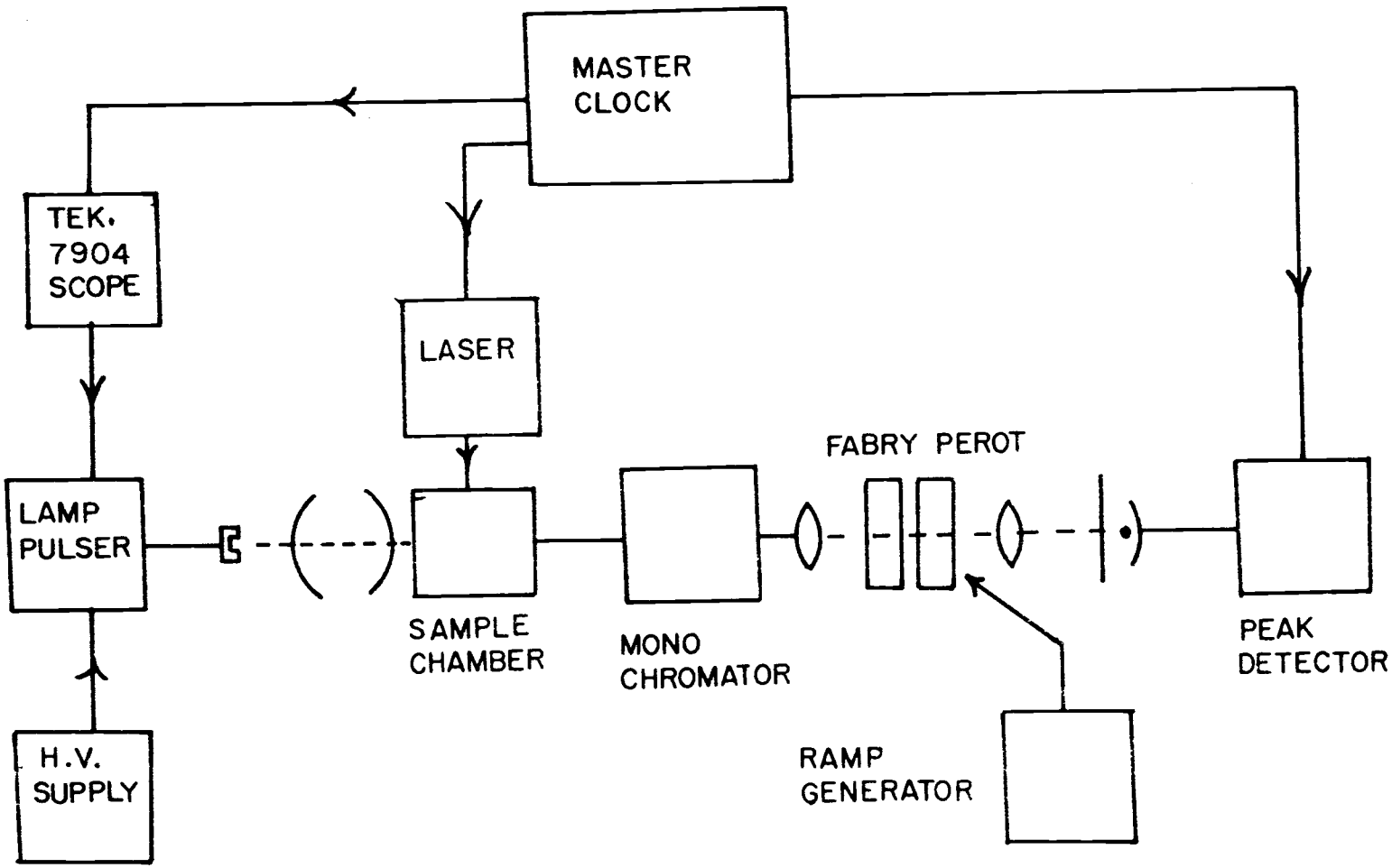

Figure 9. Block diagram of the instrumental configuration for atomic absorption line profile measurements.

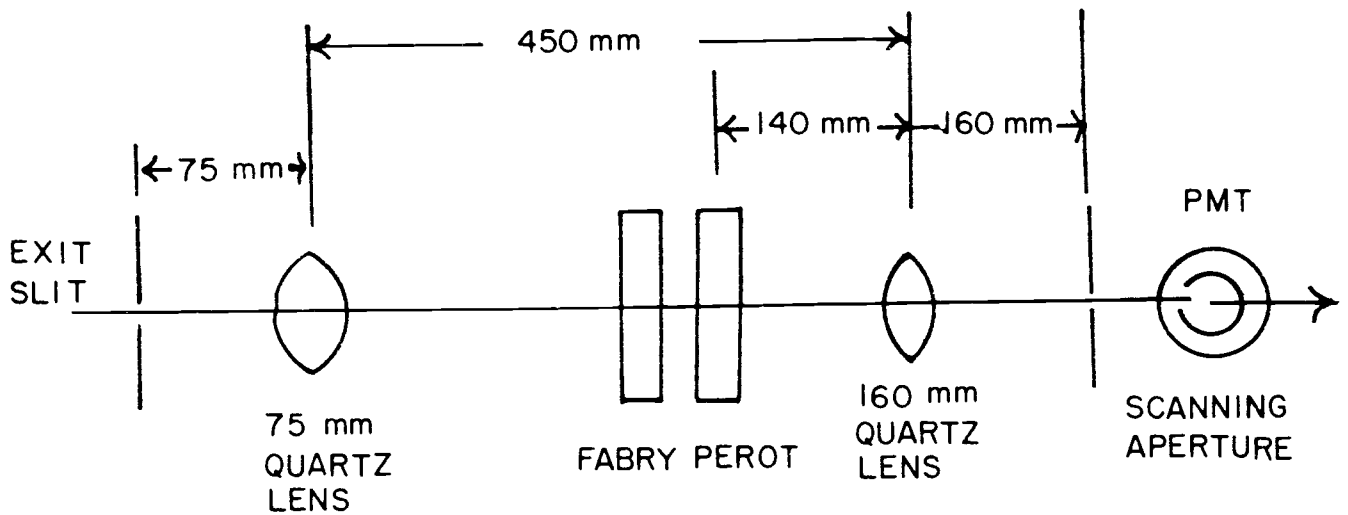

Figure 10. Optical diagram of the scanning Fabry Perot interferometer cavity.

Interferometer Alignment

Coarse Alignment. Figure 11 shows the optical arrangement used for the initial alignment of the interferometer plates. A helium neon laser was used as a monochromatic light source to aid in the alignment. A pin hole aperture was placed at the exit of the helium neon laser to cause divergence of the laser beam. This was done to totally fill the working aperture of the interferometer.

Initially the laser was placed in close proximity to the interferometer (~ 0.5 m). The position of the laser was adjusted such that the reflections from the plates were almost coincident with the exit aperture of the helium neon laser. Four reflection spots were noted. These were due to the 4 surfaces of the two interferometer plates. There are four possible ways of superimposing these spots upon one another. One combination was arbitrarily picked. The coarse micrometer adjustments on the interferometer were turned until the chosen pair of spots were coincident upon one another. The micrometers were adjusted until a series of fringes were observed on the reflection spot at the exit aperture of the laser. The adjustments were fine tuned until the spacings between the fringes were at a maximum. This procedure brought two surfaces into parallelism. A low pressure Hg lamp was placed in the axis of the interferometer. Corning Glass 3-72 and 4-68 filters were placed in front of the Hg

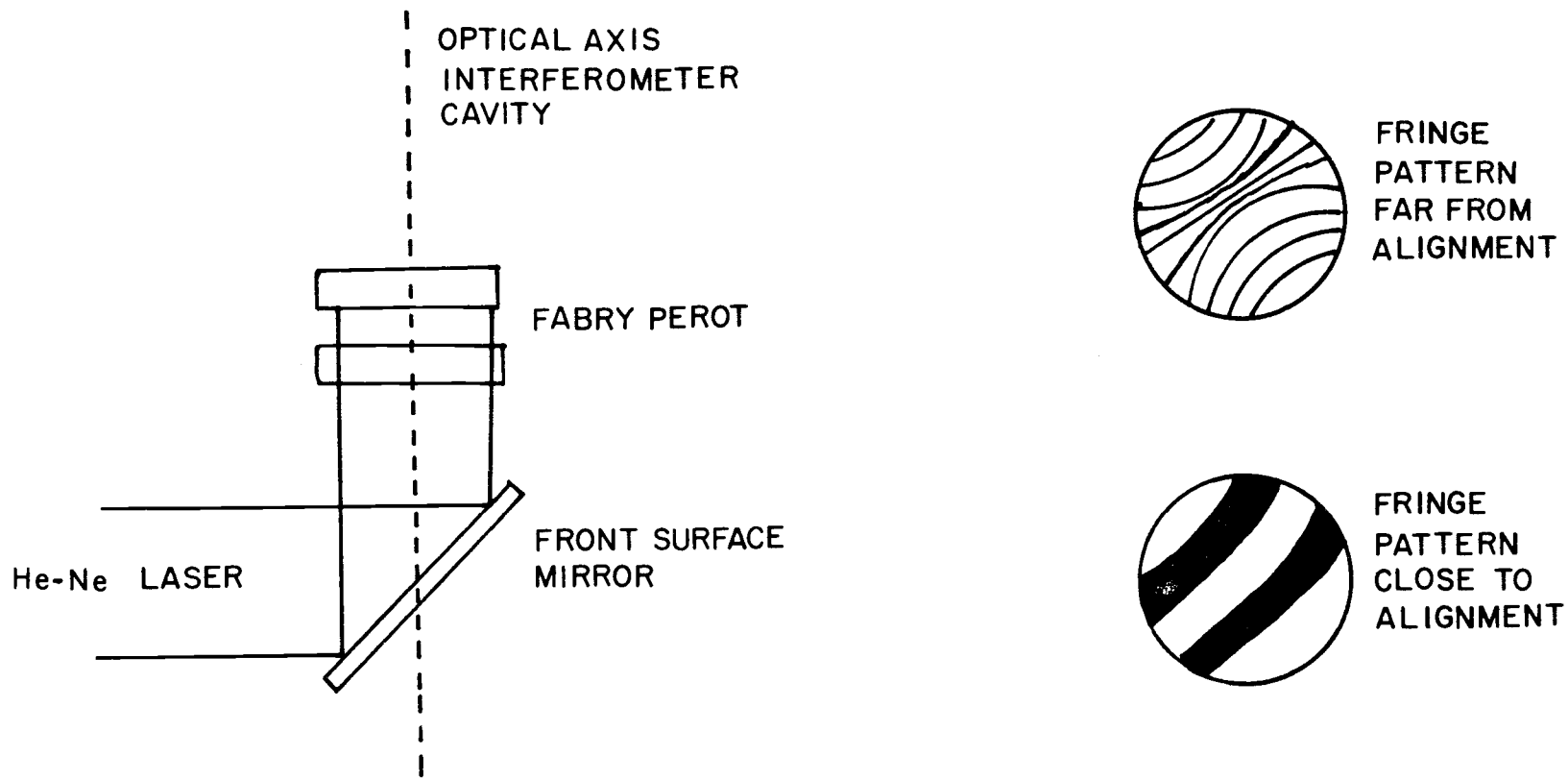

Figure 11. Fringe pattern for critical alignment of the Fabry interferometer plates.

source to allow only the green line of Hg (546.0 nm) to pass through. If the proper two mirror surfaces were picked a series of concentric fringes can be seen with the naked eye. The eye must be focused at infinity before these fringes can be observed.

If no fringes can be seen the wrong pair of spots was chosen. The above process was repeated with another combination until a pair of surfaces produced a series of concentric fringes with the Hg source.

Placement of the Interferometer in the Optical System. The interferometer must be placed in a very precise location along the optical axis of the monochromator and detection system. To aid in the alignment, three 0.6-mm apertures were placed in the optical path. The first was placed in front of the entrance slit of the monochromator, the second at the exit slit, and the third behind the interferometer in front of the focusing lens in the scanning aperture cavity (see Figure 9).

The three apertures defined an optical axis that lies in the center of the acceptance angle of the monochromator. If a helium-neon laser is passed through these apertures a visible optical axis is formed. All of the optical components of the interferometer cavity can be easily referenced to this optical axis.

A 1-mW helium neon laser was placed at the normal location of the hollow cathode lamp described in Figure 8. The position of the

He-Ne laser was adjusted until the beam passed through the three apertures. The monochromator wavelength adjustment was set to 628.3 nm to allow the laser line through.

Once the laser was adjusted, the interferometer was inserted into the optical system. The height of the interferometer was adjusted with metal shims until the laser beam passed through the center of the interferometer plates. Additional shims were placed under the appropriate leg of the interferometer to insure that all reflections from the plates were coincident upon the exit apertures of the monochromator. To aid in the visual observations of the reflection spots, the aperture disk at the exit slit was painted white. This procedure insured that the incident radiation to the plates was perpendicular to the etalon reflection surfaces.

Adjustment of the focusing lens was accomplished by placing the scanning apertures over the central portion of the cathode surface of the photomultiplier circuit. The scanning aperture lens was moved until the laser beam passed through the scanning aperture.

The collimating lens was placed into the optical axis. Its height was adjusted until the laser beam passed through its center. Fine adjustment of the position of this lens was done while observing the line profile from a line source such as a hollow cathode lamp.

Critical Alignment of the Interferometer Plates. The He-Ne laser was placed 10-20 feet away from the interferometer at right

angles to the optical axis of the interferometer axis (Figure 11). The laser beam was deflected through the interferometer by means of a plane front reflecting mirror. The pin-hole aperture was placed over the exit of the He-Ne laser. The position of the laser and the position of the reflecting mirror were adjusted until the reflection spot from the plates was superimposed upon the exit aperture of the He-Ne laser. The purpose of this was to insure that the reflections traverse the same axis as the incident laser radiation.

If the adjustment to the etalon done previously has not been disturbed, a fringe pattern should be noted on one of the reflection spots. The coarse micrometer adjustments were then carefully adjusted until the fringes were widely separated.

Once this procedure was completed, the plates were in sufficient alignment that only fine tuning of the piezoelectric drive elements of the micrometer adjustment was needed.

The fine tuning was accomplished by the observation of the line profiles of the Cu(I) 324.7-nm line. The lamp was operated in the dc mode with a current of 15 mA. The photoanodic currents were displayed on a Tektronix 555 scope. The scanning piezoelectric drive (pz) was driven from the 150 V sawtooth from the horizontal sweep amplifier of the oscilloscope. Typical instrumental parameters were as follows: Tektronix 555 time base setting, 2 sec/sweep; PMT voltage, 700 V; vertical preamplifier sensitivity, 0.005 V/div;

slit width; 1000 μm, hollow cathode current, 15 mA.

Before any modulation can be observed on the oscilloscope trace, the scanning aperture must be placed at the precise location of the central fringe. Location of the central fringe was by trial and error. The search task can be simplified if a larger aperture (5 mm) is substituted for the scanning aperture (0.5 mm). By this procedure, the region surrounding the central fringe can be easily located. The profile observed on the oscilloscope face will lack finesse but modulation of the signal can be readily observed. The actual scanning aperture was then placed in this region. Its position was carefully adjusted until modulation was observed on the trace. The location of the central fringe is the position of the scanning aperture that yields the maximum finesse or resolution.

The piezoelectric tuning drives were then adjusted for maximum finesse. For small changes in the tuning drives, adjustment of the scanning aperture was not necessary. It is however worthwhile to recheck the scanning aperture position for gross changes in the tuning drives such as those required during the initial alignment procedures.

An enclosure was placed over the interferometer cavity when the alignment procedure was completed. The size of the enclosure was such that a 0.25-m air space completely surrounded the interferometer cavity housing. This entire dead volume was filled with

styrofoam pellets to thermally insulate the interferometer from temperature variations in the laboratory. The entire system was allowed to equilibrate over a 24 hr period.

The alignment stability was greatly enhanced by leaving the power to the tuning p-z drives on continuously. By doing this the alignment of the interferometer was stable over a 2 month period. During this time, only fine adjustment of the tuning p-z drives were required to obtain maximum finesse.

Events Sequencing

To measure the absorption profile of the transient laser plume, a homogeneous sample would have to be atomized many times during the scan of the line profile. This required an extremely slow scan rate due to the delay time required between laser shots for maximum reproducibility of the laser and the insurance of not overheating the flashlamp and power supply. To accomplish this, an automated data acquisition system was developed which controlled experimental events with little operator interaction.

A typical experimental sequence of events was as follows. The sample was introduced into the sample chamber. The pressure of the atmosphere surrounding the sample was adjusted to the desired value. The pulse width and pulse current of the hollow cathode were set. To start the automated timing sequence of the laser and hollow cathode

pulses, the master control clock of Figure 9 was turned on. The laser was not fired on the first pulse of the hollow cathode in order to give a photoanodic signal corresponding to transmittance (I_0). The laser was then allowed to fire on the next hollow cathode pulse, and the resulting photoanodic signal (I) corresponded to the transmitted light that passed through the absorbing sample. All during this time the interferometer was slowly scanned through the free spectral range by the ramp generator.

The servo recording device of the peak detection circuit recorded the atomic absorption signal due to the analyte in the sample. At the end of the experiment, an almost simultaneous record of $\underline{I}$ and $\underline{I}_0$ alternating with each other was present on the chart paper for each wavelength (see for instance Figure 41). Approximately 50 hollow cathode pulses with laser shots alternating with 50 hollow cathode pulses without laser sampling were used to obtain a complete profile.

Sequencing of events during the absorption profile measurements was controlled by a master clock system assembled on a Heath model ADD-11 digital designer. Figure 12 shows the schematic diagram of the control module. An EU 801-13 clock was used as the timing device. Its frequency was set between 0.2-0.25 Hz.

Monostables M1 and M2 provided a delayed pulse to the scope external trigger. This allowed time for the analog switch of the peak

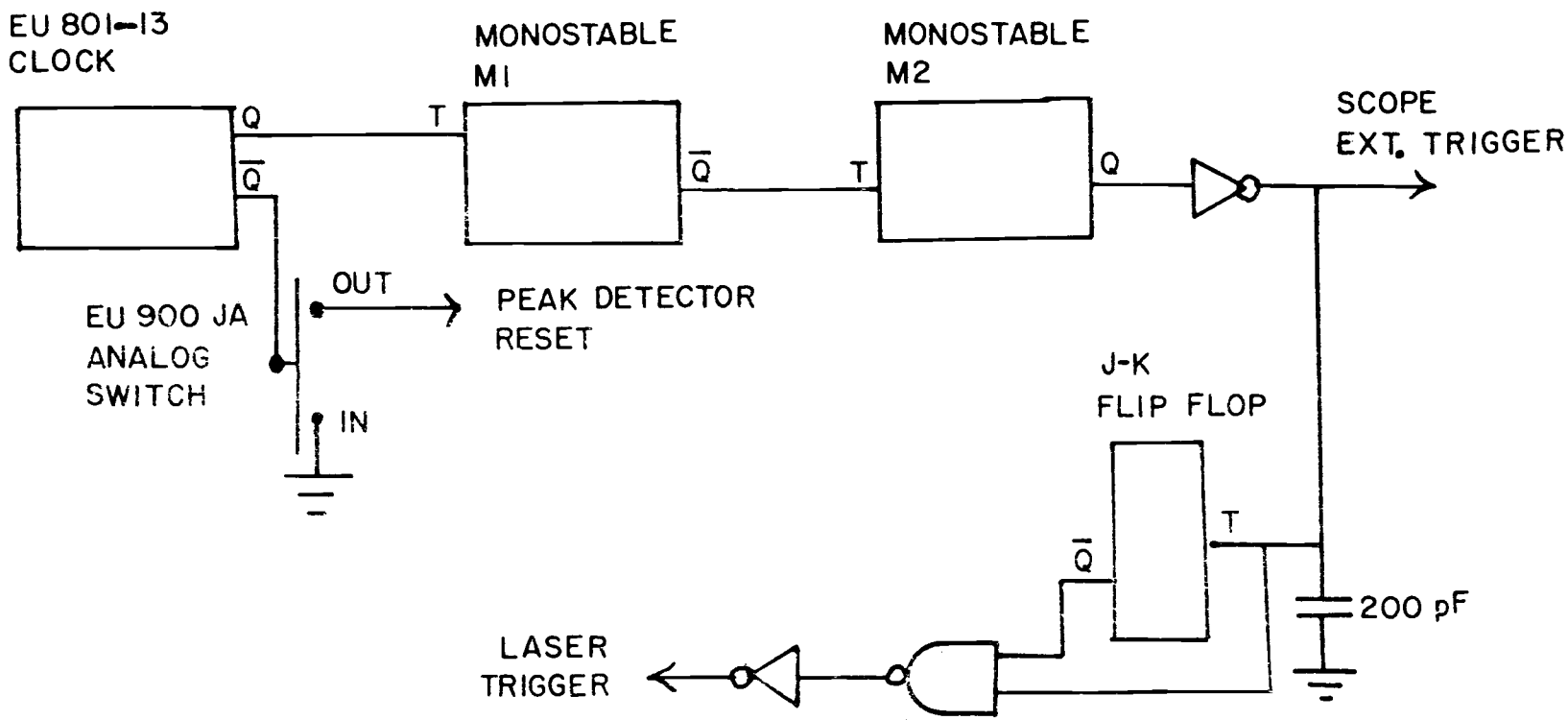

Figure 12. Schematic diagram of the control circuit for atomic absorption line profile measurements.

detection reset mechanism to close. The J-K flip-flop was used to allow only every other trigger pulse to be sent to the laser triggering circuit. The 200 pf capacitor was used to bypass any high frequency noise to ground to prevent false triggering of the laser.

Figure 13 shows the various waveforms at different points along the signal path of Figure 12. The bottom waveform is the output of the master clock. The next waveform is the output from the $\overline{Q}$ output of monostable M1. This provides the delay time since the monostables require a positive going signal to trigger. The combination of the J-K flip-flop and NAND gate allowed only every second laser trigger pulse to be passed.

The driving sawtooth potential required for the slow scanning of the p-z drive was supplied from a 50 KΩ ten-turn potentiometer. The potential across the pot was 100 V. The center tap was attached to the p-z drive connector. A 1/2 RPM synchronous motor was used to drive the potentiometer to generate the required ramp voltage. The output resistance of the pot reached a maximum of 25 KΩ. The input impedance of the p-z drive was found to be greater than 15 megohms; thus any loading effect of the ramp generator could be neglected. Capacitance loading was not important at the scan rates used. A scan time of 10 minutes was required to scan one free spectral range (FSR). The slope of the ramp could be altered by varying the potential across the pot.

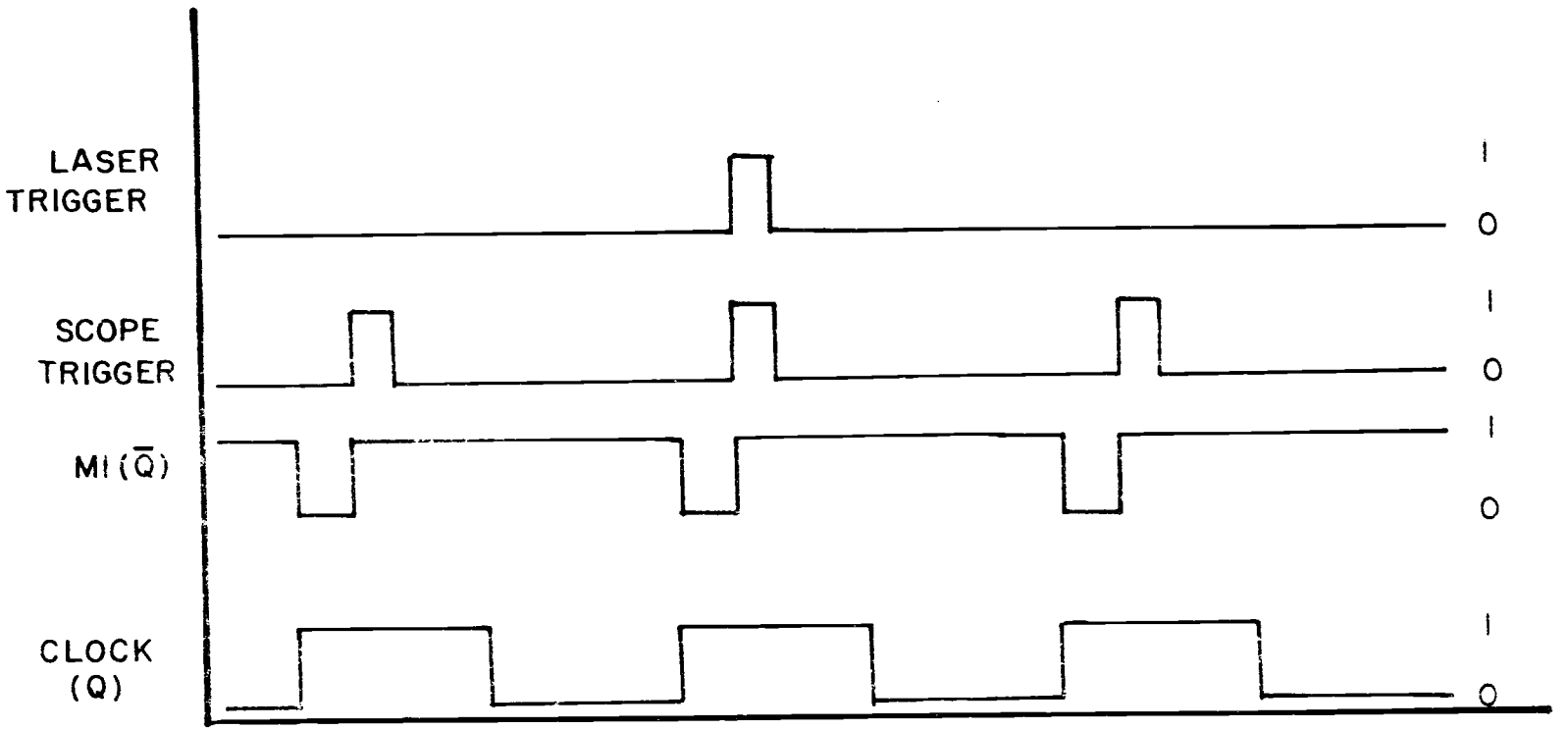

Figure 13. Output waveforms of the schematic diagram of Figure 11.

To insure a fresh sample surface to be atomized during the absorption profile runs, a 1/2 RPM synchronous motor was attached to the lead screw of the Y' translational stage (Figure 4). This caused the sample to be moved along the Y axis at a constant rate so that a fresh surface was present for each laser pulse.

IV. RESULTS AND DISCUSSION

A. Dependence of Crater Diameters on Laser Energy

Piepmeier and Osten (16) have shown that for a Q-switched Nd-glass laser microprobe system, the diameters of the resultant craters increase with laser energy at one torr, but did not change with increasing laser energy at amospheric pressure in the energy range of 1×10^5 W to 1.7×10^6 W. To explain these results Piepmeier and Osten (16) developed the concept of the formation of a radiation supported shock wave above the sample surface at atmospheric pressure. The shock front absorbs the laser energy masking the laser radiation from the sample surface during the latter part of the laser pulse. The net result is the transmission of a relatively constant amount of laser radiation to the sample surface for the energy densities that they used.

For the dye laser sampling system used in this investigation, similar results were not obtained, even though the Q-switched and dye laser pulses both contained the same energies, 0.1 J. Figure 14 shows the dependence of crater diameters for a pure Cu target at atmospheric pressure and low pressure. Note the increasing trend of the crater diameters with increasing laser energy at both pressures. Figure 15 shows the relationship between crater diameters and laser energy for a steel sample at atmospheric pressure. These results

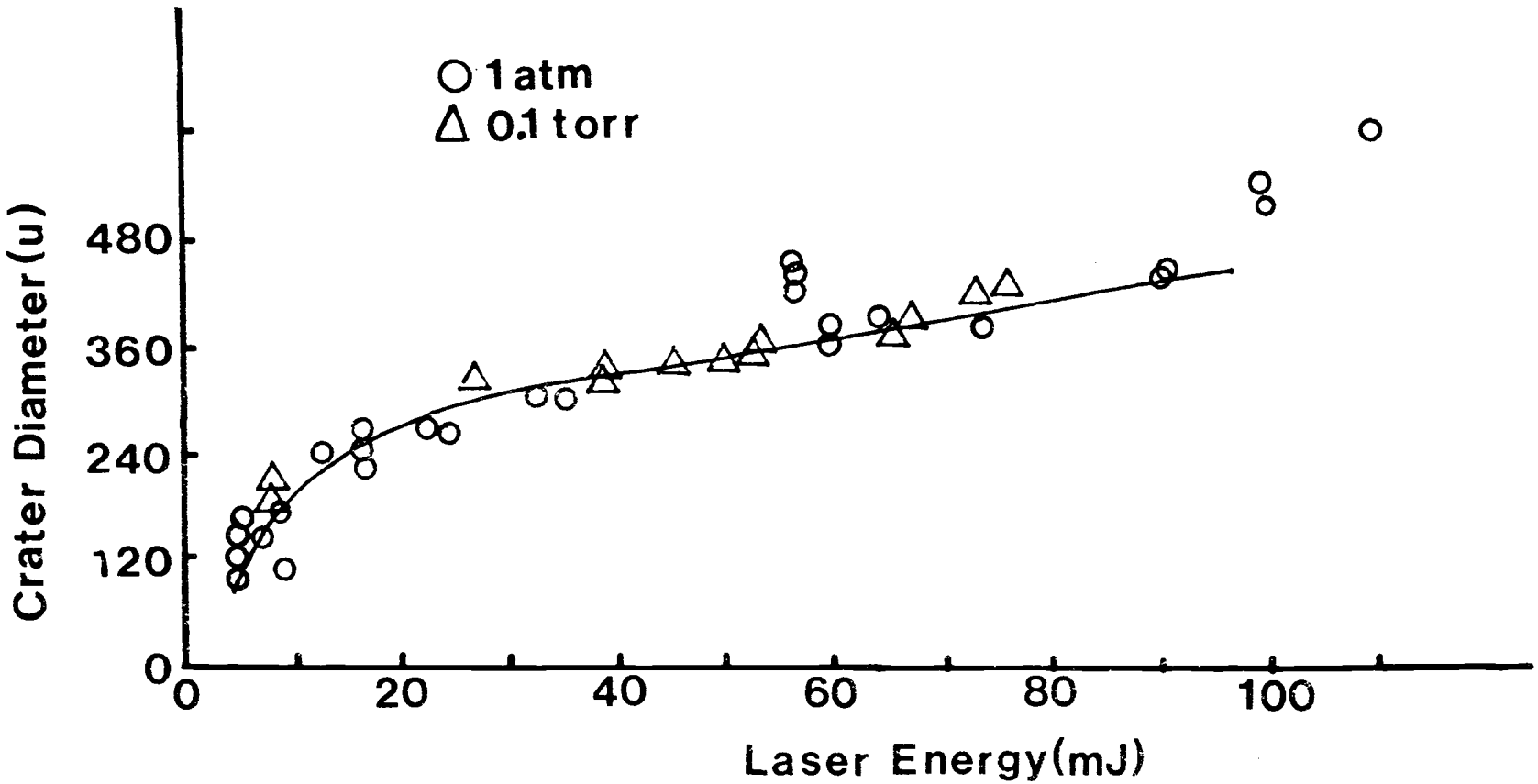

Figure 14. Crater diameter versus laser energy at atmospheric pressure and low pressure (0.1 torr) for a pure copper target.

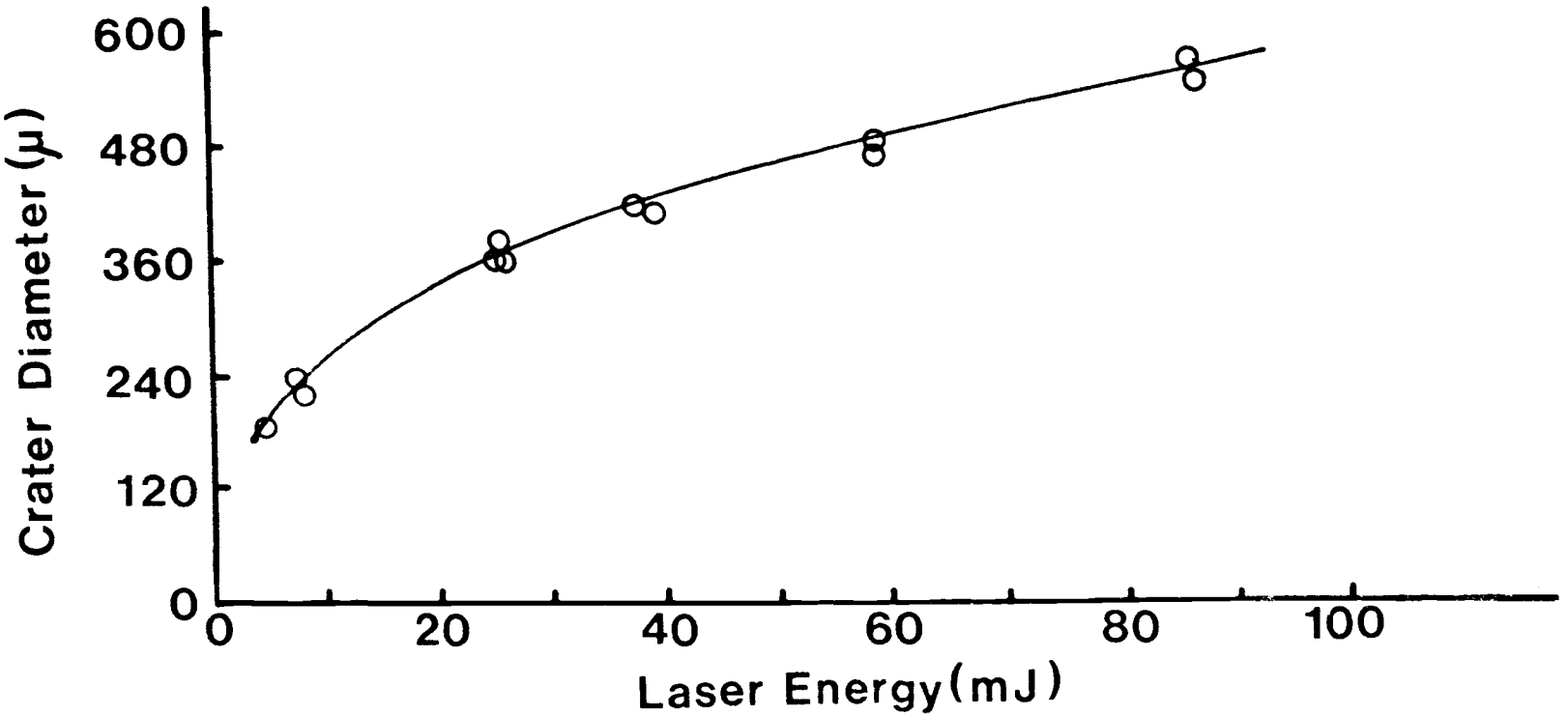

Figure 15. Crater diameter versus laser energy at atmospheric pressure for a NBS 461 steel sample.

indicate that the formation of the shock wave above the surface is minimized with the dye laser system.

The results depicted in Figures 14 and Figure 15 may be distorted by an increase in the divergence of the laser as a function of flashlamp voltage. To verify this, the beam diameter was measured with black Polaroid prints at two locations along the beam axis. The distance between the two locations was 0.9 m. The divergence at a flashlamp potential of 24 KV was found to be 2 milliradians. The minimum spot diameters can be estimated from the following equation

$$d = f \times \theta \tag{1}$$

where

f = focal length of laser focussing lens in mm

θ = divergence of laser in milliradians.

Substituting 35 mm for the focal length of the lens used in this investigation a minimum crater size of 70 microns is obtained. At a lower flashlamp voltage of 20 KV the divergence angle was slightly less than 2.0 milliradians. The exact value is uncertain due to the poor image that was produced on the Polaroid film at 0.9 meters from the laser. It is apparent, however, that the crater diameter values of greater than 200 microns are real and not due to a large increase in the divergence angle of the laser at high flashlamp potentials of 24 KV.

To help explain this variation in the dependence of crater diameter to laser energy, a comparison of the operating parameters of both laser systems was made. The Q-switched laser system employed by Osten (19) had a pulse width of 60 ns with a maximum peak power of 1.7×10^6 W. The dye laser system used in this study had a pulse width of approximately 600 ns with a maximum peak power of 1.7×10^5 W. The maximum energy flux at the focal point was 2×10^{11} W/cm^2 for the Q-switched laser and 2×10^9 W/cm^2 for the dye laser system. For the calculation of the light flux at the focal point the assumption was made that the focal spot area was equal to the minimum crater area observed.

Osten (19) has determined a value of 5×10^9 W/cm^2 as the threshold power density for the onset of atmospheric blockage of the laser beam focused on a copper sample. The maximum power density of the dye laser (2×10^9 W/cm^2), is below this threshold value indicating that the presence of the radiation supported shock wave is minimal.

Piepmeier and Osten (16) also reported that the absorption coefficient of the shock wave plasma is expected to be inversely proportional to the frequency of the laser radiation. The operating wavelength of the pulsed dye laser was 590-nm compared to 1,060-nm for the Nd glass laser. Thus the shorter wavelength or higher frequency of the dye laser should further reduce the support of the shock wave.

B. Time Integrated Atomic Emission Spectra

To compare the spectra and background produced by a dye laser microprobe with that produced by the Q-switched laser microprobe, time integrated spectra were recorded on type 57 Polaroid film. The image of the plume was focused on the entrance slit with an image ratio of 1:1. The vertical axis of the spectra represents the emission at various heights above the sample surface. The horizontal position of the slit was placed at the center of the impact crater.

Figure 16 shows the time integrated spectra for Cu, Mg, and Al. The Mg sample concentration in the graphite was approximately 10%. The slit width of the spectrograph was 50 μ corresponding to a spectral bandpass of 0.04 nm. The laser energy varied from 30-50 mJ. Each spectrum is the result of three laser shots. The sample surface is located just at the bottom of the visible part of each spectrum. The top spectrum was taken at a pressure of 0.1 Torr. The bottom three spectra were taken at atmospheric pressure.

The top spectrum, Figure 16a, was produced by Cu at low pressure. The profile of the Cu(I) 324.7-nm line is unreversed. The line emission was also observable to a height of approximately 7 mm above the sample surface compared to a height of 1 mm for the bottom spectra taken at atmospheric pressure. The bottom spectra also exhibited extreme self-reversal for Cu, Mg and Al.

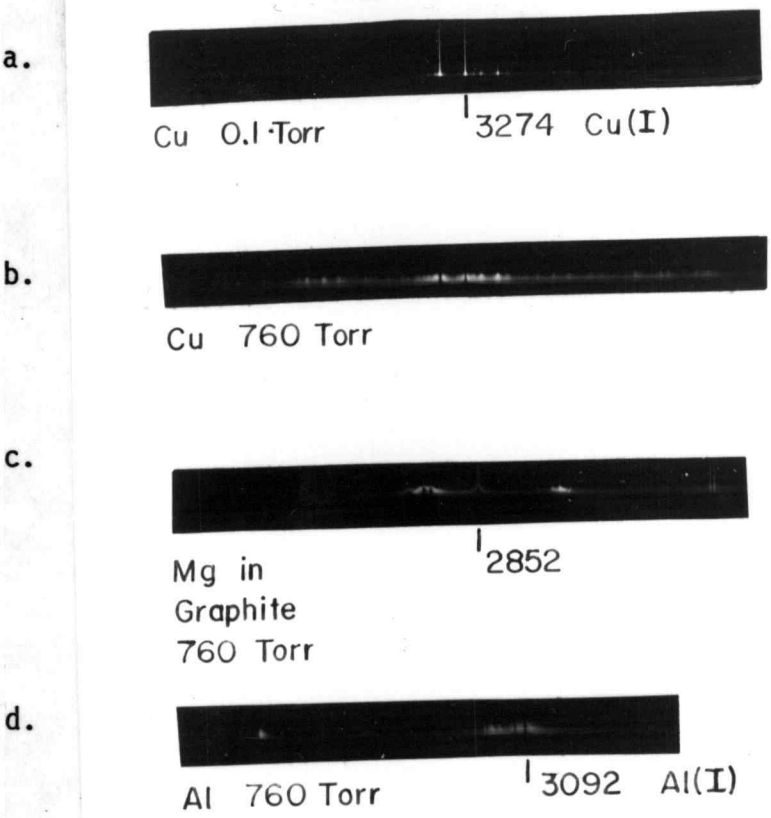

50 μ slit

Figure 16. Time integrated spectra for various elements.

At the surface of the Cu target, the emission line was broadened at both low pressure and atmospheric pressure. This broadening may be due to the increased Doppler temperatures near the sample surface, and the influence of collisional interaction due to the initial high pressure of the plume before significant expansion has taken place. Mg and Al at atmospheric pressure show similar broadening in the width of the self-reversed emission profile near the sample surface. For all three elements the self-reversal was broader near the surface than farther away from the surface. This character is particularly noticeable in the Mg(I) 285.3-nm line. The spectral profile of the Mg line was self-reversed throughout its vertical profile. This indicates that the cool Mg atoms are widely distributed over the sample surface, even to a height of 5 mm above the surface.

For comparison purposes Figure 17 shows similar spectra for a pure copper target with a Q-switched laser system. The photograph was taken from the thesis of Osten (17). Figure 17a shows the spectrum from Cu at the laser focus. Note the presence of a significant amount of continuum emission above the sample surface. Direct comparisons of Osten's data and the data produced in this investigation must be guarded since the experimental parameters used for the production of Figure 17 are unknown. The continuum produced may be due to an overloading of the emulsion due to a large slit width.

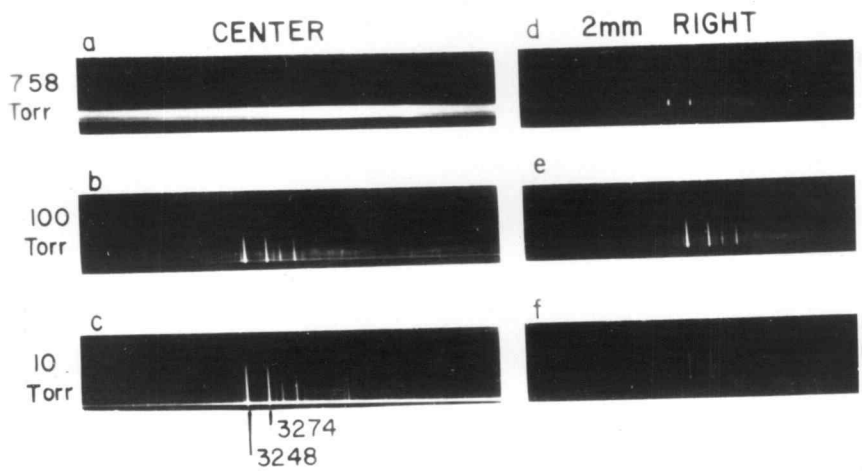

Figure 17. Appearance of spectra at two pressures and positions in the laser plume produced by a Q-switched laser.

However, the optical system used by Osten was the same as that used for the dye laser microprobe system. The film was also the same. The low pressure spectra of Figure 17c and Figure 16 indicate that the exposure was similar. Assuming that the laser energy was the same for Figure 17, it may be concluded that the dye laser microprobe exhibited relative freedom from continuum emission. The spectral profile of the lines emitted from Cu do not appear to be self-reversed as in the case for the dye laser system. This might be due to the Q-switched laser vaporizing less material, distributing the sample material in a different way, and/or causing excitation of the sample copper atoms in the outer region of the plume due to the atmospheric plasma that was generated by the laser energy absorbed in the atmosphere.

C. Photoelectric Atomic Emission and Continuum Measurements

Atomic emission signals from the Cu(I) 324.7-nm resonance line and background continuum emission at 323.9-nm were time resolved by the use of a photoelectric detection system utilizing a photomultiplier detector. The photoanodic currents were transmitted to the oscilloscope with 50-ohm coaxial cable. The cable was terminated by the 50-ohm input impedance of the Tektronix type 7A18 vertical preamplifier. The resulting time constant of the cable was less than 2 ns. The slit width of the monochromator was 200 microns.

This wide slit allowed good signal to noise ratio with spectral bandpass of 0.16-nm. This large bandpass allowed wavelength integrated emission signals to be monitored. This allowed observation of the wings of the self-reversed profiles.

Figure 18 shows the oscilloscope tracings of the time resolved emission of the Cu(I) 324.7-nm line. At a pressure of 0.1 torr, Figure 18a, the duration of the emission signal and the laser pulse were about the same. The background signal was undetectable. At a pressure of 100 torr, Figure 18b, the duration of the emission signal increases and the magnitude of the continuum signal increases. At a pressure of 200 torr, Figure 18c, the magnitude of the continuum and 324.7-nm emission plus continuum increases further.

It is apparent that the duration of the continuum at high pressure is much longer than the duration of the laser pulse itself. The presence of this plasma produced by atmospheric breakdown appears to prolong the excitation of the Cu atoms. The duration of the continuum implies that the temperature above the sample remains quite high after the termination of the laser pulse. The Cu atoms suspended in this plasma would therefore remain thermally excited to undergo spontaneous emission for a longer time period.

At low pressure a smaller fraction of the laser energy is absorbed above the sample surface. A greater fraction of the energy is transmitted into the target material. As the atoms of copper are

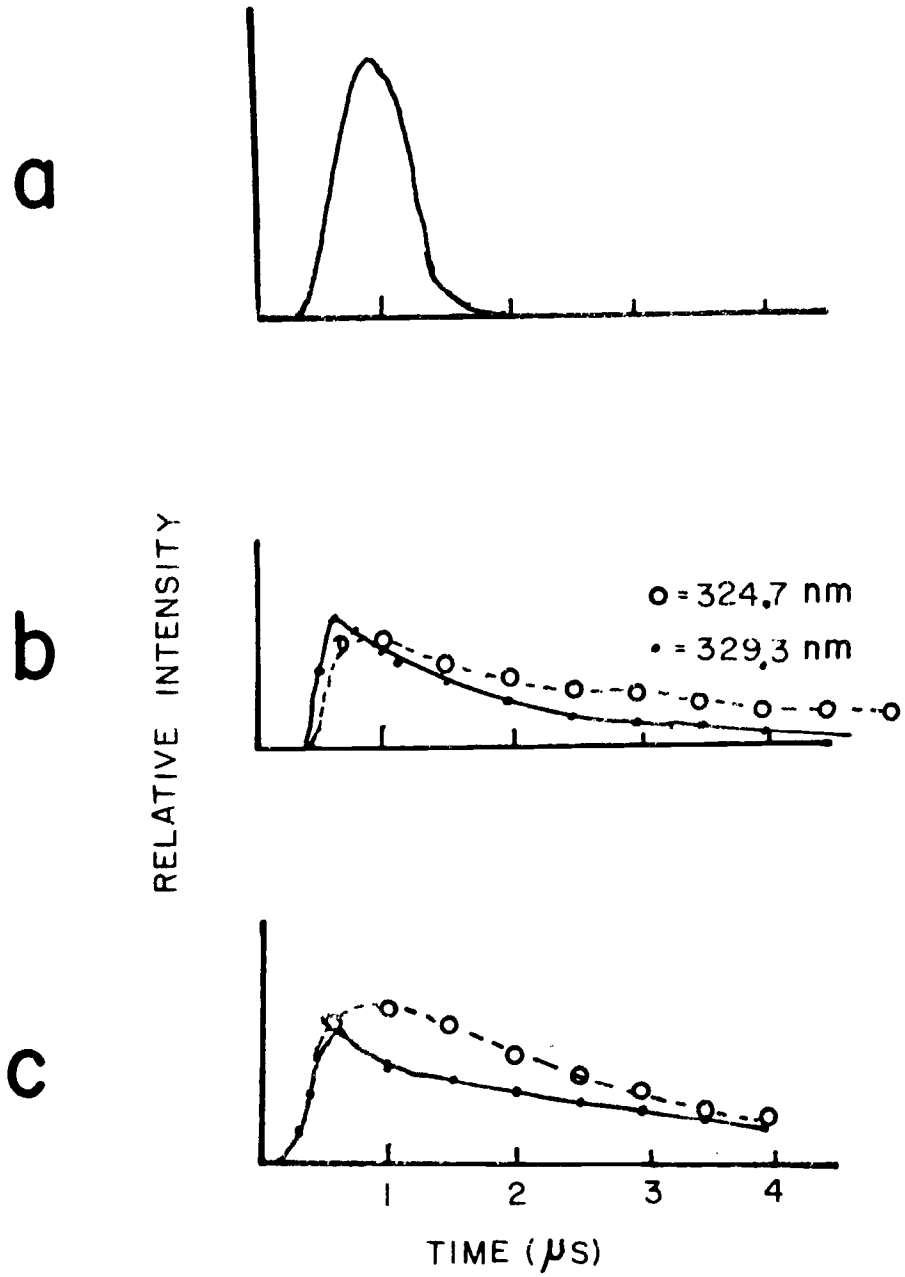

Figure 18. Time resolved atomic emission and continuum emission of a pure Cu target. (a) Pressure = 0.1 torr. (b) Pressure = 100 torr. (c) Pressure = 200 torr.

ejected from the sample surface there is no hot plasma above the sample surface to reexcite the Cu atoms into emission. The number density of the atoms is also lower at low pressure. This would decrease the rate of thermal collisions resulting in reduced spontaneous emission. The net result is a rapid termination of the emission process.

The lack of self-reversal observed at low pressure may be misleading. Self-reversal depends mainly upon the concentration-pathlength product of a region of relatively unexcited species between the main source of emission and the detector. Since at low pressure the rate of diffusion should be higher than at atmospheric pressure, there should be an appreciable pathlength of relatively unexited neutral Cu atoms interposed between the sample and detection system. Self-reversal may be present but unresolved by the spectrograph in the low pressure spectra of Figure 16.

D. Atomic Absorption in the Laser Plume

Many authors have demonstrated the use of atomic absorption measurements for the spectrochemical analysis of plumes produced by a laser microprobe (18, 19, 20, 21). Osten and Piepmeier (20) have

shown that the duration of the atomic absorption signal for pure Cu at atmospheric pressure was 200 μs. This is approximately an order of magnitude longer than the duration of atomic emission at atmospheric pressure. It was also noted that as the pressure was decreased, the duration of the absorbance for pure copper increased to 9 ms. The increased residence time of the free atoms above the sample surface, particularly at low pressure, should allow more time for blending of the concentration gradients in the plume. An improvement in the precision of the spectrochemical analysis should result.

Atomic Absorption Precision of NBS 461 Standard

To study the precision of atomic absorption measurements in the plume, a homogeneous sample was needed. A National Bureau of Standards reference steel alloy #461 was chosen because of its certified homogeneity to a spot size of 1 micron. The sample surface was finished with a lathe cutoff tool.

Most of the previous work at this laboratory on atomic absorption measurements was done at the sample surface on axis with the laser beam. It was felt that to improve the precision, observation above the sample surface would be preferable. This would allow the plume to expand before the atomic absorption measurements were made. Moving the observation point away from the sample surface also prevents the emission from the surface continuum ~~to be~~ detected.

This would minimize overloading the detection system from the intense continuum emission.

The pressure of the atmosphere over the sample surface was chosen to be 0.2 torr because this was the lowest constant pressure obtainable with the vacuum system in use. A low pressure was chosen because of the observed increase in the residence time of the atoms over the sample surface.

Time resolved atomic absorption measurements were performed as described in the experimental section. The minor constituent chosen in the steel alloy was Mn. Its concentration in the alloy was 0.3%. The analytical line chosen was 403.1-nm Mn(I) line, because it had the highest signal to noise ratio of the pulsed hollow cathode signal. The slit width of the monochromator was 200 microns. The observation point of the monochromator was 2 mm above the sample surface.

Figure 19 shows the plot of the peak absorbance of manganese vs shot number at the same sample location. After the initial three shots the peak absorbance reached a constant value of 0.2 with a relative standard deviation of 5.9%. This was a significant improvement over the relative 10-20% precision of the peak absorbances on different sample sites of the NBS alloy. This improved precision may be a result of sample conditioning of the initial laser pulses. Once the sample surface was sufficiently cleaned or prepared by the first three

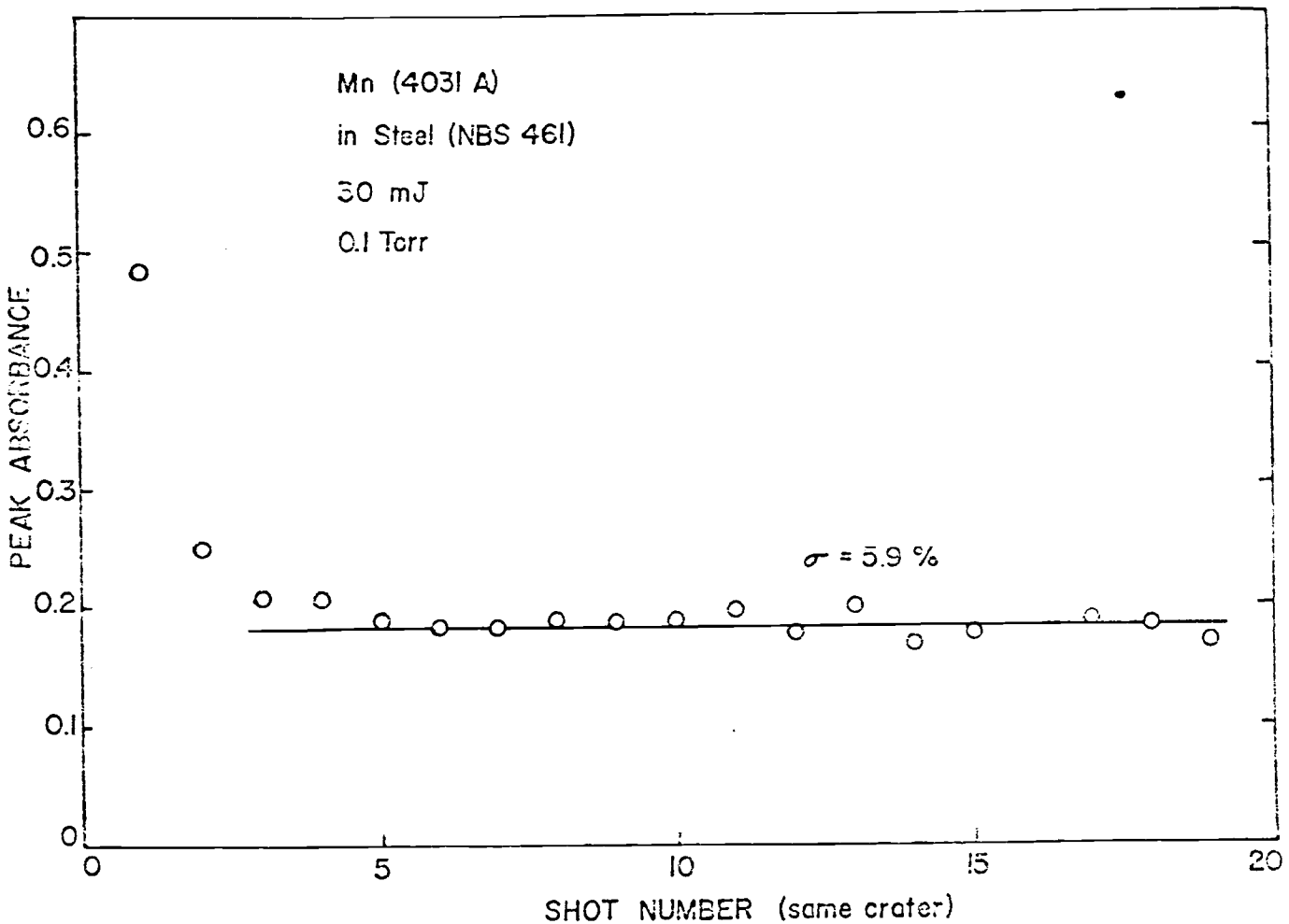

Figure 19. Peak absorbance vs shot number. Height was 2 mm above sample surface.

laser pulses, the exposed sample surface would have the same physical appearance for each subsequent laser shot. The initial drop in absorbance may be due to a depletion phenomenon similar to that observed in aluminum (20). The important point to make here is that a reproducible composition of the resultant plume is produced. This will allow investigation of the physical process of the plume to be carried out with increased confidence.

Spatial Distribution Peak Absorption of Atomic Absorption Signals

The improved precision at low pressure above the sample surface implies that the plume is quite homogeneous. To determine the extent to which the plume is homogeneous, the plume was spatially resolved into 200-μm square cross sections. This was accomplished by placing a 200-μm horizontal slit behind the vertical entrance slit. The slit width of the vertical slit was 200 μm. Since the plume was imaged upon the slit in a 1:1 image ratio, this resolved the plume into 200 μ, sections. The observation point of the plume was controlled by the X and Z axis translational stages of the sample module positioning system, Figure 4. The X axis adjustment controlled the radial distance away from the plume. The Z axis controlled the height of the observation point above the sample surface.

Figure 20 shows the radial distribution of Mn absorbance at 0.2 torr for various heights above the sample surface. Near the laser focus, Figure 20a, there is a decrease in the peak absorbance detected by the readout system. Direct interpretation of this would imply that at the focal spot the Mn atoms are ejected away from the crater much faster than the response time of the detection system. However, another contributing factor to the decrease in absorbance at the focal spot may be due to the decrease in the value of the absorption coefficient of the absorption profile central maximum. This is a result of the broadening of the absorption line profile by either an increase in temperature or pressure at the focal spot area. A more detailed discussion of line broadening mechanisms will be presented in Section IV-F.

A possible model for the depletion of free-ground-states-Mn atoms from the focal area is shown in Figure 21. The inner circle represents an area void of Mn atoms. The area between the circles represents the area in which the Mn atoms are confined. The two path lengths are represented as two different sections observed by the monochromator. Path A represents observing the plume at a distance away from the laser focal spot and path B represents a path traversing the laser focal spot. If the assumption is made that the atoms have a uniform density between the circles it is apparent that path A has a longer effective path length of analyte vapor than does

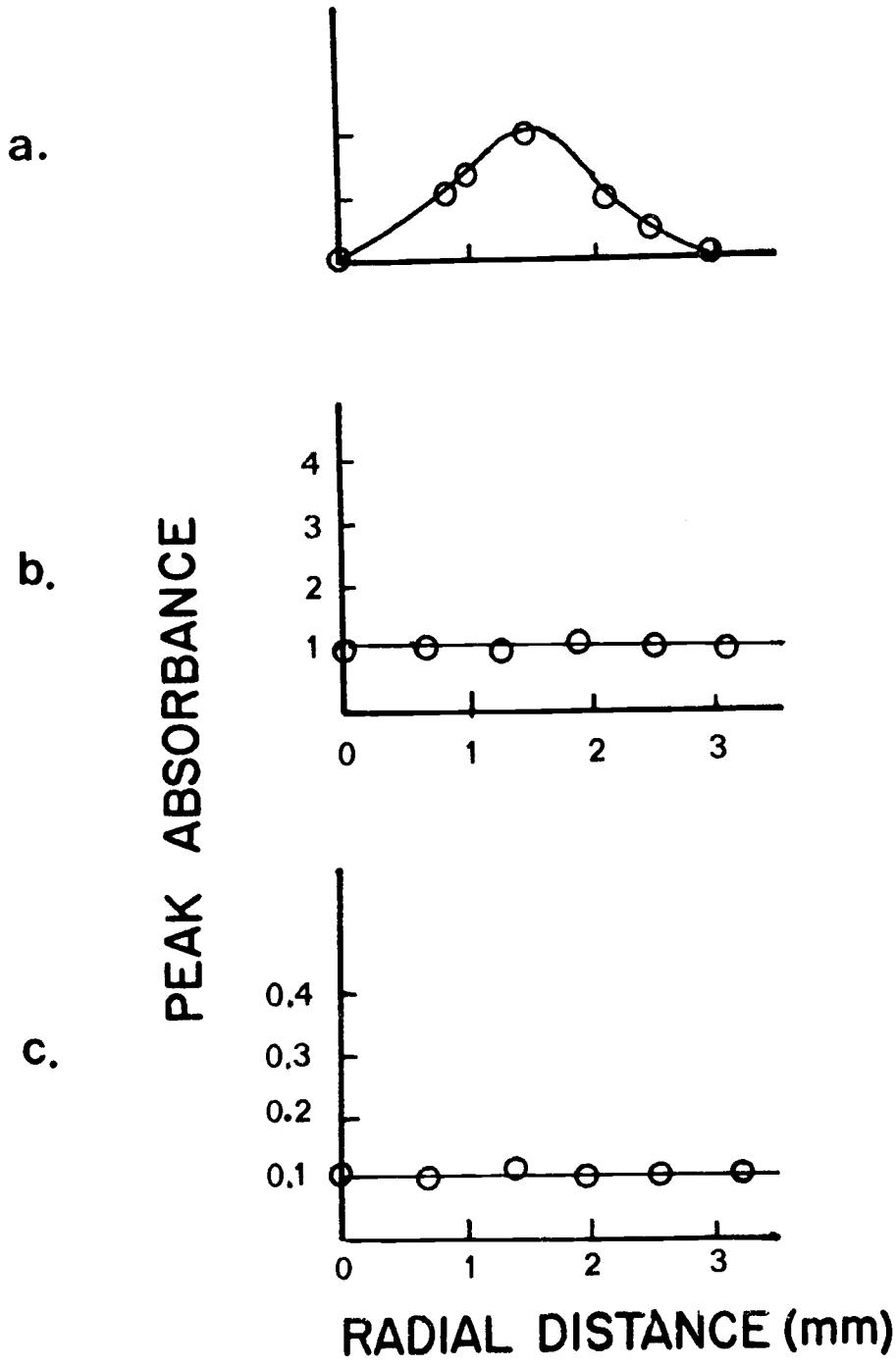

Figure 20. Peak absorbance versus radial distance from laser focus for Mn in NBS 461 steel. Mn(I) 402.1-nm line. Pressure Pressure = 0.2 torr. (a) Height = 0.0 mm. (b) Height = 1 mm. (c) Height = 2 mm.

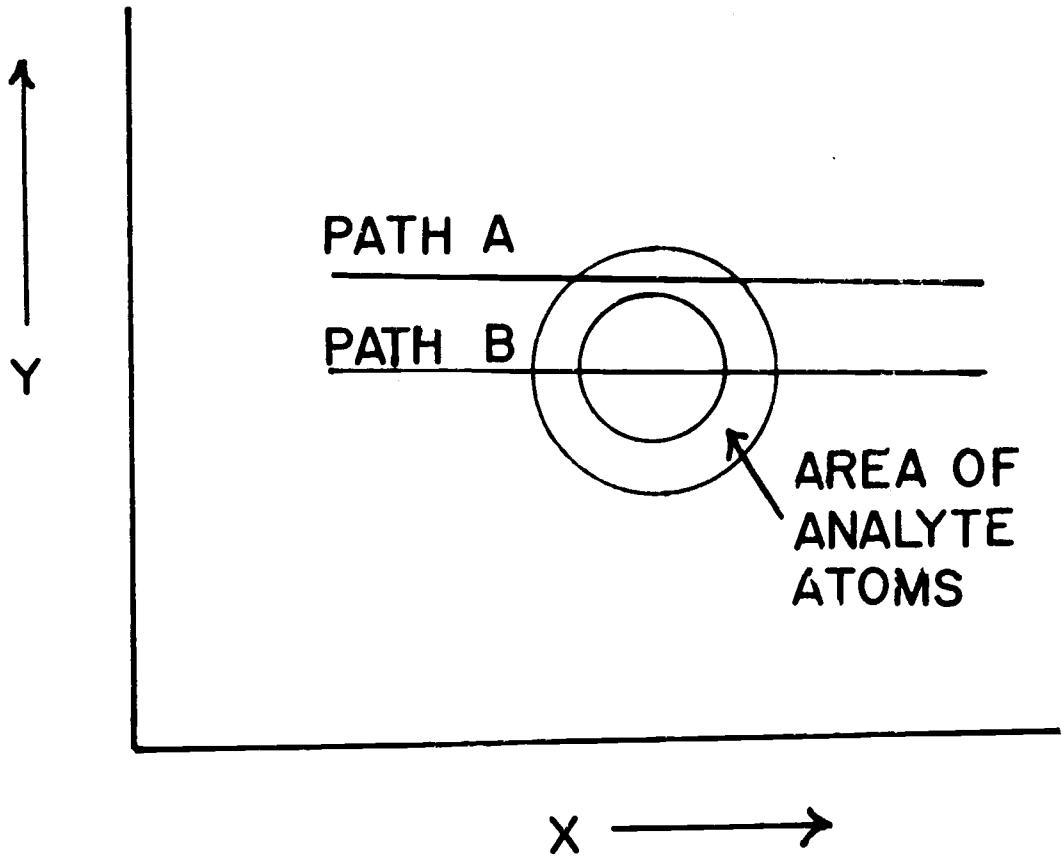

Figure 21. Cross sectional model for inhomogeneous plume.

path B. The net result should be a stronger absorbance signal of path A compared to path B.

The above model does not take into account the effect of the time constant delay of the detection system. Figure 22 shows the effect of the time constant upon the recovery time from the continuum emission spike. Figure 22a depicts the waveform produced by the detection system on a pure emission signal. Figure 22b represents the waveform of the atomic absorption signal if no emission spike was superimposed. Figure 22c shows the combined waveform of an emission spike superimposed on the absorption signal. Note that in Figure 22c there is a finite delay time before the signal crosses the 100%T line. If the duration of the absorption maximum occurred in this portion of the waveform its peak value would be severely distorted. If the free Mn atoms are no longer available to absorb the hollow cathode radiation during this time frame the absorption signal could be totally masked.

Figure 23 shows oscilloscope tracings of time resolved atomic absorption signals at 10 torr. Figure 23a is representative of absorption signals at 0.5 mm above the sample surface. A strong continuum emission peak is present. At a height of 2.5 mm, Figure 23b, the continuum peak superimposed on the hollow cathode pulses were not greater than the noise level. The duration was longer when compared to the absorption peaks at 0.5 mm. The absorption signal also reached a constant value minimum transmittance with a duration

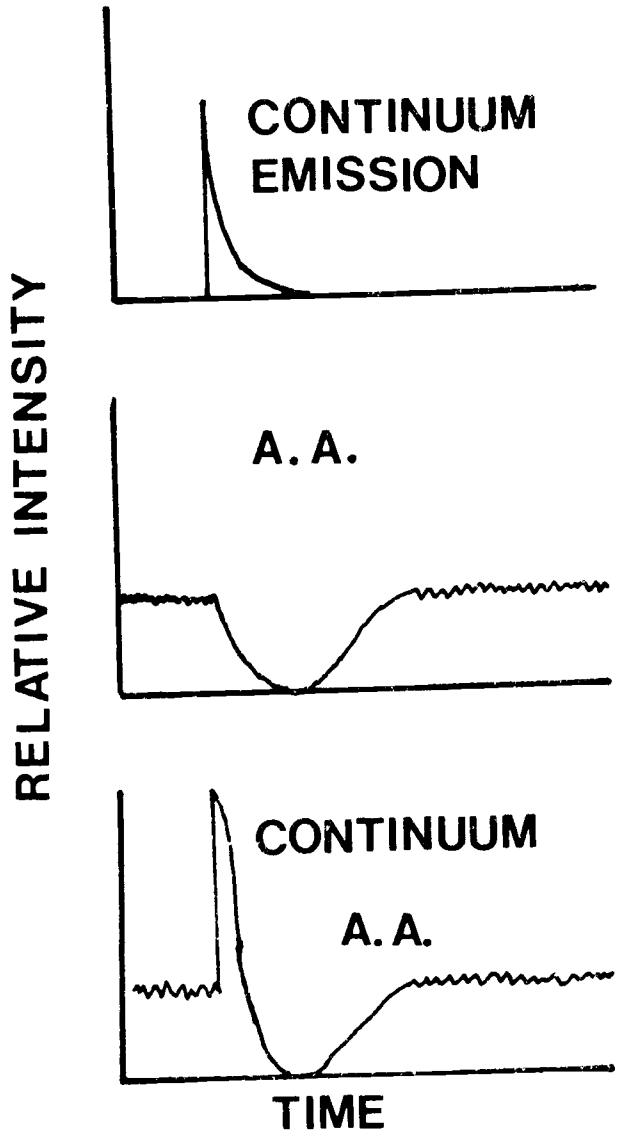

Figure 22. Effect of continuum and atomic emission spike on atomic absorption signals.

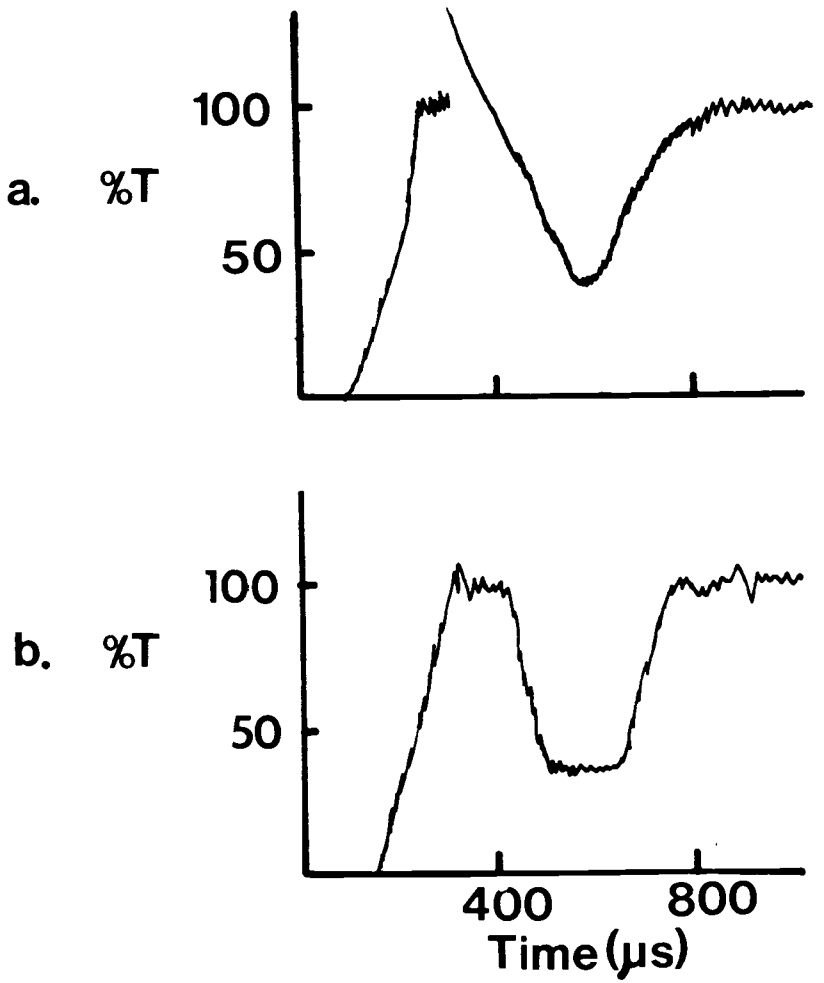

Figure 23. Oscilloscope tracings of time resolved Mn atomic absorption 403.1-nm. Pressure = 10 torr. (a)Height = 0.5 mm (b)Height = 2.5 mm

of 100 μs. At a height of 0.5 mm the transmittance never reached a constant minimum value. It is apparent from the data that the plume at low pressure is homogeneous if the point of observation is greater than 2 mm above the sample surface. It appears that the vigorous dynamic conditions present in the formation of the plume rapidly damp out in the time that it takes the atomic absorption signals to reach their maximum values.

Spatial Distribution of Peak Absorbance of Atomic Absorption Signals at Atmospheric Pressure

Spatially resolved measurements were also performed with the sample at atmospheric pressure. Figure 24 shows the radial distributions of the maximum atomic absorption signal at different heights above the sample surface. It is interesting to note that at a height of 0.5 mm, Figure 24b, no absorption was detected directly above the sample surface. At this height, the absorption was present away from the laser axis and reached a maximum value between 1-2 mm away from the laser axis. At a height of 2 mm above the sample, Figure 24c, absorption on the laser axis reappeared but decreased to the noise level at a distance of 1.5 mm away from the laser axis.

Figure 25 summarizes the data obtained along the vertical axis described by the incident laser beam. As noted earlier, the atomic absorption signal disappears at 0.5 mm above the sample. Absorption

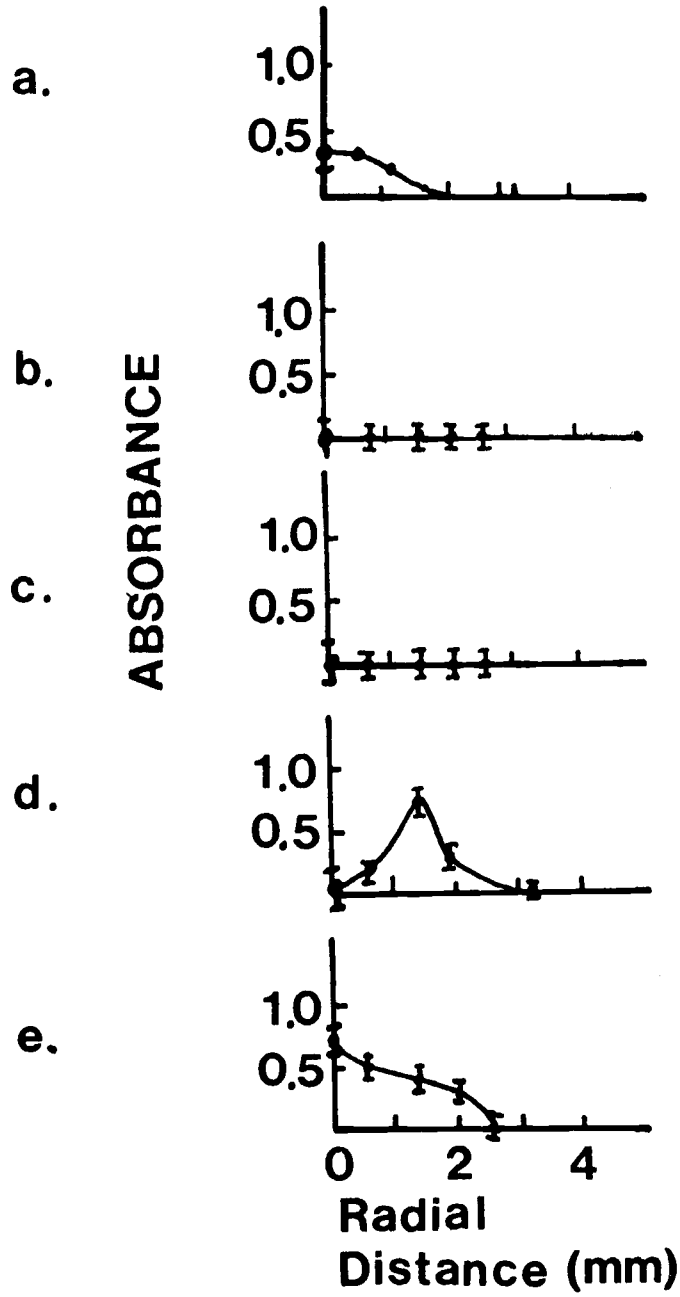

atmos. press

Figure 24. Peak absorbance vs radial distance for Mn(I) 403.1-nm atomic absorption at various heights. Pressure: atmospheric. (a) Height = 0.0 mm. (b) Height = 0.5 mm. (c) Height = 1.0 mm. (d) Height = 1.5 nm. (e) Height = 2.0 mm.

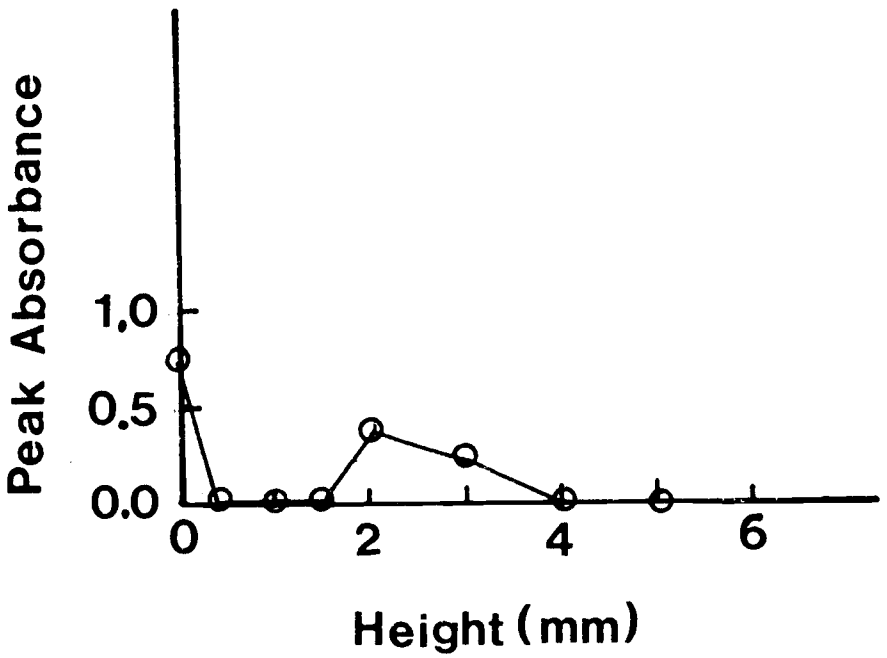

Figure 25. Peak absorbance vs. height directly above the laser focal spot at atmospheric pressure. Sample was NBS 461. Analyte was Mn 403.1-nm.

reappears at a height of approximately 2 mm above the surface and disappears into the noise level at a height of 4 mm above the sample surface.

The spatial distribution of the maximum atomic absorption signals may be distorted by the presence of the continuum emission present at atmospheric pressure. The apparent inhomogeneity of the plume at atmospheric pressure may be due to a time constant limitation of the readout system. For a simple RC decay, four time constants are required before the signal is diminished to 2% of its peak value. For the atomic absorption instrumentation this presents a dead time of approximately 60 μs. It is possible that the free atoms are no longer available for atomic absorption during this time frame.

Figure 25 shows representative oscilloscope tracings of the atomic absorption signal at various heights above the sample surface at atmospheric pressure. At a height of 0.5 mm above the sample, Figure 26b, there was a time span of 50-60 μs before the trace returned to the steady state hollow cathode signal before the laser fired. During this time interval the absorption of the hollow cathode radiation by the plume could have been masked because of the slewing conditions of the detection system. As the observation point is raised above the sample surface the delay time before the trace reaches the reference hollow cathode intensity decreases. Assuming a first order exponential decay, this delay time can be related to the peak

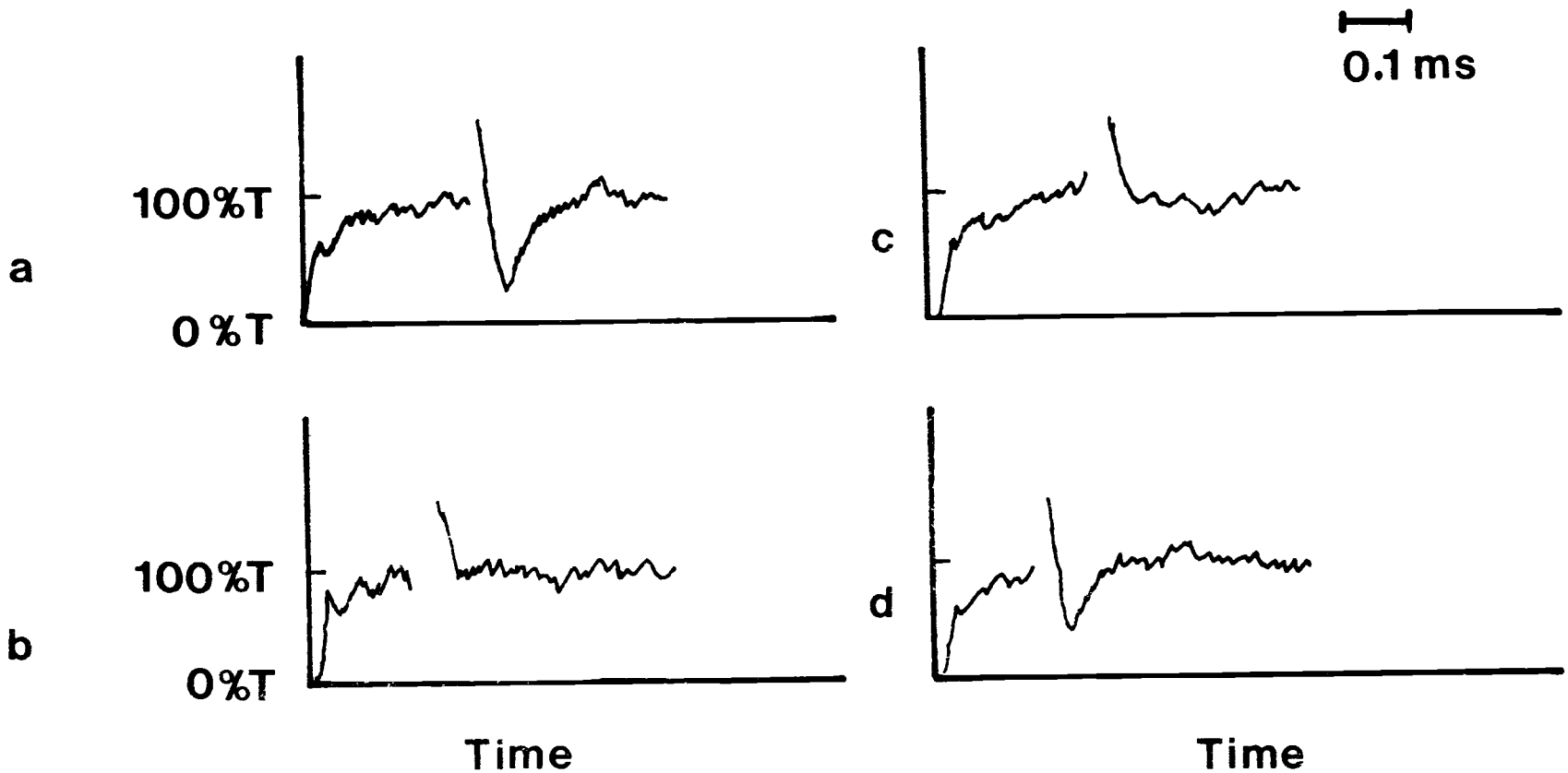

Figure 26. Representative oscilloscope tracings of Mn 403.1-nm atomic absorption in NBS 461 at various heights. Pressure = atmospheric. (a) Height = 0.0 mm. (b) Height = 0.5 mm. (c) Height = 1 mm. (d) Height = 2 mm.

value of the continuum spike superimposed on the hollow cathode pulse. The greater the delay time the greater the peak intensity of the continuum. As the observation point is raised above the sample surface the delay time is reduced indicating that the magnitude of the continuum decreases.

An interesting point evident in Figure 26 is that at the sample surface, Figure 26a, the magnitude of the continuum seems to be smaller than at a height of 0.5 mm above the sample surface. This may be further evidence for the existance of a radiation support shock wave discussed earlier (16).

To determine the spatial dependence of the temporal behavior of a major constituent of a metal sample, a pure copper target was substituted for the NBS 461 steel sample. Figure 27 shows the oscilloscope tracings of atomic absorption signals for the Cu(I) 324.7-nm line at atmospheric pressure. At a height of 1 mm above the sample, Figure 27b, there was a delay time of 50-60 μsec before the absorption signal crossed below the 100%T point of the hollow cathode intensity pulses. This delay time indicates again the presence of a large continuum peak superimposed on the hollow cathode pulses. As the observation point was raised above the sample surface the continuum again decreased at heights above 2 mm. At a height of 3 mm, Figure 27d, the continuum peak was completely absent.

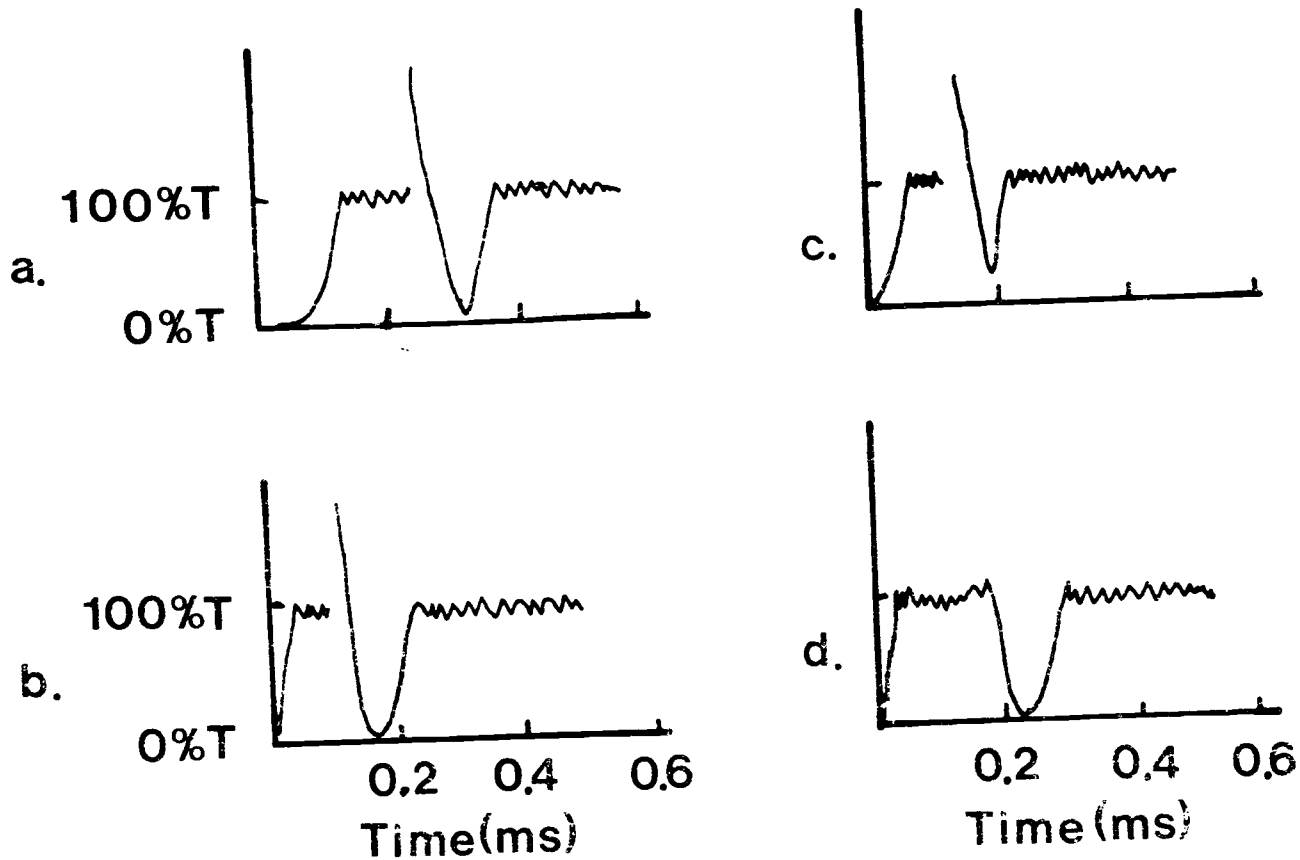

Figure 27. Oscilloscope tracings of Cu(I) 324.7-nm. Atomic absorption at various heights at atmospheric pressure. Sample is pure Cu. (a) Height = 0.0 mm. (b) Height = 1.0 mm. (c) Height = 2 mm. (d) Height = 3 mm.

Figure 28 shows oscilloscope tracings in which the observation point was lowered to the sample surface but moved to one side of the focal point of the laser beam. It appears that if the observation is moved away from the focal spot the magnitude of the continuum decreases rapidly. At a horizontal displacement of 12.7 mm, Figure 28b, the emission spike was not observed above the noise level. At a horizontal distance of 2 mm away from the focus, Figure 28d, no copper atomic absorption was detected above the noise level. This indicates that at atmospheric pressure the free Cu atoms are restricted to a much smaller volume than at lower pressure. The presence of the atmosphere seems to increase the rate of the depletion of the free atom population by chemical combination or thermal quenching caused by the surrounding atmosphere.

In summary, the results from the spatial distribution of the atomic absorption signals indicates that at low pressure the plume will offer greater utility for spectrochemical analysis than at high pressure. The free atom population was found to be distributed as far as 6 mm away from the focal spot of the laser. The increased time duration of the free atom population above the surface minimizes any distortion resulting from the response time of the detection system. These factors should yield a more homogeneous plume and better precision of the analytical results.

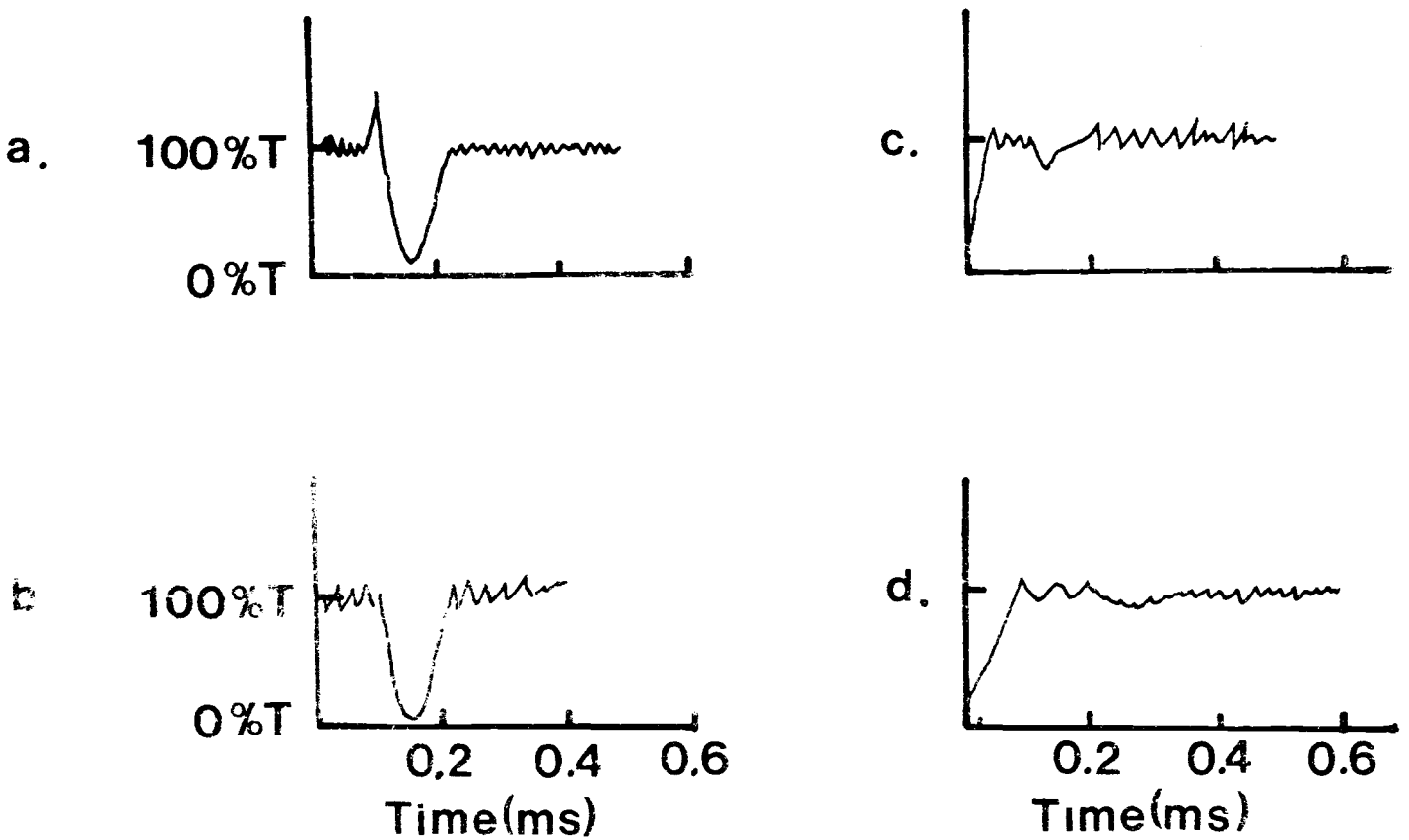

Figure 28. Oscilloscope tracings of Cu(I) 324.7-nm atomic absorption at various horizontal distances from the laser focus along the sample surface. Pressure = atmospheric. (a) Displacement = 0.7 mm. (b) Displacement = 1.27 mm. (c) Displacement = 1.5 mm. (d) Displacement = 1.0 mm.

At atmospheric pressure the spatial distribution of the free atoms was confined to a much smaller cross section. The magnitude of the absorption signal was not spatially constant. The interpretation of the results was further complicated by the increase in the level of the background emission spike that is superimposed on the hollow cathode signal. This coupled with the decrease in the residence time of the free atom population resulted in distortion of the signals by the time constant of the readout system.

Dependence of Minor Constituent Atomic Absorption Signals with Pressure

The effect of varying pressure above the sample surface upon the sensitivity and duration of the atomic absorption signals of the minor constituents of a sample was investigated. The experimental data was obtained from a NBS 461 reference steel sample. The minor constituent was Mn because of its demonstrated good precision at low pressure.

Figure 29 shows oscilloscope photographs of representative pressures. The general trend is that increases in the pressure decreased the time duration of the absorption signal. This is consistent with the time behavior of the atomic absorption signals of major constituents of metallic samples (20). The magnitude of the peak absorbance reaches a maximum value of 50 torr. The time jitter that

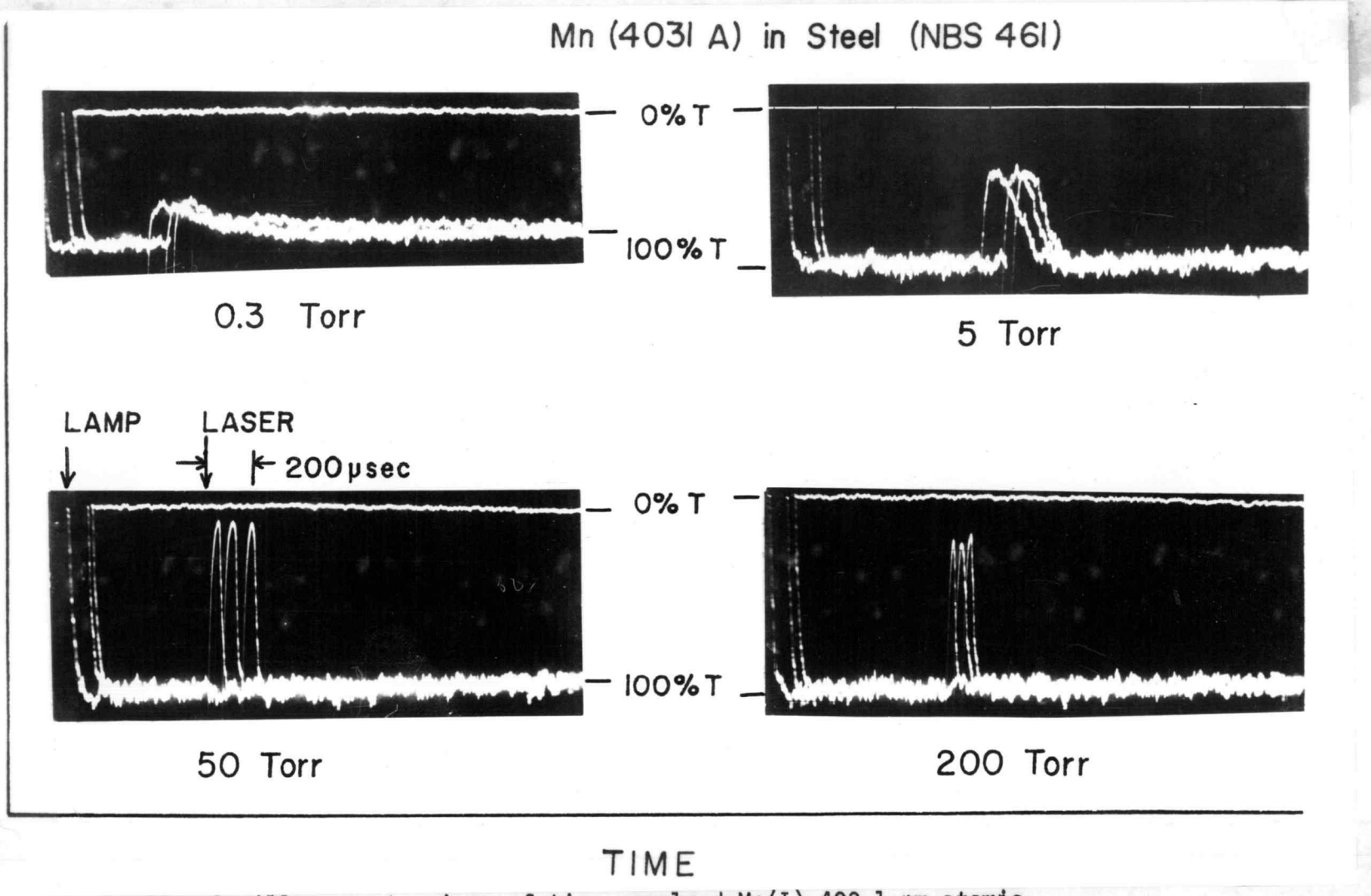

Figure 29. Oscilloscope tracings of time resolved Mn(I) 403.1-nm atomic absorption at various pressures. Sample height = 2 mm.

appears in the photographs is a result of the jitter time of the spark gap of the laser triggering mechanism.

The decrease of the peak absorbance at low pressure is perhaps due to the lower density of the free Mn atoms at low pressure. The spatial distribution of the atomic absorption measurements indicated that the expanded plume was observable over a much wider cross sectional area at low pressure than at high pressure. Thus for an equivalent amount of material vaporized, the smaller physical dimensions of the plume would result in a higher density of the analyte atoms.

A compensating effect is the increased path length of the plume at low pressure. This effect should increase the peak absorbance value. This effect is, however, overshadowed by the fact that the plume is expanding in all directions. The peak absorbance would increase if the plume was confined and only allowed to expand in a unidirectional manner along the observation axis. If the assumption is made that the plume is spherical in 3 dimensions, it can be readily seen that the atom density decreases as $1/R^3$, where R is the radius of the expanded plume. The magnitude of the absorbance is directly proportional to the path length. Since the absorbance is a product of the atom density and path length the net result would be a decrease in absorbance as a function of $1/R^2$.

Figure 30 summarizes the width of the absorption peak as a function of pressure. The decrease of the peak absorbance at pressures greater than 50 Torr may be due to a time constant limitation. From Figure 30 as the pressure is increased, the duration of the absorbance peak is continuously decreasing up to a pressure of 50 Torr. The width soon reaches a point in which the readout system cannot recover from the continuum emission spike fast enough to respond accurately to the peak absorption signal. The decrease in the residence time of the free atoms of Mn are due to the increased rate of interaction of the Mn atoms with the surrounding atmosphere. This would cause a rapid depletion in the free atom population over the sample. At low pressure, interaction between the free Mn atoms and the surrounding atmosphere will be less rapid, allowing the free atoms of Mn to remain for a longer period of time.

Duration of Ion Species in the Plume

The duration of ions in the plume was unknown. To study the time behavior of ionized species in the plume, a metallic sample of calcium was used as the sample target. Atomic absorption measurements were done using the Ca(I) 422.7-nm and Ca(II)-393.3 nm lines. The ion line was used for the study of ion population of the plume.

Figure 31 shows the time resolved atomic absorption at 0.2 torr. The duration of the free atoms of calcium was on the order of

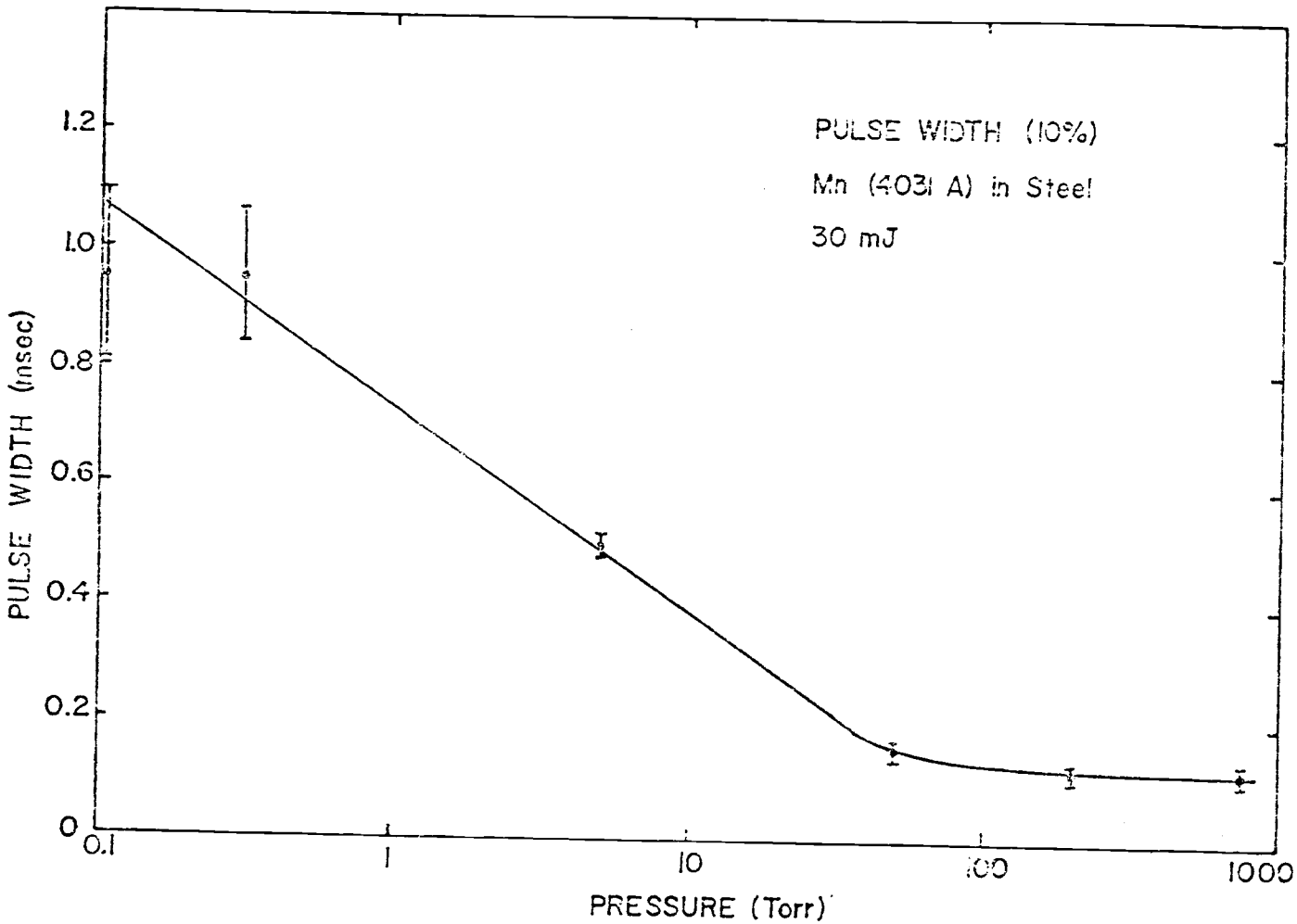

Figure 30. Absorption pulse width (ms) vs pressure for Mn atomic absorption in NBS 461 sample.

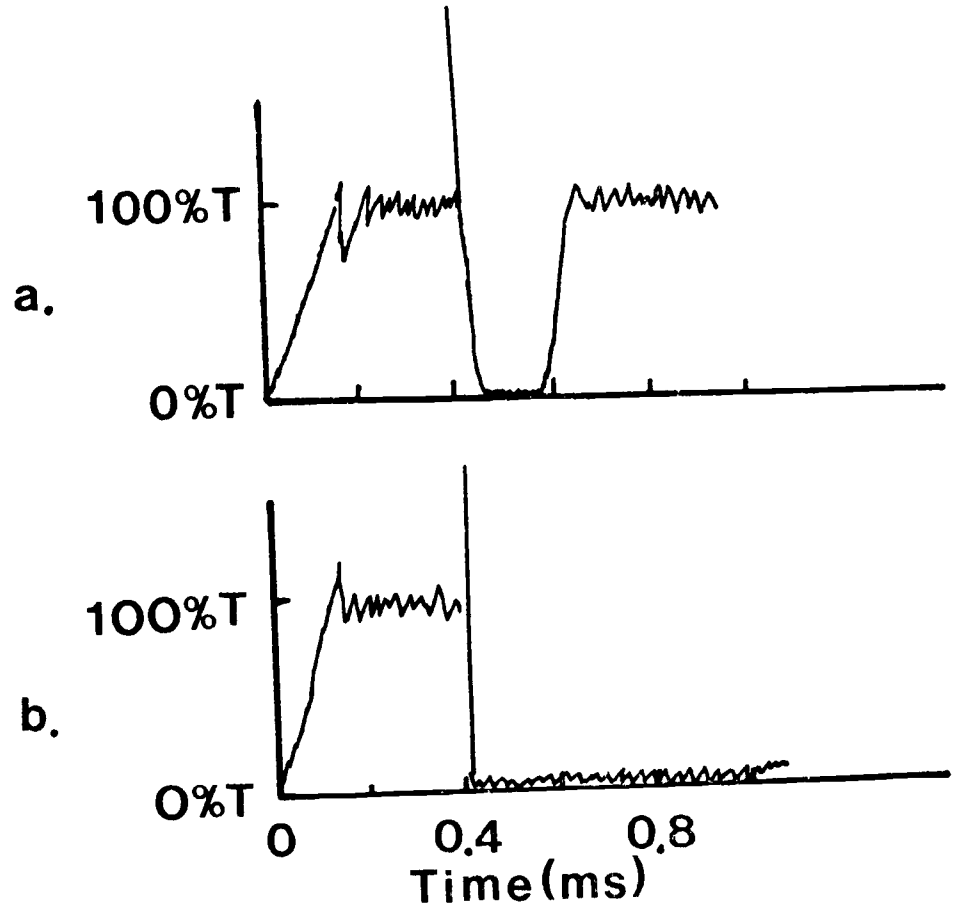

Figure 31. Calcium atomic absorption at 0.2 torr and at a height of 2 mm above the sample surface.
(a) Ca(II) 393.3-nm line. (b) Ca(I) 422.7-nm line.

milliseconds. This is consistent with the results of other pure metals (20). The duration of the absorption signal for the ion line was much shorter, 0.2 ms. This indicates that the calcium ion remains a comparatively short time compared to the free neutral atom population.

Figure 32 shows the duration of the absorption signals at atmospheric pressure. The duration of the 422.7-nm line was 150 μs. This is also consistent to that reported for other pure metal samples. The duration of the Ca ion line was so short that the response time of the readout system masked the true duration and magnitude of the absorption peak. This indicated a time duration of less than 60 μs.

It appears from this experiment that the recombination rate for ions appears to be rapid compared to the time required for the depletion of the free atom population, and that the recombination rate is slower at lower pressures as expected due to lower collisional rates caused by lower densities.

E. Measurements of Atomic Absorption Line Widths of the Plume

The work of Osten and Piepmeier (20) on the use of pulsed hollow cathode lamps for the measurement of laser plume atomic absorption has yielded nonlinear calibration curves in most instances.

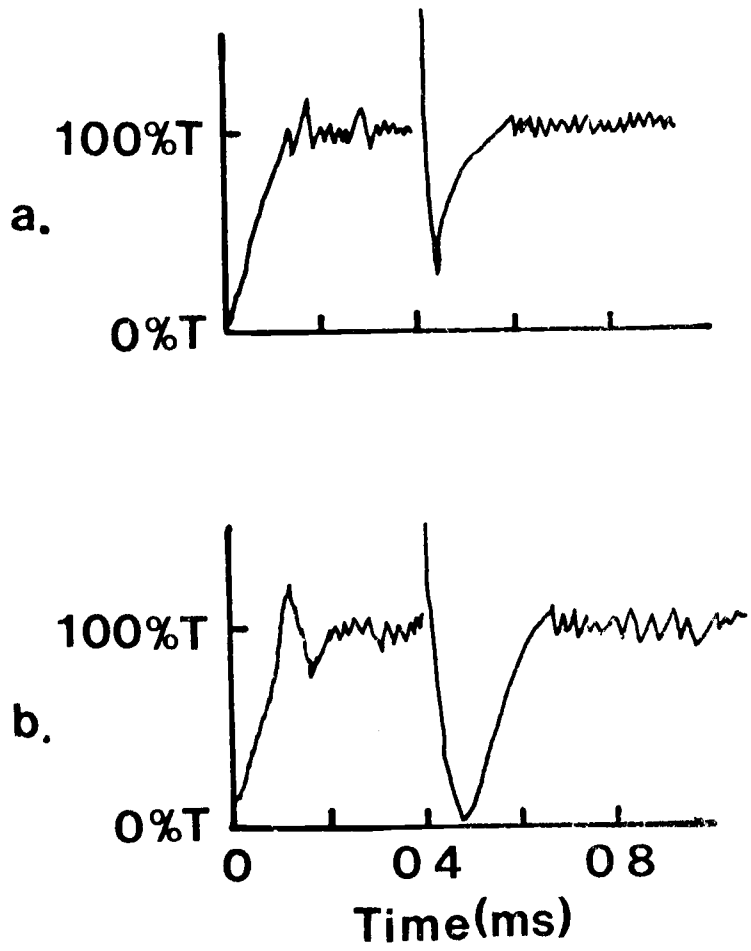

Figure 32. Calcium atomic absorption at atmospheric pressure and at a height of 2 mm above the sample surface. (a.) Ca(II) 393.3-nm line (b) Ca(I) 422.7-nm line

Osten's pulsing parameters were similar to those used by DeJong and Piepmeier (28). They have shown that significant self-reversal and line broadening occurs after the initial 21 μs of the hollow cathode pulse. The measured half widths were on the order of 200 mK. It is therefore conceivable that the basic assumption used in atomic absorption of the applicability of Beer's law may be invalid. The absorption width of the plume may no longer be wide in relationship to the line width of the primary source.

To resolve this, absorption profile measurements of the plume produced by the dye laser microprobe were made. Wagenaar, Pickford, and de Galan (29) have demonstrated the use of a Fabry Perot interferometer in conjunction with the high resolution monochromator to measure the absorption line width for Cu(I) at 324.7-nm in an air acetylene flame. They reported a Doppler width of 135 mK and a collisional width of 93 mK. The total width of each of the two major peaks in the line profile was approximately 200 mK. Since typical line widths of low current dc operated hollow cathodes have been shown to be 65-90 mK (38), the absorption line profile is therefore actually only approximately twice the width of the emission profile of a dc operated hollow cathode at low currents. For pulsed hollow cathodes the absorption width and emission profile of the hollow cathode are approximately the same.

For the low pressure plumes produced in this investigation the absorption line width may be much narrower than that observed in flames. This is because at low pressure it is often assumed that the contribution of collisional broadening is negligible compared to the magnitude of the Doppler half width (24, 25).

It is therefore desirable to know the exact width of the atomic absorption profiles in the low pressure plume to guide the selection of the types of primary sources that may be of utility for microprobe atomic absorption measurements. The pulsed hollow cathodes of the past (20) may not be useful for the observation of atomic absorption at low pressure because the width of the primary source may be much wider than the width of the absorbing atoms of the plume.

To measure the absorption profile, an extremely high resolution detection system is needed. This requirement is met with the use of a scanning Fabry perot interferometer in conjunction with a dispersive monochromator for order selection (24, 25, 26, 27, 28). Before discussing the results of the measurements, the determination of the extent of instrumental distortion caused by the interferometer will be considered.

Determination of the Instrument Function

The interferometer has a distorting effect upon the measured profile due to its imperfections. The measured profile is a

convolution of the true profile with the instrument function of the interferometer. In order to compensate for this distortion, the instrument function of the interferometer must be known.

The instrument function of a Fabry Perot interferometer has been measured in the past by observing a line source at very close mirror spacings (1 mm). This method assumed that the free spectral range (FSR) of the interferometer was sufficiently large that the spectral line width was infinitely narrow in relation to the FSR. The line profile observed was therefore essentially that of the instrument function.

This technique has the disadvantage that the instrument function at close mirror spacings may differ from that at wide spacings. For instance, if the light entering the interferometer was not exactly collimated, the effective aperture of the etalon will not be the same at different mirror spacings. This will cause the instrument profile to be different at the operating spacing compared to the profile measured at close mirror spacings.

Stacey (33) has suggested the use of a dual etalon system. The first etalon is used as an interference filter producing line profiles that are narrow compared to the FSR of the second etalon under test. The line profile produced by the second etalon is due entirely to the instrumental function of the second etalon.

In this laboratory a second etalon was not available. However, if a sufficiently narrow line could be found, the first etalon could be eliminated. A monoisotopic Hg^{198} electrodeless discharge lamp (EDL) was used at the reference line source. The 312.6-nm line (35,36) was chosen because of its proximity to the 324.7-nm Cu(I) line. Figure 33 shows the line profile produced by the interferometer. The full width at half maximum (FWHM) was 60 mK. The peaks appeared symmetrical and free of isotopic shifts.

The line profiles produced by a Fabry Perot interferometer are a convolution of the true spectral line profile with an instrument function. The distorting instrument function is often described as a convolution of a Gaussian function arising from the plates not being perfect flats and a Lorentz function resulting from the reflectivity of the plates being less than 100%. This reflection profile is more accurately described by the Airy function, which has a distinctly Lorentz character (24).

The function resulting from the convolution of a symmetrical Gaussian function and a symmetrical Lorentz function is a Voigt Profile. The mathematical equation describing this function is as follows:

$$H(a,v) = \frac{a}{\pi} \int_{-\infty}^{+\infty} \frac{e^{-y^2} dy}{(a^2)+(v-y)^2} \qquad (2)$$

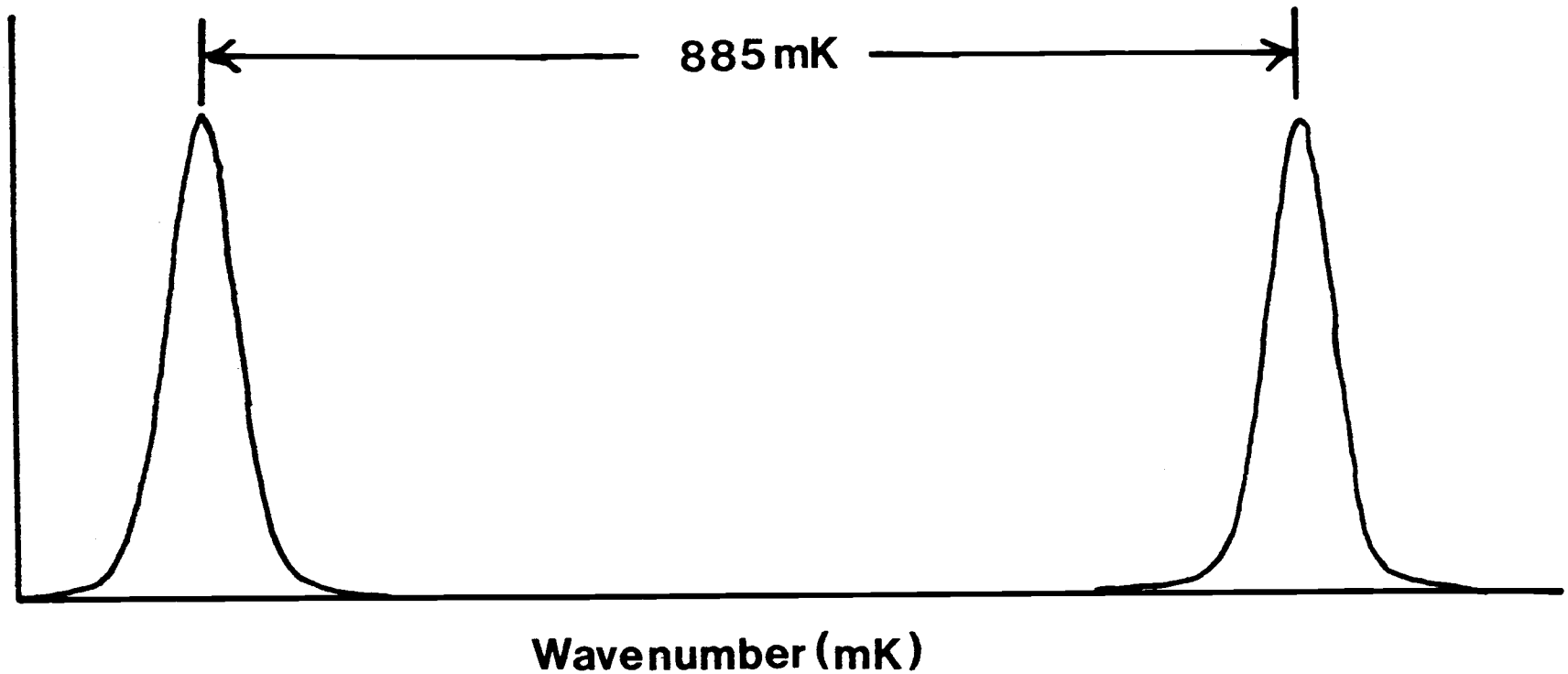

Figure 33. Experimental profile for Hg^{198}(I) 312.6-nm electrodeless discharge. FSR = 885 mK. Microwave power = 10 W.

where $v = (w-w^0)/\frac{1}{2}\Delta V'_G$. v is the distance from the line center (w_0) in units of $\frac{1}{2}\Delta V'_G$. $\Delta V'_G = (\ln 2)^{-1/2}\Delta V_G$ where ΔV_G is the Gaussian halfwidth if no Lorentz contribution were present. The variable a is equal to the ratio of $\Delta V_L/\Delta V'_G$ where ΔV_L is the Lorentz half width. The variable a is often referred to as the a parameter and is a measure of the relative amount of Lorentz broadening present in the profile.

Posener (37) has tabulated the shapes of different normalized Voigt profiles. The tables represent various families of Voigt functions with varying amounts of Lorentz and Gaussian character. By comparison of an experimental profile shape with a known Voigt profile, a graphical deconvolution is possible.

The data tables of Posener contain values of the widths of Voigt profile at various heights. The widths, k, are expressed in units of the measured width at half height (or simply halfwidth) of the experimental profile. The value of k of the width at half height is therefore unity. The ordinate values, h, along the peak are expressed in units of the maximum peak height, so that the value of h is unity at the center of the peak.

A curve fitting routine is done by minimizing the difference between the value and h for the experimental profile and a known Voigt profile. Once this is accomplished the value of the a parameter is obtained from the table and the profile can be deconvoluted for

the Gaussian half width and the Lorentzian half width.

Figure 34 shows the Hg(I) 312.6-nm line on an expanded scale. The lines represent the width of the experimental profile at various heights.

Table 1 contains a data summary of the line profile shown in Figure 34. The first column contains the normalized peak widths of the experimental Hg profile. The second column contains the normalized heights corresponding with the values of k. The next six columns are values from the tables published by Posener (37). The values of columns 3 through 8 are the differences between the experimental data and the tabulated values of h for Voigt profiles with different values of a. The numbers present at the bottom of the difference columns are the sum of the squares of the differences. The smaller the value the better the fit. The smallest absolute difference occurs for the value of $a = 0.18$. The confidence limit of the a parameter is less than 0.02, the tabulation interval used by Posener. Further interpolation to obtain a better estimate of a seemed unnecessary because of the small change in the sums of the squares of the differences from $a = 0.16$ to $a = 0.18$. The magnitude of the difference rapidly increases for values of the a parameter outside the region of 0.16-0.20.

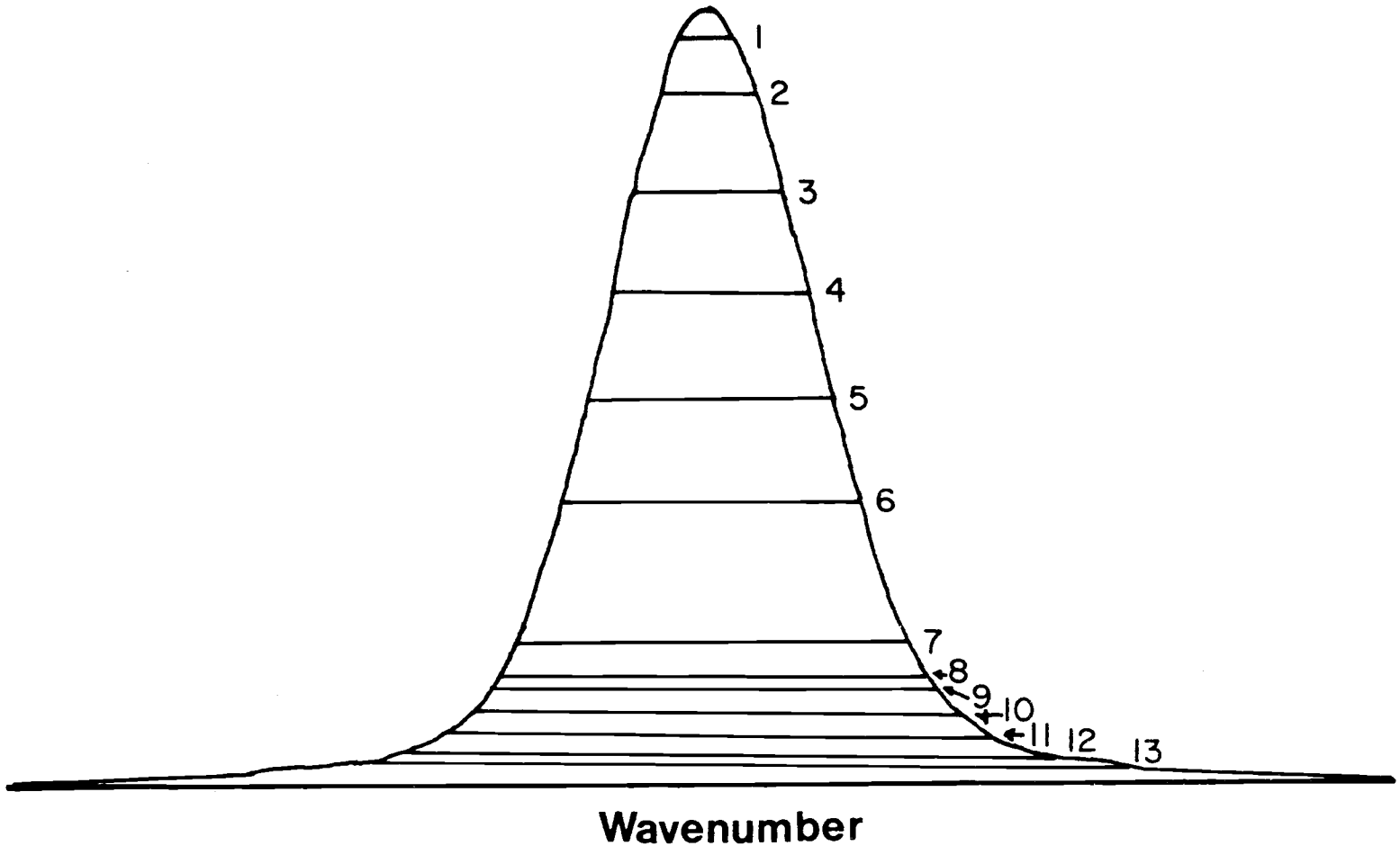

Figure 34. Hg^{198}(I) 312.6-nm profile. Half width = 60 mK.

Table 1. Tabulation of peak widths and peak heights of the experimental profile of Figure with known Voigt profiles.

k	h	Values of h											
		a = 0.14		a = 0.16		a = 0.18		a = 0.20		a = 0.22		a = 0.24	
0.2	0.969	0.972	+ 3	0.972	+ 3	0.972	+ 3	0.972	+ 3	0.972	+ 3	0.972	+ 3
0.4	0.896	0.893	- 6	0.893	- 3	0.893	- 3	0.892	- 4	0.892	- 4	0.892	- 4
0.6	0.766	0.776	+10	0.776	+10	0.776	+10	0.775	+ 9	0.775	+ 9	0.774	+ 8
0.8	0.640	0.639	- 1	0.639	- 1	0.638	- 2	0.638	- 2	0.638	- 2	0.638	- 2
1.0	0.500	0.500		0.500		0.500		0.500		0.500		0.500	
1.6	0.180	0.184	+ 4	0.186	+ 6	0.187	+ 7	0.189	+ 9	0.191	+11	0.193	+13
1.8	0.122	0.124	+ 2	0.126	+ 4	0.129	+ 7	0.131	+ 9	0.133	+11	0.135	+13
2.0	0.090	0.081	- 9	0.085	- 4	0.088	- 2	0.091	+ 1	0.093	+ 3	0.096	+ 6
2.2	0.061	0.056	- 5	0.059	- 3	0.061	+ 0	0.064	+ 3	0.066	+ 5	0.069	+ 8
2.6	0.036	0.028	- 8	0.031	- 5	0.033	- 3	0.035	- 1	0.037	+ 1	0.040	+ 4
3.0	0.024	0.017	- 7	0.019	- 5	0.021	- 3	0.023	- 1	0.024	+ 0	0.026	+ 2
3.6	0.014	0.010	+ 4	0.012	- 2	0.013	- 1	0.014	+ 0	0.015	+ 1	0.016	+ 2
Absolute difference			401		250		240		284		388		555

Once the value of the $\underline{a}$ parameter is known, the contribution from the Gaussian and Lorentzian function to the total profile can be calculated.

The Gaussian contribution is obtained from the tables by use of the $\underline{w}$ parameter. Posener has calculated the value of $\underline{w}$ for each value of $\underline{a}$. The value of $\underline{w}$ corresponds to the measured width of the profile in units of $\Delta V'_G$. The values of $\underline{w}$ for a value of $\underline{a} = 0.18$ is 0.933. Thus for an observed width of 60 mK

$$\Delta V'_G = \frac{60 \text{ mK}}{0.933} = 64 \text{ mK} \tag{3}$$

The actual Gaussian width can now be calculated

$$\Delta V_G = \Delta V'_G (\ln 2)^{\frac{1}{2}} = 54 \text{ mK} \tag{4}$$

The magnitude of the Lorentz contribution can now be calculated from the $\underline{a}$ parameter by use of equation:

$$\Delta V_L = (\underline{a})\Delta V'_G \tag{5}$$

$$\Delta V_L = (0.18)(64.4) = 12 \text{ mK} \tag{6}$$

If the assumption is made that the total Lorentz broadening is contributed from the Airy function of the interferometer, one obtains a value of 95.7% for the reflectivity of the plates. If one substitutes

the values of $\underline{a} = 0.16$ and $\underline{a} = 0.20$ the values of the reflectivity of the plates turns out to be 96.4% and 95.4% respectively. One basis for the assumption that the total Lorentz character of the profile is due entirely to the instrument function is that the total broadening of the emission profile from the Hg discharge lamp is due entirely to Doppler broadening since it is operating under low pressure. The experimental value of the reflectivity is lower than the manufacturers specification of 97.5%. A low value of the reflectivity may be due to the aging of the coatings. A reflectivity of 96% gives a reflection finesse of 76 which was essentially negligible compared to other finesse imperfections.

The Gaussian portion of the Voigt profile consists of the convolution of the Gaussian Doppler width of the line with the Gaussian portion of the instrument function. The instrumental contribution can be obtained by the subtraction of the Doppler line width from the total Gaussian half width.

$$\Delta V_{GI}^2 = (\Delta V_{GEXP})^2 - (\Delta V_G{}^{Hg^{198}})^2 \qquad (7)$$

where ΔV_{GEXP} is the measured experimental width and ΔV_{GHg}^{198} is the Doppler width for Hg at room temperature.

The Doppler half width for a Hg EDL operating at room temperature can be calculated as follows:

$$\Delta V_{GHg}^{198} = 7.16 \times 10^{-7} \sigma \sqrt{\frac{T}{198}} \qquad (8)$$

σ = Energy of the transition in mK.

$$\Delta V_{GHg}^{198} = 28 \text{ mk} \; @ \; T = 300°K \qquad (9)$$

therefore the Gaussian contribution to the instrument function is:

$$\Delta V_{GI}^{2} = (53)^2 - (28)^2 = (45 \text{ mK})^2 \qquad (10)$$

The total instrument function is therefore estimated to be a Voigt profile with $\underline{a} = 12/45 = 0.27$.

In obtaining the value of the instrument function it was assumed that the radiative Hg atoms were in translational equilibrium with the inert argon atoms and ions present in the EDL lamp. This assumption may not be valid because the effective translational temperature of the EDL in the microwave cavity may be higher than room temperature. The value of an estimated upper limit for the temperature of a EDL could be assumed to be that of a hollow cathode, 400°K. This would correspond to a Doppler half width of 32 mK for the Hg(I) 312.6-nm line. The increased value of the Doppler width would decrease the Gaussian instrument function by a corresponding amount.

Emission Profile of a Cu Hollow Cathode

The analyte chosen for the atomic absorption profile measurements was copper in lead foil. The analytical line was the Cu(I) 324.7-nm line. This particular line was chosen because of its high intensity during pulsed lamp operation. To insure that the interferometer was properly aligned, line profile scans of a Cu hollow cathode lamp were made. Figure 35 shows an experimental profile of a Westinghouse lamp #23042 operating at 5 mA dc. The 324.7-nm line was a doublet separated by 380 mK as reported by Brix (34). The measured half width was 95 mK for the larger peak. The peak ratio of the intensity of the major peak to the minor peak was 1.65.

A corrected half width for each line in the Cu 324.7-nm doublet can be determined in the following way. We assume as before that the lamp line profile is entirely Gaussian with a negligible Lorentz contribution. The Gaussian shape of the Doppler width of the lamp line combines with the Gaussian part of the instrument function to give the total Gaussian contribution to the measured profile. Since the Lorentzian and Gaussian contributions from the interferometer are known, the tables of Posener can be used with an iteration technique to estimate the amount of added Gaussian character (due to the line) required to obtain the measured half width of the experimental profile. The method is as follows.

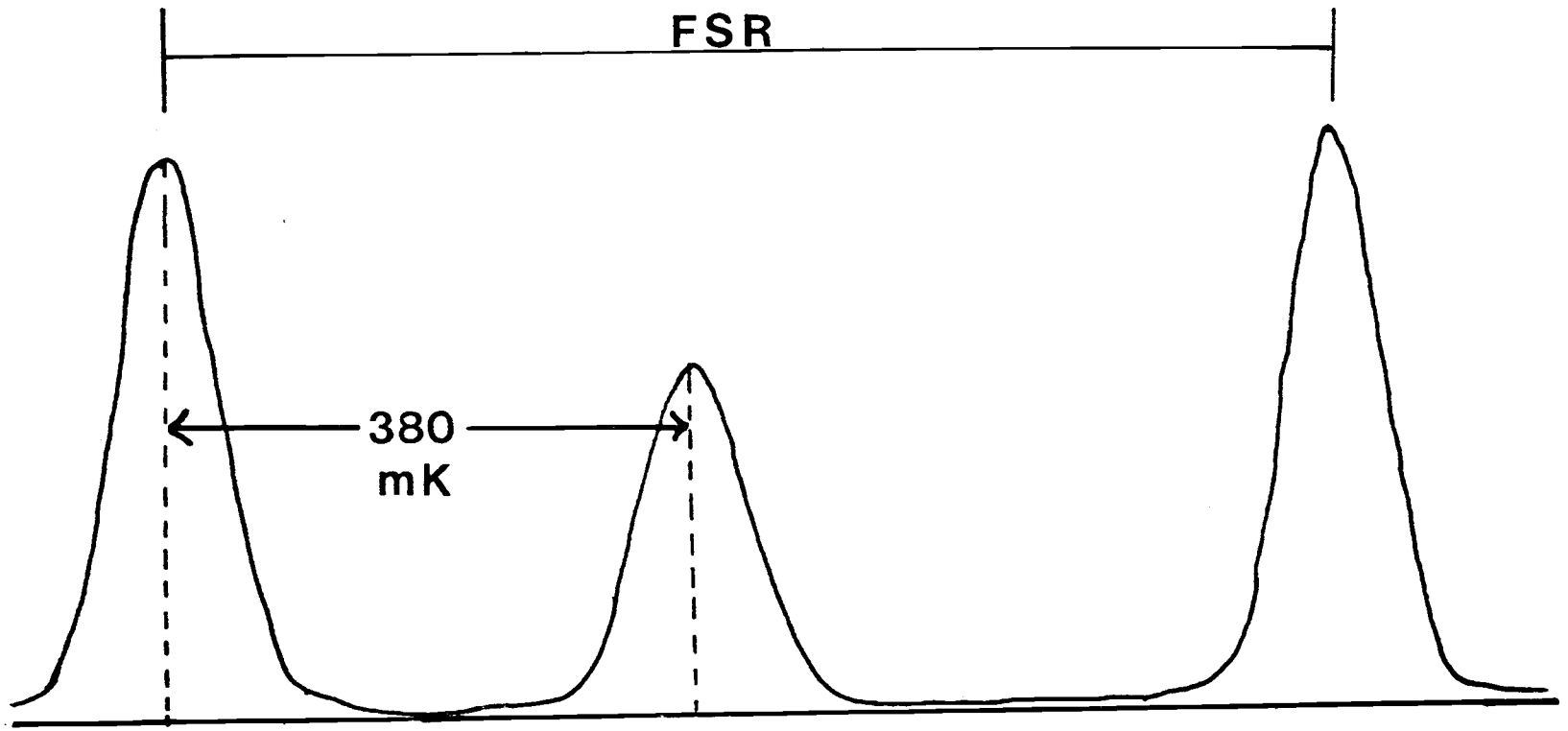

Figure 35. Experimental profile of Cu(I) 324.7-nm emission from a dc hollow cathode lamp. FSR = 853 mK.

A value of $\underline{a}$ is assumed and its corresponding value of the $\underline{w}$ parameter is used to determine the Gaussian part of the experimental profile from the measured half width. The measured half width is then divided by the value of the assumed $\underline{w}$ parameter to yield a value of the Gaussian half width $\Delta V'_G$. A new $\underline{a}$ value is calculated from the ratio of the known Lorentz half width (12 mK) to the value of $\Delta V'_G$. The proper value of the $\underline{w}$ parameter is determined by calculating the value of the $\underline{a}$ parameter. If agreement between the calculated $\underline{a}$ parameter and the assumed $\underline{a}$ parameter and the $\underline{w}$ parameter is not obtained the wrong choice was made. Another value of $\underline{a}$ and its corresponding $\underline{w}$ are chosen and the process is repeated.

For the experimental Cu profile of Figure 34 the measured half width was 95 mK. The best correlation from the estimated $\underline{w}$ parameter and $\underline{a}$ parameter was obtained for a value of $\underline{w} = 0.898$ and $\underline{a} = 0.12$. This combination of parameters yielded a Gaussian half width of the profile of 88 mK. Removal of the Gaussian contribution of the instrument function yielded a value of 76 mK for the Doppler width of the Cu hollow cathode profile.

For Cu hollow cathodes under normal low current conditions, Doppler half widths on the order of 60 mK are expected. The value of 76 mK obtained in this investigation is quite high, indicating a high source temperature. This was the cause of some concern.

Wagenaar and de Galan (38) have measured the line profile emitted from a Varian Cu hollow cathode. Corrected half width of 71 mK @ 5 mA was obtained for the major peak. The peak ratio of the minor to major peak was 1.67. At a lower current of 2 mA a corrected half width of 60 mK and a peak ratio of 1.87 was obtained. The measured half width at 2 mA corresponds to a Doppler temperature of 400°K. This temperature corresponds closely with the source temperature observed for other hollow cathode lamps. Since the peak ratio of the experimental profile of this investigation was lower than 1.87, a significant amount of self-absorption may be present yielding a half width that is wider than the actual Doppler half width.

Other authors have reported high Doppler half widths for other hollow cathode lamps. Kreye (39) has reported the Doppler temperature of a Au hollow cathode to be 1600°K by measurement of the line profile of the Au(I) 312.3-nm line. Measurements of the Argon ion lines of the same hollow cathode discharge yielded temperatures of 400-600°K. Kreye's explanation for this difference was based on the large value of the 312.3-nm transition probability. Kreye calculated the mean interval of 25 ns between excitation and emission.

Kreye also states that for a hollow cathode lamp with an internal pressure of 6 torr and a translational temperature of 400°K, the mean interval of the collisions between Au(I)-Ar(I) atoms is approximately 29 ns. It is therefore possible for a Au(I) atom to emit

before it has had a chance to collide with the surrounding Ar(I) atoms.

Stuart and Wehner (40, 41) have measured the energy distribution of sputtered Cu atoms by various sputtering agents. They have found for a filler gas of Kr, Cu atoms are ejected off the cathode surface with an average energy of 4 eV. This was for a hollow cathode potential of 150 V which is common among hollow cathodes used for analytical purposes. For a neon filled lamp, the average energy of sputtered atoms is approximately 0.1-0.3 eV. If one assumes the lower limit of 0.1 eV, an effective temperature can be calculated as follows:

$$T = \frac{(0.1\ \text{eV})(1.69 \times 10^{-19}\ \text{J(eV)})^{-1}}{1.388 \times 10^{-23}\ \text{J(K)}^{-1}} \qquad (11)$$

$$T \approx 1200°\text{K}$$

If the sputtered atoms possess a higher energy and hence a higher translational temperature than the filler gas, and if the transition probability is sufficiently high, the sputtered atoms can emit radiation with a Doppler width that is significantly higher than predicted from the measurement of the surrounding gas.

The transition probability for Cu(I) is 4.8×10^{8}/sec (42). The transition probability for the Au(I) 312.3-nm line is 1.9×10^{8}/sec. The mean time for a fast sputtered Cu atom to undergo spontaneous emission before it is slowed by a collision is even shorter than for Au.

Therefore, the line broadening due to high Doppler width resulting from a nonequilibrium condition should be more pronounced.

The above arguments assumed that the hyperfine structure of the copper 324.7-nm line had no effect on the line width. Stuart and Wehner (41) could not use the Cu(I) 324.7-nm line to verify their velocity measurements by determining the Doppler shifts produced by observing atoms with velocities normal and parallel to the observation axis of a Fabry Perot interferometer. They claim that the hyperfine structures consisting of 12 components split over a range of 0.05 Å became unresolvable at the high sputtering potentials they used.

The exact cause of the artifically high Doppler width observed in this investigation may be a simple case of self-absorption resulting in a decrease in the peak ratio of the major and minor component of the 324.7-nm Cu(I) transition. It is more likely a combination of both self-absorption, and a non thermal equilibrium condition in which the radiating atoms on the hollow cathode discharge may possess a much higher translational energy than the temperature of the cathode would indicate.

Consideration of Pulsing Parameters of Hollow Cathodes for Absorption Line Profile Measurements

Measurement of atomic absorption of atoms in the laser plume requires a light source with special characteristics. Due to the transitory nature of the plume the response time of the detection system must be fast. Thus, shot noise will be a significant source of variance in the analytical signal. Therefore, to maximize the signal to noise ratio, the intensity of the source must be high. Another consideration is that the physical characteristics of the laser plume are changing constantly throughout its duration. To attach any physical meaning to the absorption line profile measurements, the source duration should be such that the plume looks stationary. The above requirement suggests the use of a pulsed source to gain intensity and also to possess a short duration in relation to changes occurring during the lifetime of the plume. This second requirement indicates that the shortest pulse duration should be used that is consistent with adequate signal to noise ratio.

The spectral characteristics of the lamp are also important. The ideal light source for the measurement of the absorption line profiles would have a rectangular spectral profile in which the intensity of the source was constant over the entire width of the absorption spectral profile. Wagenaar, Pickford and de Galan (29) used a continuum source with a high resolution monochromator to approximate this.

The response time of their system was on the order of tens of seconds. Due to the transitory nature of the plume and the resolution of the monochromator available, this approach was not acceptable.

A broadened spectral profile obtained from a pulse hollow cathode lamp should be an adequate light source for atomic absorption in the laser plume. The pulsing parameters can be varied to yield an unreversed line profile. The duration of the lamp can be made to be sufficiently short such that the absorption of the plume will be reasonably constant during the duration of the pulse. The use of a hollow cathode also eliminated the need of a ultra-high resolution monochromator as an order selector for the Fabry Perot. For a continuum source, the bandwidth of the monochromator must be less than the free spectral range of the interferometer. If a line source such as a hollow cathode is used, the resolution of the monochromator need only separate one emission line from another.

In summary, to measure the absorption line profile in the laser plume, the spectral profile of the lamp should be broader than the absorption profile but narrower than the FSR of the interferometer. The lamp profile should be unreversed since the location of the absorption peak of the plume will coincide approximately with the location of the self-reversal in the lamp profile. The pulse width should be as narrow as possible to minimize the variation in the plume during the measurement. Sufficient photons must be detected by the PMT

during a pulse to insure good signal to noise ratios.

Figure 36 shows the emission line profile of a pulsed Cu hollow cathode with a pulse duration of 200 μs. The peak current was 250 mA. The location of the Cu emission peaks from a dc operated lamp are at the plus signs. It is evident that extreme self-reversal is present and therefore this would be undesirable as a light source for the absorption profile measurements. The presence of the self-reversal is consistent with the work of DeJong and Piepmeier (28).

Figure 37 shows a line profile of a pulse duration of 400 μs with a pulse current of 750 mA. Although the S/N ratio is good, the peaks are extremely broad with strong self-reversal. Order overlap from one FSR to another is also present.

Figure 38 shows a line profile with a pulse duration of 60 μs and a peak current of 500 mA. This profile represents the best compromise of a non self-reversed profile consistent with sufficient signal to noise ratio. As indicated above, increasing the pulse duration introduces self-reversal. Increasing the pulse current does not increase the integrated intensity, but the spectral profiles become broadened and overlap of the FSR occurs. Decreasing the pulse duration decreases the signal to noise ratio to an unacceptable level.

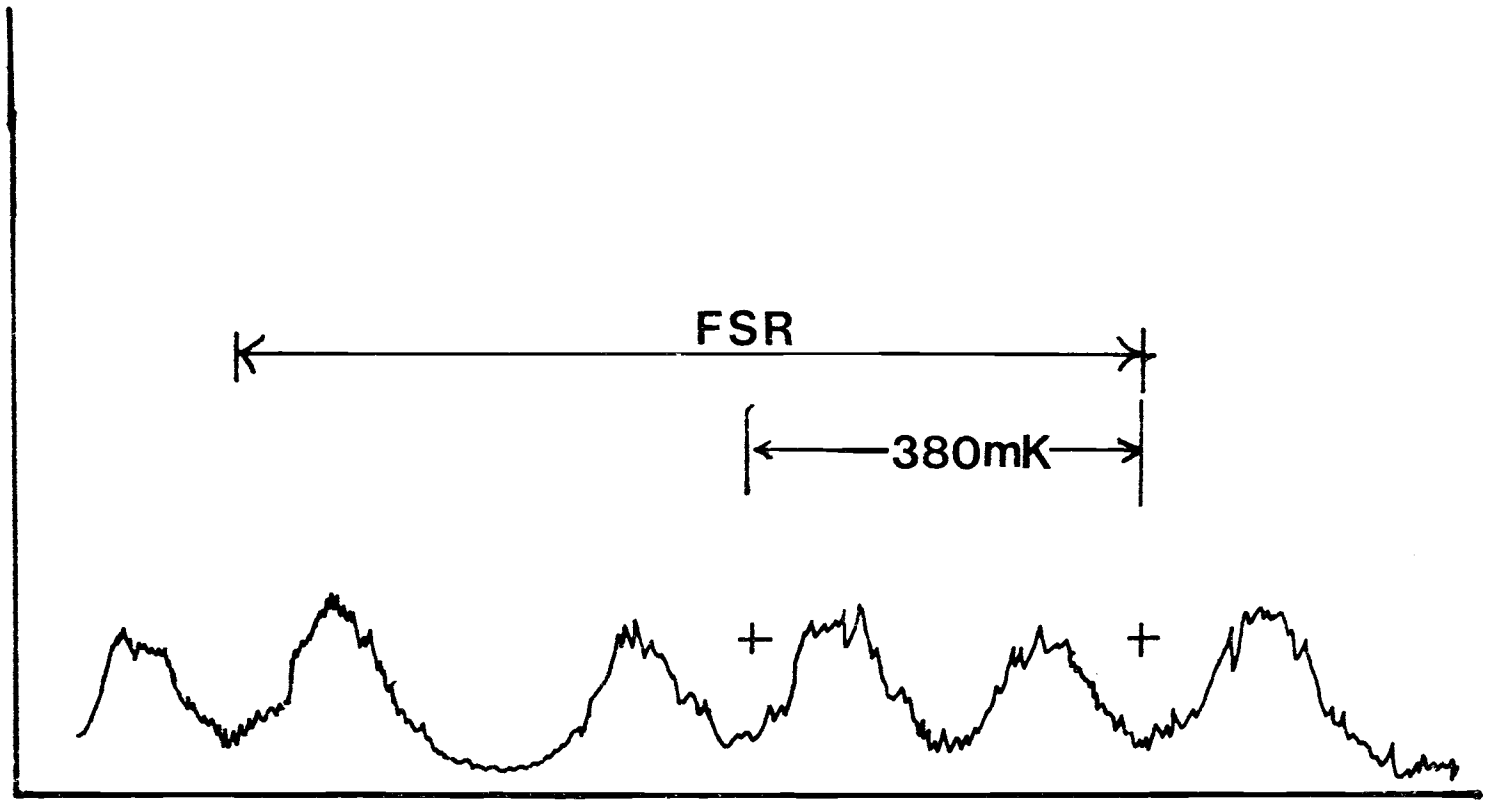

Figure 36. Emission profile of Cu(I) 324.7-nm emission from a pulsed hollow cathode lamp with a duration of 200 us and a pulse current of 250 mA.

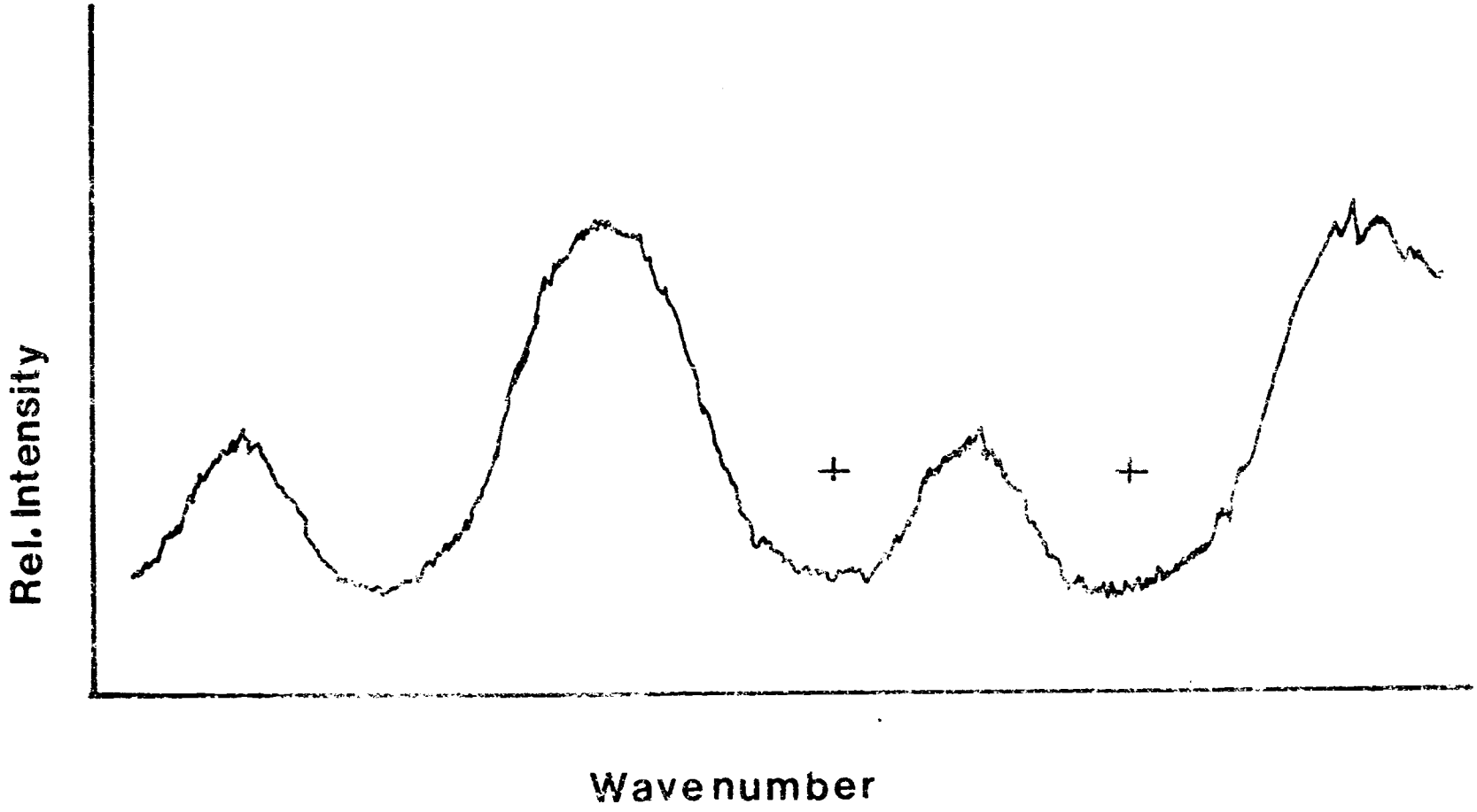

Figure 37. Emission profile of Cu(I) 324.7-nm emission from a pulsed hollow cathode lamp with a duration of 400 us and a pulse current of 750 mA.

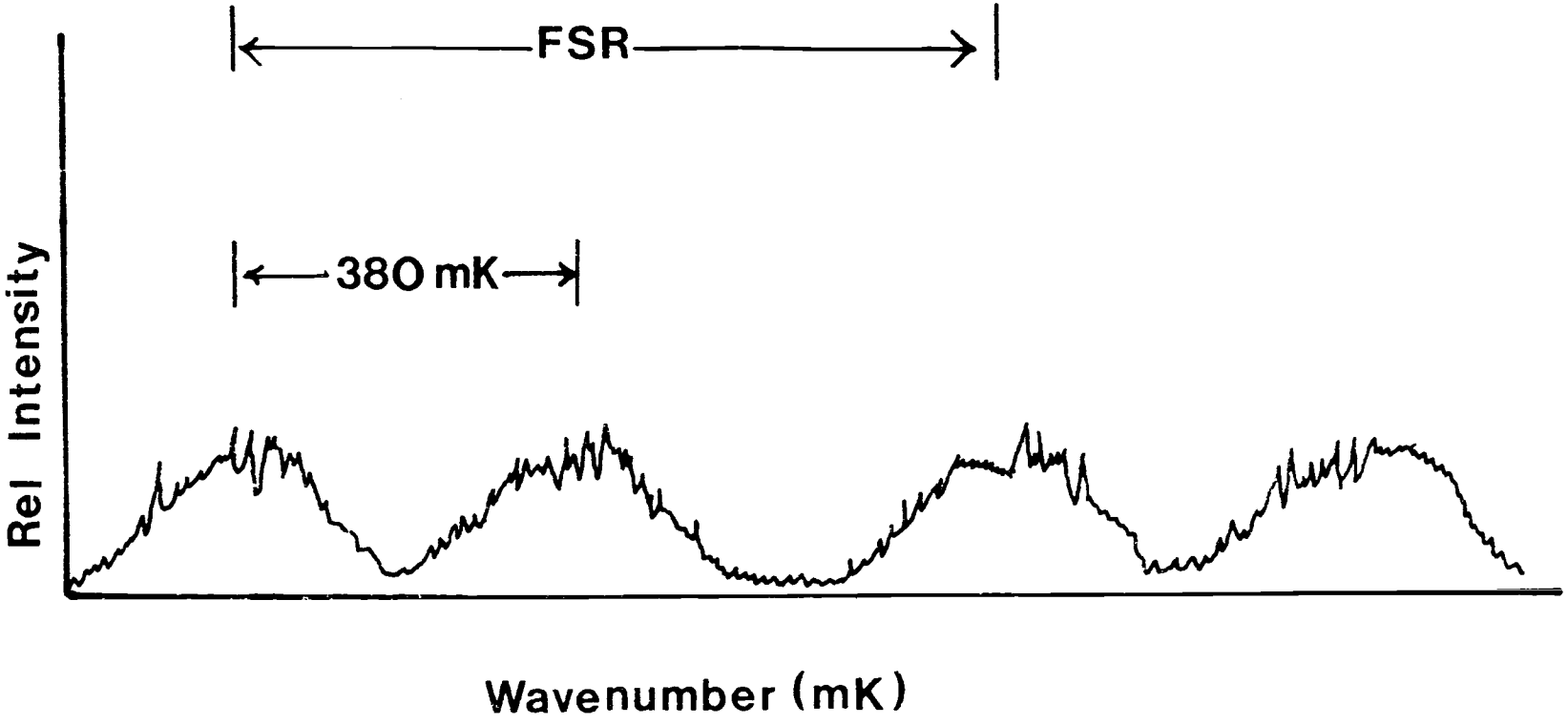

Figure 38. Emission profile of Cu(I) 324.7-nm emission from a pulsed hollow cathode lamp with a pulse duration of 60 us and a pulse current of 500 mA.

Experimental Absorption Line Measurements

The timing and control system allowed the laser to fire on every other hollow cathode pulse. This allowed almost simultaneous determination of the I_0 (100%T) curve (no laser plume) and the absorption curve I (laser fired), to reduce the influence of thermal drift of the interferometer.

Figure 39 shows experimental data from a typical profile run. Figure 39a is the emission profile from a dc operated Cu hollow cathode lamp. Figure 39b is the emission profile of a pulsed hollow cathode lamp with a duration of 60 μs and a pulse current of 500 mA. Figure 39c shows the absorption profile obtained with the laser firing on every other hollow cathode pulse. This profile represents the Cu absorption profile in the plume during the initial 60 μs after the laser has fired.

Figure 40 shows a plot of the absorbance calculated from the experimental data. The absorbance profile was obtained by manually passing a continuous line through the I_0 and I data points of the data in Figure 39c. The absorbance was calculated at each point along the profile and plotted. The upper curve, Figure 40, is a tracing of the line profile from a dc operated hollow cathode lamp. The measured half width of the absorption profile of Figure 40 was between 60-100 mK. The odd shape is probably due to the uncertainties of the

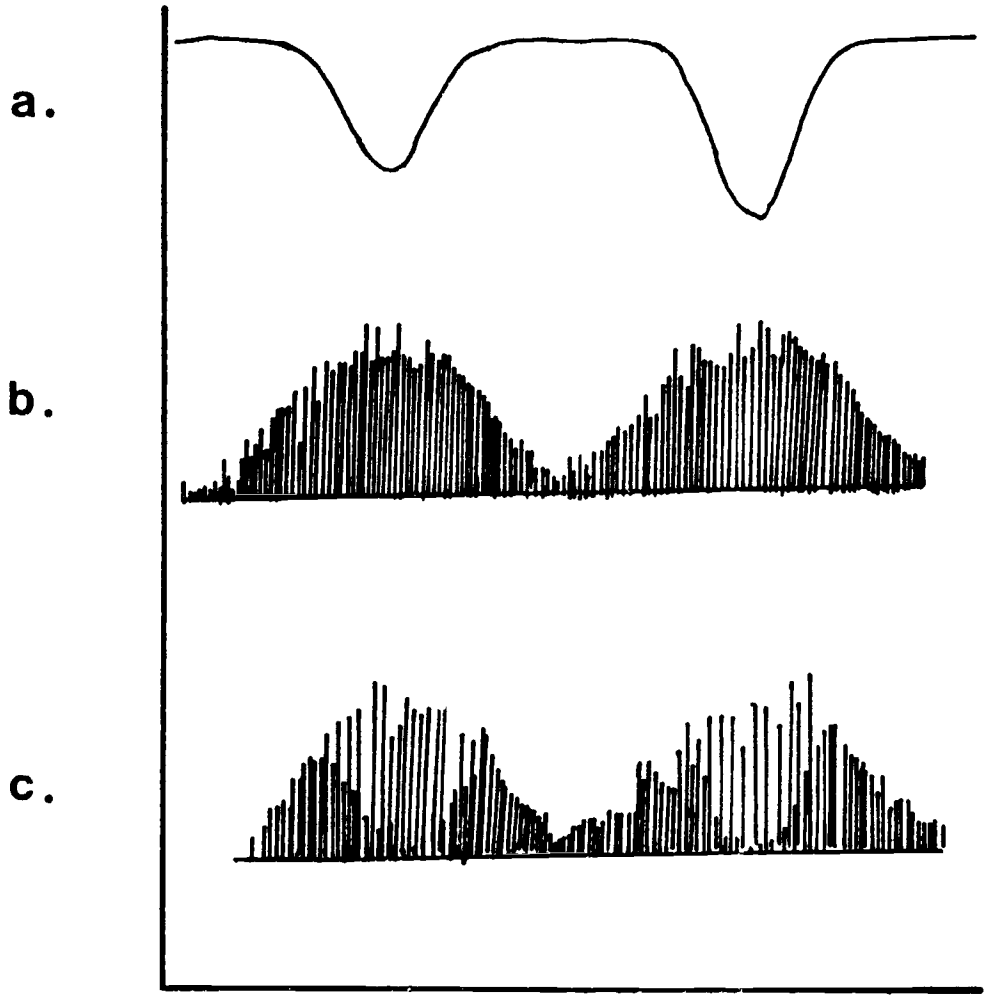

Figure 39. Experimental data of atomic absorption line profile measurements of Cu in Pb foil. Analyte line = Cu(I) 324.7-nm. Pressure = 1 torr.

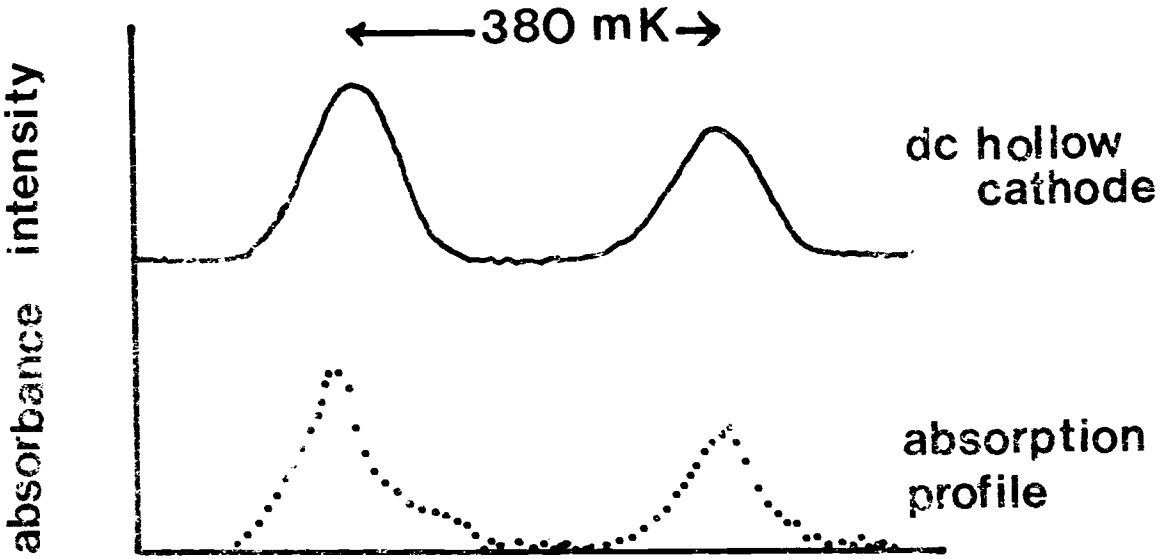

Figure 40. Absorption profile of Cu(I) 324.7-nm atomic absorption in a low pressure plume (1 torr). Sample was a Pb foil.

data points. From the data it appears that the width of the absorption profile at low pressure is quite narrow and approximates the width of a dc operated hollow cathode. Since it has been documented that typical operating temperatures of hollow cathodes are on the order of 400-600°K (25,26), the temperature of the plume, from the half width, is therefore less than approximately 1000°K at low pressure.

This temperature implies that the plume has undergone rapid cooling after the termination of the dye laser pulse. Typical temperatures of laser induced plasmas are on the order of 10,000°K during its initial formation.

It is also interesting to note that the width of the absorption profile is much narrower than the width of the line profiles from hollow cathode lamps commonly used in the past for the investigation of laser plume atomic absorption. The assumption that the absorption profile is infinitely wide compared to the width of the source appears to be invalid. The net result will be nonlinear calibration curves for the analyte and reduced sensitivity of the determination.

Figure 41 shows the experimental data obtained for the plume at 50 torr. The profile appears to be much broader at initial inspection. Conclusions must be guarded because the plume showed complete absorption in the region of the maximum peak absorption. The width of the source was also not wide compared to the width of the absorption profile, causing the exact behavior of the profile to be

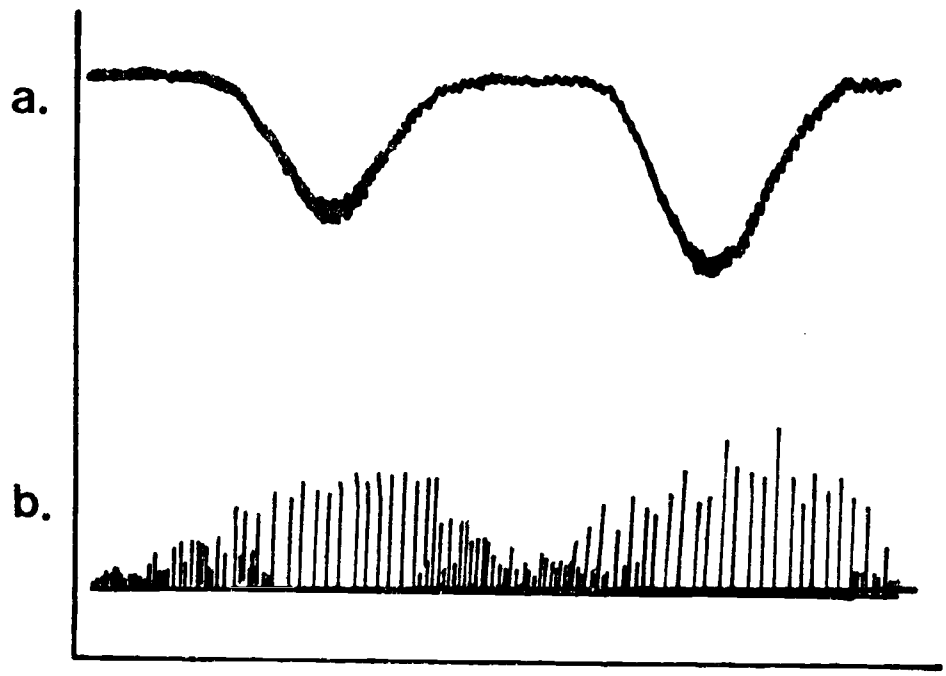

Figure 41. Absorption profile data for the Cu(I) 324.7-nm line at a pressure of 50 torr.

unknown in the wings. Another type of source such as a tunable laser would be helpful for future measurements of laser plume absorption profiles.

F. Estimates of the Contribution of Lorentz and Doppler Broadening to the Absorption Line Profile

The pressure dependence of the absorption half width discussed in Section IV-D may be explained by an increase in the collision half width as the pressure is increased. In this section estimates of the collisional half width calculated according to the Lorentz classical theory will be discussed.

The major contribution to the collisional half width of a spectral line in the uv or vis spectral band is the interaction of a radiating atom in a gaseous medium with unchanged atoms of other species in the surrounding atmosphere. The forces involved are Van der Waals interactions. The contribution of resonance broadening and quadratic stark broadening mechanisms were found to be negligible (21).

The half width due to collisional broadening can be calculated by use of the following equation resulting from classical Lorentz theory (24).

$$\Delta V_L = \frac{2}{\pi}\sigma_L^2 Nh \cdot 5.02 \times 10^{15}\ \text{cm}^{-1}\text{erg}^{-1}\sqrt{2\pi RT\left(\frac{1}{M_1}+\frac{1}{M_2}\right)} \qquad (12)$$

where

σ_L = collisional cross section

N = number density of perturbing atoms

M_1 = molecular weight of radiating atom

M_2 = molecular weight of perturbing atoms.

h = Planck's constant

Parsons and Windfordner have found that the values of σ_L, the collisional cross section, lie between 2.0×10^{-15} and 1×10^{-14} cm^2 (43). A more refined value of σ_L for Cu can be calculated by use of the recently reported absorption profile measured for Cu in an air acetylene flame (29). A value of 93 mK was obtained for the collisional half width for the Cu(I) 324.7-nm line. By solving Equation 12 for σ_L and substituting 93 mK for the Lorentz or collisional half width and value of $\sigma_L = 6.3 \times 10^{-15}$ cm^2 was calculated. The temperature of the air acetylene flame was assumed to be 2200°C. The number density $\underline{N}$ was calculated from the ideal gas law. The pressure of the flame was assumed to be atmospheric. The average molecular weight of the flame was assumed to be approximated by the average molecular weight of the atmosphere. This assumption was based on the fact that nitrogen is the major component of the atmosphere and does not undergo chemical changes for flame temperatures of 2200°C.

The refined value of σ_L for the Cu(I) 324.7-nm transition will allow estimation of the contribution of the collisional profile at other

pressures. From the data on the absorption line profile measurements of the plume at low pressure, an estimated upper limit of 1000°K was obtained for the Doppler temperature of the expanded plume. Using this value for T the pressure of dependence of the Lorentz half width can be derived from Equation 12. If the temperature is assumed to be constant, the collisional half width is proportional to the number density of the perturbing atoms or molecules. For a gaseous state under the assumption of the applicability of the ideal gas law, the number density is proportional to pressure. The net result is that the collisional half width is proportional to pressure.

Figure 42 shows a log-log plot of the calculated Lorentz half width as a function of pressure. In the pressure region of 10-100 torr the collisional half width changed only from 2 to 15 mK. The total width of the absorption profile can be approximately calculated by use of the following equation (26).

$$\Delta\nu_T = \frac{\Delta\nu_L}{2} + \left[\left(\frac{\Delta\nu_L}{2}\right)^2 + (\Delta\nu_g)^2\right]^{1/2} \qquad (13)$$

where

$\Delta\nu_L$ = Lorentz half width

$\Delta\nu_g$ = Gaussian half width.

Equation 13 was found to be within 1% of the correct half width for values of the a parameter of the Voigt function between 0 and

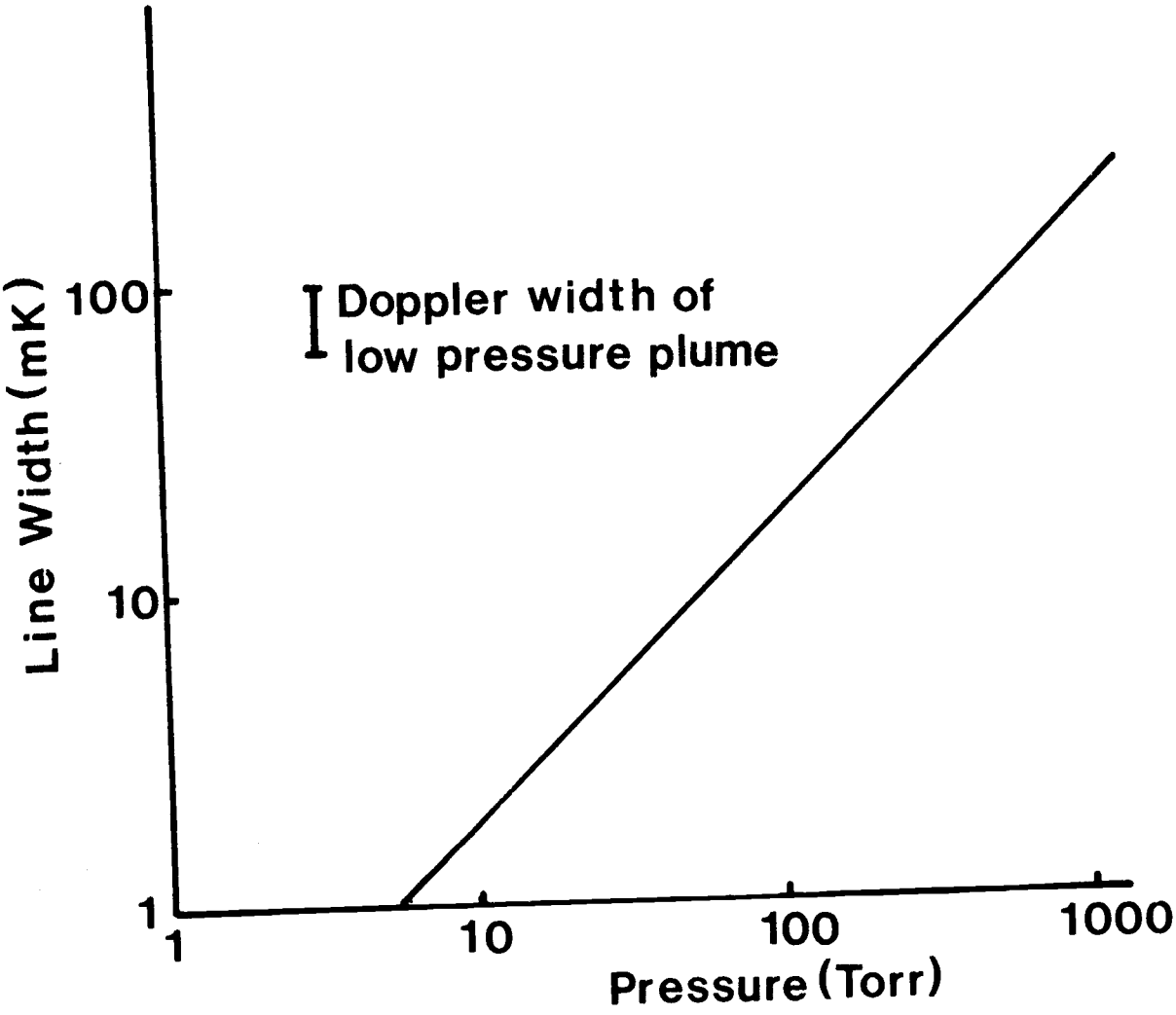

Figure 42. Plot of pressure dependence of Lorentz half width as a function of pressure.

1. Assuming a value of 90 mK as the upper limit of the Doppler half width for the low pressure plume and substituting boundary values of 2 mK and 15 mK for the Lorentz half width, total line widths of 100 and 108 mK were obtained. It appears that the contribution of the collisional width is still small (<10%) at pressures up to 100 torr.

The observed increase in the absorption profile at increased pressures is evidently not due to the increase in pressure broadening at pressures below 100 torr. Another possible broadening mechanism is the increase in Doppler width due to the increase in temperature at higher pressures. As the temperature is raised the contribution of collisional broadening decreases further. From the data on the time resolved emission data on pure copper, it was evident that as the pressure was increased to 10-100 torr there was a dramatic increase in the amount of continuum production. This duration of continuum emission lasted for a period that was ten times longer than the duration of the laser pulse itself. The presence of this continuum indicates that the temperature above the sample surface is quite high for a relatively long period of time (10-20 μs).

Figure 43 shows the temperature dependence of the Doppler width. The second curve is the temperature dependence of the Lorentz half width as a function of temperature for a pressure of 10 torr. Note as the temperature of the plume increases the contribution of the

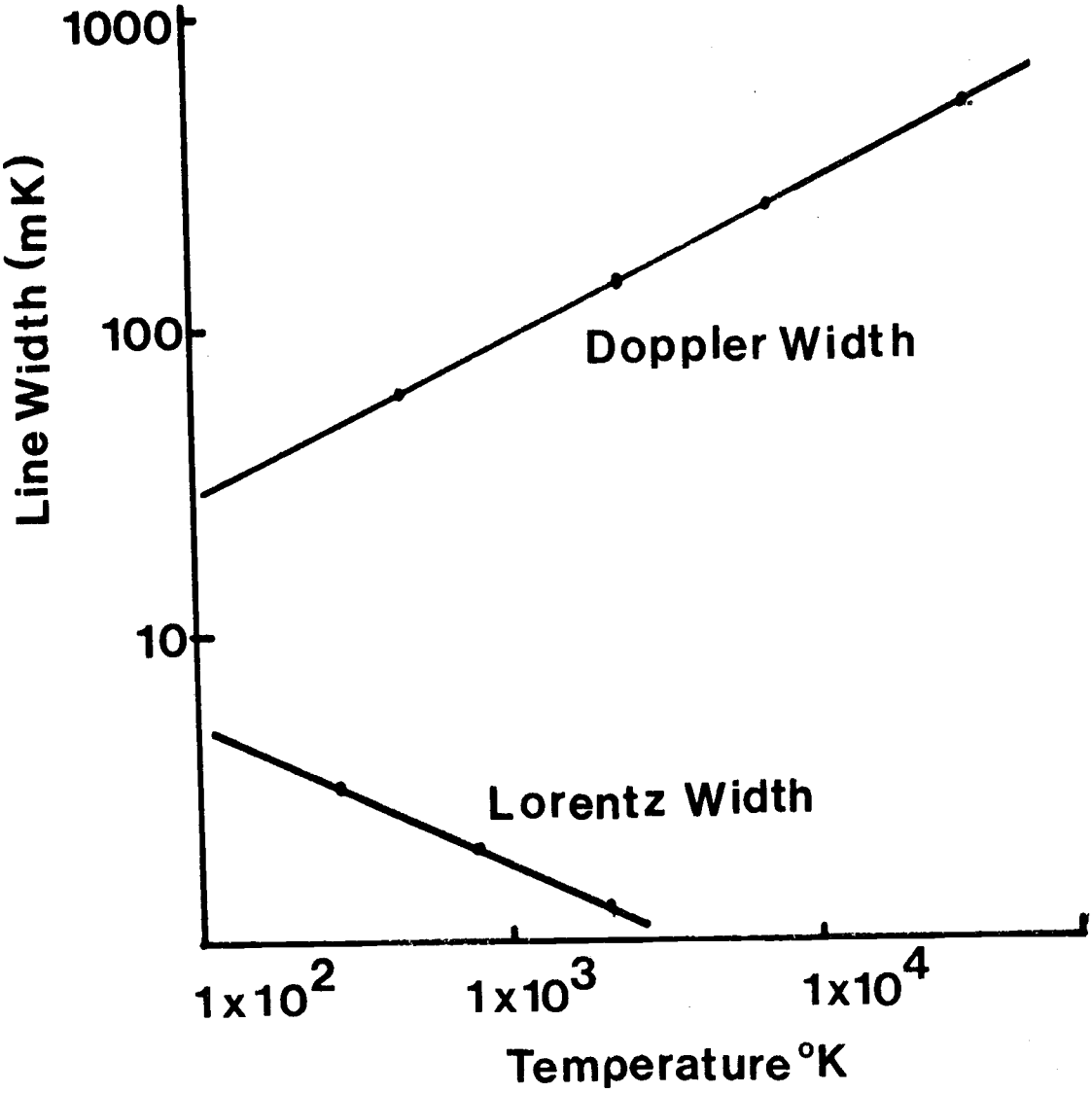

Figure 43. Temperature dependence of Doppler width and Lorentz width of collisional broadening at a pressure of 10 torr.

Lorentz half width continuously decreases. For a temperature change from 1000°K to 5000°K the Doppler width increases from a value of 90 mK to a value of 200 mK. Doppler broadening is a far more significant contribution to the total absorption width than the increase in Lorentz broadening with increase in pressure from 1 torr to 100 torr. The experimentally observed absorption line with 60-100 mK corresponds to a Doppler temperature from 400°C to 1200°K in the laser plume.

Since the earlier work of Osten (20) employed pulsed hollow cathode parameters that have been shown to be severely self-reversed and broadened with half widths on the order to 200 mK for the Cu(I) 324.7-nm line, linear calibration curves based on the assumption of the applicability of Beer's law should not result. The basis of the applicability of Beer's law is that the width of the absorption profile is much wider than the width of the monochromatic radiation used to measure the absorbance. From the considerations of the previous section on the sources of broadening in the plume, and from the measured half width of Cu (200 mK) in an air acetylene flame it is apparent that at the best case the emission profile of Osten's hollow cathode lamp equalled the absorption profile of the Cu in the plume.

G. Production of Microsecond Duration Hollow Cathode Pulses

From the absorption profile measurements of Cu in the plume it became evident that commercially pulsed hollow cathode lamps of long duration may have severe limitations due to their broad and reversed emission profile. Piepmeier and de Galan (30) have shown that as the duration of the hollow cathode pulse was decreased the line profile exhibited less self-absorption and self-reversal. The shortest pulses that they reported were 10 μs.

There is another advantage to the use of short duration hollow cathode pulses for laser plume atomic absorption. By coupling microsecond hollow cathode pulses with a current charge integration detection system employed for the absorption line profile measurements, improved time resolution of the laser plume atomic absorption would result. The time constant limitation of the measurements would now be limited by the duration of the actual hollow cathode pulse itself and not on the time constant of the photodetection system.

By the use of the solid state pulsing circuit used for the production of the hollow cathode pulses in this investigation, hollow cathode pulses as short as 0.5 μs could be observed. The observation of these short duration pulses was made possible by removing the interferometer from the optical path of the monochromator-readout module. This increased the light throughout of the optics to allow observation

of the pulses with good signal to noise ratio. The photoanodic currents were observed by use of the Tektronix type 7A18 preamplifier. This reduced the time constant of the resistance with the cable to less than 2 ns.

Figure 44 shows the time behavior of the intensity of the Cu(I) 324.7-nm line produced by a 1 μs pulse. Figure 44b shows the current waveform as measured by a current sensing resistor. The ringing evident in the current waveform is probably due to the very dynamic conditions occurring during the initiation of the high current sputtering operation. Figure 44c shows the time behavior of the collector voltage referenced to ground. Note that the collector voltage rises after the pulse is terminated to a value equal to the voltage of the power supply. Figure 44d is the reciprocal of Figure 44c to depict the voltage across the lamp as a function of time.

After a period of approximately 400 μs, the collector voltage returns to the value of the supply minus the typical voltage drop across the hollow cathode of 150 V. A possible explanation of this is that the resistance of the lamp may be changing during the recombination of the space charge set up during the high current pulse. If the resistance of the lamp decreases to a very low value, then the voltage drop across the lamp will be less, resulting in a higher potential across the collector emitter junction of the switching transistor.

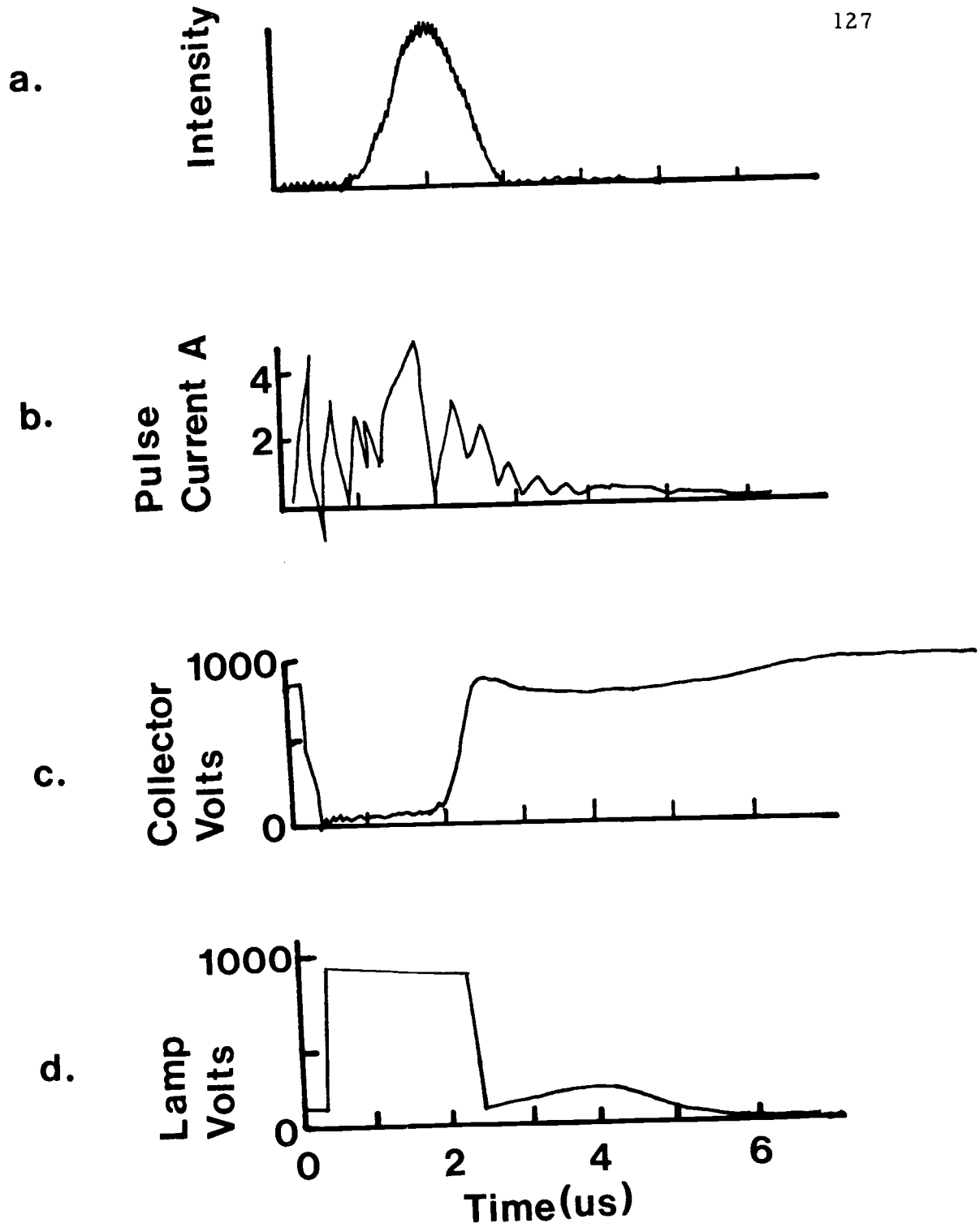

Figure 44. Time resolved waveforms for a high current pulsed Cu hollow cathode. Cu(I) 324.7-nm. (a) Relative intensity versus time. (b) Pulse current versus time. (c) Collector volts versus time. (d) Lamp volts versus time.

Figure 45 shows the time resolved intensity of a 10 μs pulse. The intensity rose after a delay of 2 μs to a peak value at 4 μs. The intensity, however, rolls off to a constant value at 6 μs. Figure 46 shows the time resolved intensity of a 60 μs pulse. The length of the plateau in the intensity increases with increasing pulse width of the trigger pulse. This decay of the emission signal was thought at first to be a power supply problem. Stiffening of the power supply with 100 μf capacitors did not improve the results.

The fall off in intensity in both Figure 45 and Figure 46 was originally thought to arise from the current gain of the transistor decreasing after the initiation of the conduction process. To check this a 500 ohm 5 watt resistor was substituted for the hollow cathode lamp. By observing the waveform of the voltage across the current sampling resistor no current fall off was noted. The fall off might be explained by the process of self-absorption. Atoms sputtered initially from the cathode can diffuse outward away from the cathode region resulting in an absorption layer of Cu atoms causing self-absorption and self-reversal of the profile.

Line profile measurements were not performed on these pulses because of the lack of good signal to noise ratio. The width of the profile can be extrapolated from the work performed by De Jong and Piepmeier (28) on high current pulsed hollow cathodes. They have reported that during the initial 21 μs of the pulse the profiles are

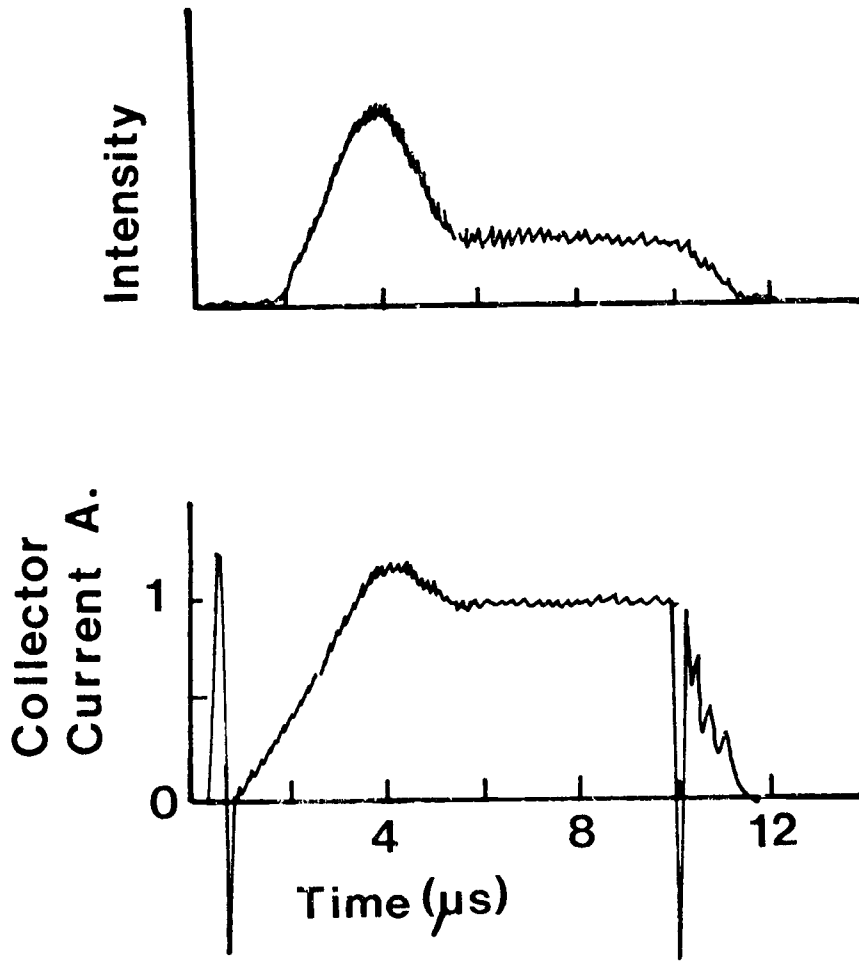

Figure 45. Time resolved intensity and current waveforms for a 10 μs duration Cu hollow cathode. Cu(I) 324.7-nm.

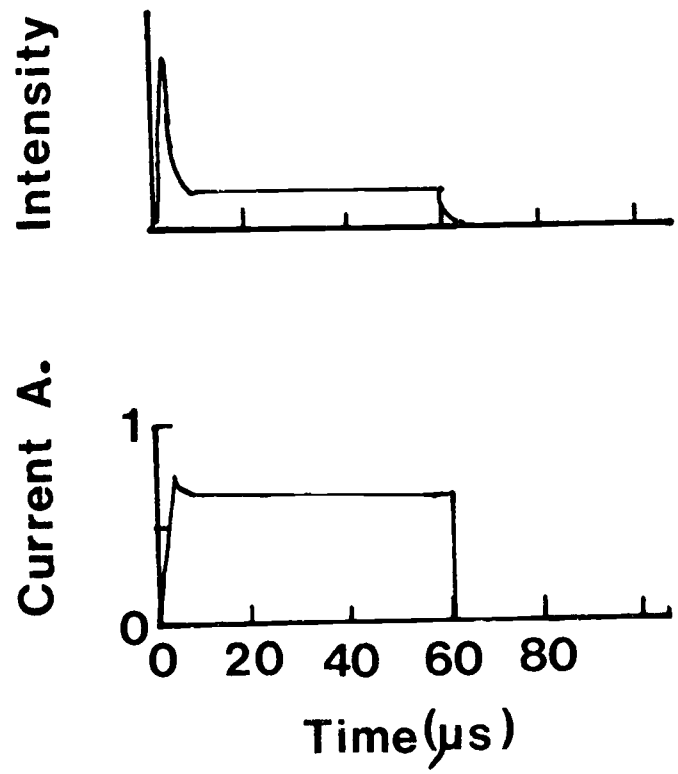

Figure 46. Time resolved intensity and current waveforms for a 60 μs pulse width. Cu(I) 324.7-nm.

unreversed though broadened by self-absorption and/or stark broadening. If the pulse width is on the order of 1 μs, the line width should also be unreversed with little self-absorption. For 1-amp pulses with a pulse duration of 10 μs a half width of 200 mK was obtained (30). For a 300 mA pulse with a duration of 300 μs a half width of 200 mK was obtained during the initial 21 μs. It is assumed that as the pulse duration is decreased, the role of self-absorption should be decreased resulting in a narrower profile than the above examples. The value of 200 mK can therefore be taken as an estimate of the upper limit of the profile width for the 1 μs pulses.

Figure 47 shows the intensity of the pulsed hollow cathode pulses as a function of supply voltage. The pulse duration of the hollow cathode was 2 μs. As the supply voltage was increased, the rise time of the intensity decreased and the pulse width decreased. A combination of effects may account for this. One effect is that at higher voltages the space charge of the hollow cathode is recharged at a faster rate. This increased rate of establishing the space charge in the hollow cathode would also increase the rate in which the current through the lamp can be used in the sputtering excitation of the cathode atoms.

The increase in the pulse width as the supply voltage is lowered may be the result of the increased time required for the high voltage transistor to terminate the conduction process. As the potential

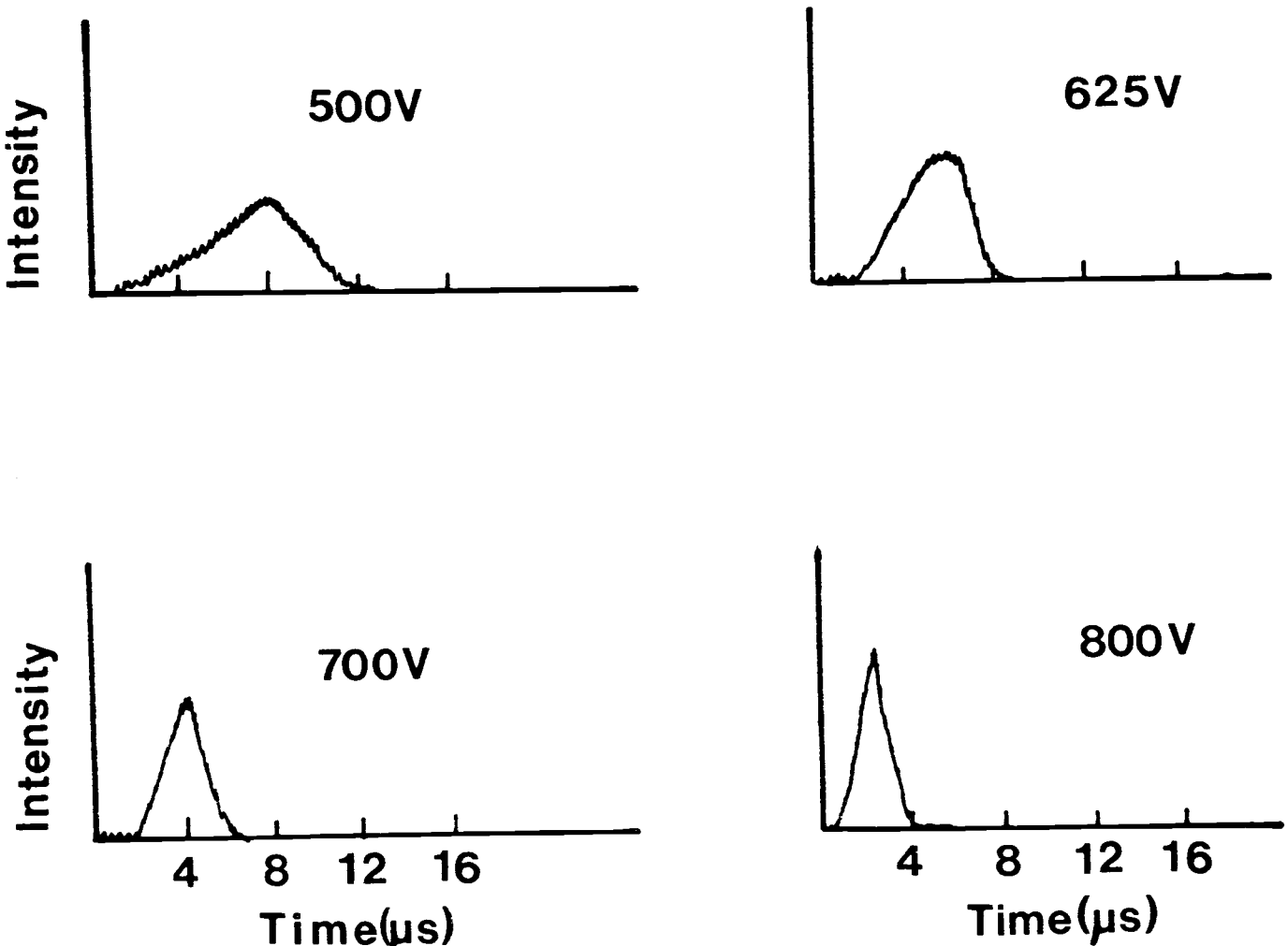

Figure 47. Time resolved hollow cathode emission of Cu (I) 324.7-nm line as a function of supply voltage.

across the transistor is lowered there is a decrease in the rate in which the charge carriers are removed from the base region. This can result in a slower turn off time for the transistor.

H. Photoanodic Charge Integration Atomic Absorption Measurements

The production of the extremely short duration hollow cathode pulses (1-2 μs) should improve the atomic absorption measurements performed on the plume. The improvements lie in two areas. The first is that the spectral profile of the emission from a hollow cathode pulsed in such a manner should be unreversed. Due to its short duration, the line profile should exhibit even less self-absorption than the 10 μs profiles published by Piepmeier and de Galan (30). The other improvement lies in the improved time resolution of the laser plume atomic absorption measurements. By coupling the 1 μs hollow cathode pulses with the photoanodic charge integration system employed for the absorption line profile measurements, temporal resolution of 1 μs is now possible. This is a tremendous improvement over the 60 μs time resolution of the atomic absorption system originally described by Osten and Piepmeier (20).

With the enhanced temporal resolution capability, experimental measurements were made to determine the time behavior of Cu atomic absorption in the initial 1-5 μs after the laser was fired. The sample

chosen was the same lead foil that was used in the absorption profile measurements. The hollow cathode pulses were delayed in relation to the laser by varying the delay time of the oscilloscope sweep function. The 7904 scope was externally triggered by the leading edge of the laser pulse. The shortest time interval between the firing of the laser and the pulsing of the hollow cathode was 2 μs. This was the result of the time required to switch the pulsing currents through the lamp and the delay time after initiation of the pulse before the lamp would emit radiation.

Figure 48 shows the relationship between the absorbance vs time. The relative standard deviations of the data points were 5%. This variance is the sum of the variance of the hollow cathode pulses with no laser sampling and the sampling variance of the laser microprobe. At 2 μs after the laser pulse, the peak absorbance was 0.4. There was a rapid decrease to a value of 0.2 at 5 μs. The absorbance then reached a steady value up to 200 μs before it began to roll off.

The higher absorbance during the initial phases of the plume might be due to a nonspecific absorption. This possibility could be checked by the use of a continuum source instead of a hollow cathode lamp. A high intensity pulsed xenon lamp was used as the continuum source. The timing of the events were controlled by a Tektronix 555 oscilloscope. The flash lamp was operated at a potential of 6 KV. The pulse width of the lamp was 6 μs. The delay time between the

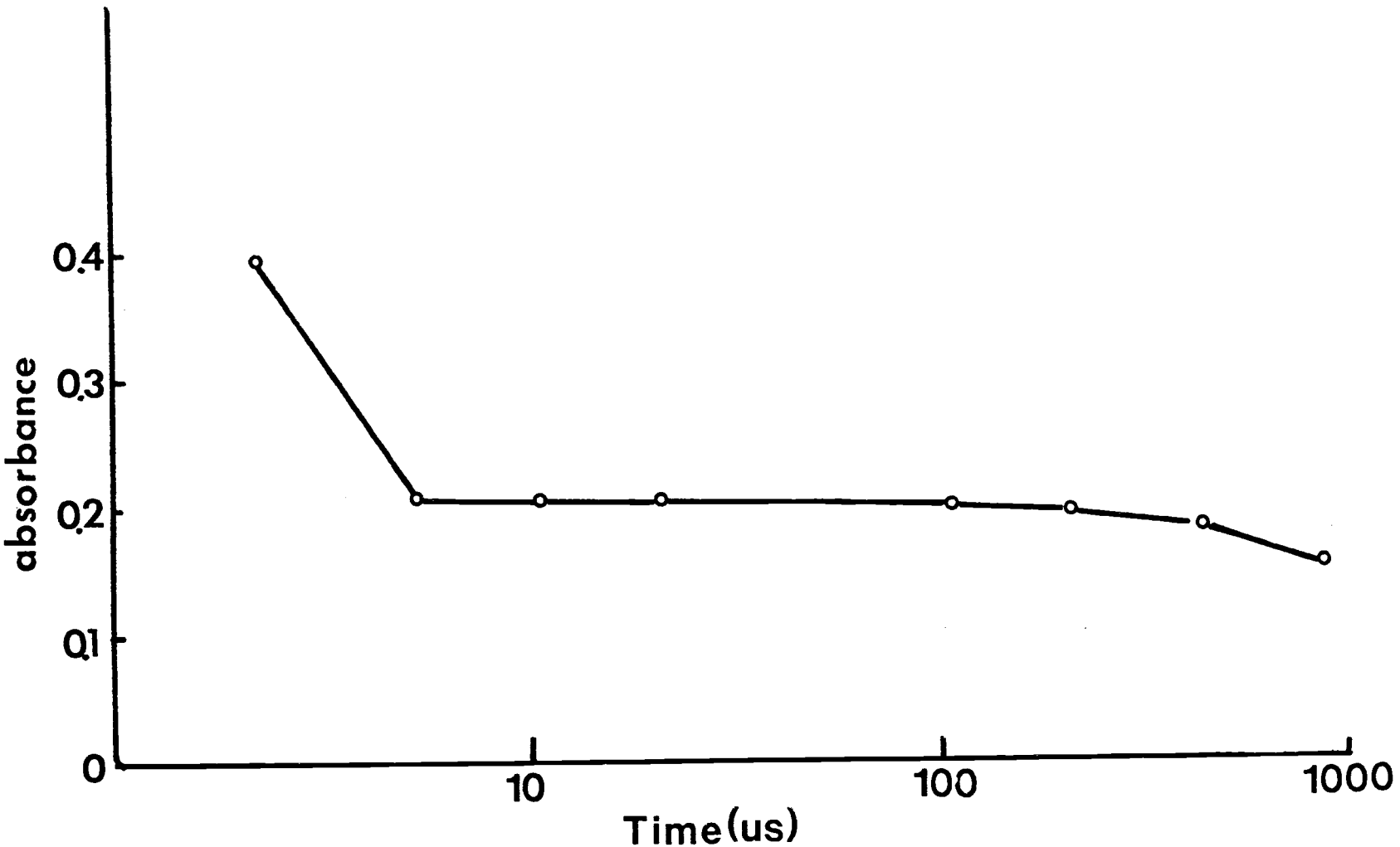

Figure 48. High temporal resolution atomic absorption measurements of Cu in Pb foil. Pressure = 1 torr. Observation height = 2 mm.

trigger pulse and light output from the lamp was 6 μsec. The jitter in the delay time was 1 μsec. The laser had a delay time of 10 μsec between the leading edge of the trigger pulse and the leading edge of the laser emission. To bring the flash lamp and laser into coincidence, the light output of each source was simultaneously displayed on the scope face. The triggering of the flash lamp was delayed until both the laser and flashlamp fired at the same time (see Figure 49).

The flashlamp was fired without the laser initially to determine the value of I_0 (100%T). The laser was then fired at the same time with the signal from the detection system equation to I. No difference in the two signals above the noise level of 10% or variation of the intensity of the flashlamp itself could be detected. This implies that there is little or no scattering of the light during the initial 5-6 μs of the plume.

Scott and Strasheim (14) have used a framing camera to photograph the formation and expansion of the laser pulse. They have measured the initial expansion velocity to be 1×10^6 cm/sec for a Q-switched single pulse laser system with a mean power density at the focal spot of 4.2×10^9 W/cm^2. Their photographs have shown that during the initial μs the plume was confined to a rather small sphere. As time increased the sphere radius increased until it reached a constant value at 20 μs. The plume at this point took on the shape of a motionless nebula cloud just hanging in space. They have also noted

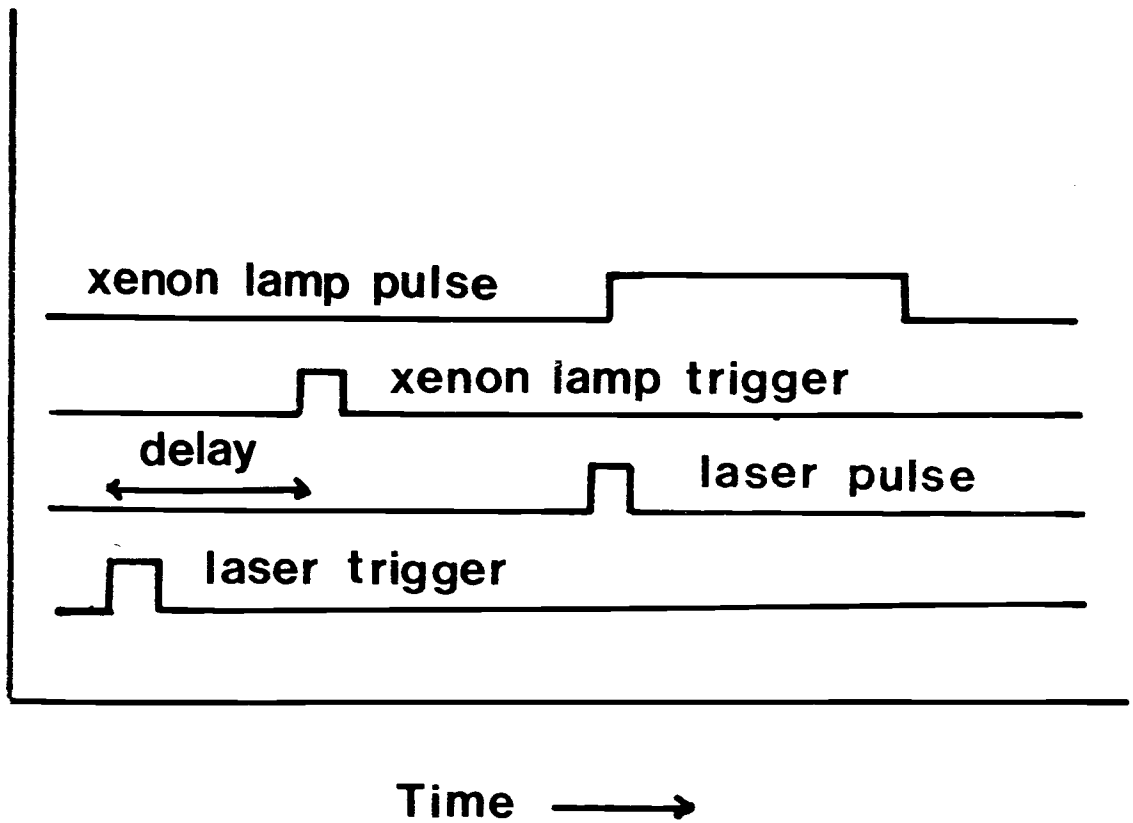

Figure 49. Timing pulse signals to bring xenon flashlamp and laser pulse into coincidence.

that as the plume expanded the amount of emission decreased.

Earlier studies on the gas dynamic expansion of the plasma produced by the laser interaction with solid samples have shown ~~that~~ the expansion velocities of the plasma to be approximately 10^6-10^7 cm/sec (14). For a dye laser system with a pulse duration of 600 ns the plasma can expand to a radial distance of 10 mm away from the impact region of the focus spot at atmospheric pressure before termination of the laser pulse. If the assumption is made that at the termination of the laser pulse the input of energy to the plume ceases, a thermokinetic expansion theory developed by Dawson can be applied (11).

For a spherically expanding plasma it has been shown that the expansion radius R can be related to the temperature T of the plasma under adiabatic expansion by the following equation.

$$2 \ln \frac{R}{R_0} = \ln \frac{T_0}{T} \tag{14}$$

R_0 = initial radius of the sphere

R = radius of the sphere

T_0 = initial temperature of the plasma

T = temperature of the plasma at radius R.

If the assumption is made that at the termination of the laser pulse the velocity is constant, then the radius is related to time by

$$R = vt \tag{15}$$

where v is the expansion velocity and t is time. Substitution of Equation 15 into Equation 14 yields the following result:

$$\ln \frac{v^2 t^2}{R_0^2} = \ln \frac{T_0}{T} \tag{16}$$

Equating the arguments of the logarithm terms yields the following relationship for the temperature as a function of time t.

$$T = (1/t^2)K \tag{17}$$

where $K = T_0/v^2 R_0^2$.

Equation 17 indicates that the temperature of the plume is inversely proportional to the square of the time interval between the termination of the laser and the observation time of the plume. If the assumption is made that the initial temperature of the plume is 10,000K, in a period of 5 μs the plume has cooled to 400 K.

The plasma, however, does not continue to cool as it expands. As the ions and free electrons recombine in the plasma they release their energy to compensate for the further cooling resulting from expansion. A constant temperature of approximately 0.1 eV is obtained until recombination of the charge is completed. This phenomenon may explain the existence of the long time plateau in

which the absorbance remained relatively constant.

The results of the microsecond atomic absorption measurements indicate that the absorption measurements should be made early after the laser pulse. In a period of a few microseconds after vaporization, the plume has still expanded to a limited extent to allow concentration gradients to blend. The plasma is still hot to prevent chemical interferences from reducing the sensitivity of the analyte measurements. Another result would be the increase in the absorption half width due to the initial high temperature. The result should be improvement in linearity of the calibration curves.

V. CONCLUSIONS

The pulsed dye laser microprobe appeared to minimize continuum production at atmospheric pressure due to its lower peak power rating and shorter operating wavelength than a Nd-glass Q-switched laser system with similar pulse energy. This reduced continuum should result in less distortion of the analytical signal for atomic emission and atomic absorption measurements.

The emission spectra and time resolved emission data indicated that as the pressure over the sample surface was decreased, the continuum production was further reduced. The time resolved emission data indicated that both the magnitude and duration of the continuum were reduced at low pressure. The reduced production of the continuum is probably a result of the increased threshold of atmospheric breakdown as the pressure was lowered.

The time resolved atomic absorption data indicated that at lower pressures the free atom population of minor constituents of metal alloys was present for a longer time than at atmospheric pressure. The spatially resolved atomic absorption measurements also indicated that at low pressure the plume was dispersed over a much larger cross sectional area than at atmospheric pressure. At low pressure the plume was found to be more homogeneous and observable up to a distance of 7 mm away from the focal spot of the sampling laser beam.

At atmospheric pressure the plume was observable to distances of only 1-2 mm away from the focal spot. The advantage of a large cross sectional area at low pressure is that the observation point for atomic absorption measurements can be removed from the laser focal spot area. This would eliminate the continuum present at the sample surface from being detected by the monochromator.

The magnitude of the peak absorbance of the minor constituents of the steel alloy was very dependent upon the pressure above the sample surface. There was an optimum pressure in which the sensitivity of the absorbance was a maximum. Varying the pressure above the sample surface can be used to adjust the sensitivity for a given sample matrix. If the sensitivity is not adequate for a given analysis, the pressure may be increased.

The absorption profile measurements of Cu in a lead alloy indicated that within the initial 60 μs, the temperature of the plume has cooled to a value that is less than 1000°K. The Doppler width of the absorbing atoms in the plume was about the same order of magnitude as the emission width of a dc operated hollow cathode lamp. This result coupled with the time resolved emission profile measurements of pulsed hollow cathodes by DeJong and Piepmeier (28) indicates that the emission profile of pulsed hollow cathodes of long duration (1 ms) was much wider than the absorption profile of analyte atoms in the plume. This is the reverse situation one would

normally want for analytical atomic absorption measurements.

This observation may explain some of the work of Osten (19, 20). He has reported laser microprobe atomic absorption calibration curves for Cu in aluminum. In almost all cases the curves were non-linear. The hollow cathode pulsing parameters were very similar to those which produced broad line profiles (28). These results appeared to indicate that the emission profile from his pulsed hollow cathode lamps may have been much broader than the absorption profile of the analyte atoms in the plume.

By narrowing the pulse duration of the hollow cathode pulses, improvements in the emission profile should result as indicated by extrapolation of the work of Piepmeier and de Galan (30). Extremely short pulses were made possible by use of a solid state high voltage switching circuit. The important parameter for the high-speed switching of hollow cathodes pulsing currents was the voltage of the lamp power supply. Increasing the voltage to 800 V allowed the pulse duration to be dramatically shortened.

The short duration hollow cathode pulses allowed the use of a photoanodic charge integration detection system. This combination allowed time resolution of the atomic absorption measurements to 1 μs. The charge integration atomic absorption system also eliminated the use of an oscilloscope as a detection system. The charge integration system allowed signals to be read directly by a digital

voltmeter or computer data acquisition system.

The time resolved atomic absorption measurements indicated that the absorbance reached a plateau value from 5-200 μs after termination of the laser pulse. This indicates that the analyte cloud of atoms is relatively stationary above the sample during this interval. This lends support to the photographic observations of Scott and Strasheim (14) who observed similar laser plumes to hang as a nebula for 10-100 μs after their initiation.

The time resolved atomic absorption measurements also indicate that the absorption sensitivity increases in the time period of 1-5 μs after the laser pulse compared to 5-200 μs later. This may be a direct result of the atoms being confined to a much smaller volume before extensive expansion of the plume has occurred. Another possibility is that since the plasma is still relatively hot at this point in time this would result in a higher percentage of free atoms suspended in the plume because the hot environment would minimize chemical recombination effects. The increased temperature would result in an increase in the Doppler width of the absorbing atoms, which should result in improved linearity of the calibration curves.

An alternative, though presently more expensive, light source for the short duration hollow cathode pulses would be a pulsed dye laser system with an extremely narrow emission profile. The advantage would be the tunability of the laser to locate the exact

absorption peak maximum. Absorption profile measurements would also be possible at higher gas pressures where the absorption profiles would be much broader than the limited line width of the hollow cathode used in this investigation. The tunable dye laser system with appropriate frequency doubling crystals could be very useful for multielement capability in the plume with one monochromatic light source.

LIST OF REFERENCES

1. F. Brech and L. Cross, Appl. Spectosc., 16, 59 (1962).

2. J.E. Mentall and R.W. Nicholls, J. Chem. Phys. 46, 2881 (1967).

3. W. Bogershausen and K. Honle, Spectrochimica Acta 24B, 71 (1969).

4. J. Baldwin, U.S. Atomic Energy Commission IN-1219, Oct., 1968.

5. J. Baldwin, U.S. Atomic Energy Commission IN-1262, Dec., 1968.

6. J. Baldwin, U.S. Atomic Energy Commission IN-1305, July, 1969.

7. J. Baldwin, U.S. Atomic Energy Commission IN-1360, Jan., 1970.

8. J. Baldwin, U.S. Atomic Energy Commission IN-1492, June, 1971.

9. J.F. Ready, J. Appl. Phys., 36, 462 (1965).

10. J.F. Ready, Effects of High-Power Laser Radiation, Academic Press, New York, 1971.

11. Heinrich, Hora, Laser Interaction and Related Plasma Phenomena, Plenum Press, New York (1971).

12. W. Bogershausen and R. Vesper, Spectrochim. Acta 24B, 103 (1969).

13. H. Klocke, Spectrochim. Acta, 24B, 263 (1969).

14. R.H. Scott and A. Strasheim, Spectrochim. Acta, 25B, 311 (1970).

15. Charly D. Allemand, Spectrochimica Acta, 27B, 185 (1972).

16. E.H. Piepmeier and D.E. Osten, Appl. Spectrosc. 25, 642 (1971).

17. E.H. Piepmeier and H.V. Malmstadt, Anal. Chem. 41, 700 (1969).

18. V.G. Mossotti, K. Laqua, and W.D. Hagenan, Spectrochimica Acta 23B, 197 (1967).

19. D.E. Osten, Ph.D. Thesis, Oregon State University, 1972.

20. D.E. Osten and E.H. Piepmeier, Apll. Spectrosc. 27, 165 (1973).

21. E.P. Krivchikova and N.M. Vasil'eva, Zhurnal Analiticheskoi Khimii, Vol. 28, 928 (1973).

22. E.K. Vul'fson, A.V. Karyakin, and A.I. Shidlovskii, Zhurnal Analiticheskoi Khimii 28, 1253 (1973).

23. E.K. Vul'fson, A.V. Karyakin, and A.I. Shidlovskii, Zavodskaya Laboratoriya, 40, 945 (1974).

24. D. de Galan and H.C. Wagenaar, Extrait de la revue du GAMS 3, 10, (1971).

25. H.C. Wagenaar and L. de Galan, Spectrochim. Acta 28B, 157 (1973).

26. G.F. Kirkbright, O.E. Troccoli, and S. Vetter, Spectrochim. Acta 28B, 1 (1973).

27. C.F. Bruce and P. Hannaford, Spectrochim Acta 26B, 207 (1971).

28. G.J. DeJong and E.H. Piepmeier, Spectrochim. Acta 29B, 159 (1974).

29. H.C. Wagenaar, C.J. Pickford and L. de Galan, Spectrochim. Acta 29B, 211 (1974).

30. E.H. Piepmeier and L. de Galan, Spectrochim. Acta 30B, 263 (1975)

31. E.H. Piepmeier, Appl. Spectrosc. 26, 100 (1972).

32. G.J. DeJong, Ph.D. Thesis, Oregon State University, 1974.

33. D.N. Stacey, V. Stacey, and A.R. Malvern, J. Phys. E.: Sci. Instrum. 7, 405 (1974).

34. P. Brix and W. Humbach, Zeitschrift fur Physik. 128, 506 (1950).

35. K. Burns and K.B. Adams, J. Opt. Soc. Am. 42, 56 (1952).

36. Victor Kaufman, J. Opt. Soc. Am. 52, 866 (1962).

37. D.W. Posener, Austr. J. Phys. 12, 184 (1959).

38. H.C. Wagenaar and L. de Galan, Spectrochim. Acta 30B, 361 (1975).

39. W.C. Kreye and F.L. Roesler, J. Opt. Soc. Am. 60, 1100 (1970).

40. R.V. Stuart and G.K. Wehner, J. Appl. Phys. 351, 1819 (1964).

41. R.V. Stuart, G.K. Wehner, and G.S. Anderson, J. Appl. Phys. 40, 803 (1969).

42. C.H. Corliss and W.R. Bozman, Experimental Transition Probabilities for Spectral Lines of Seventy Elements, National Bureau of Standards Monograph 53 (1962).

43. M.L. Parsons and J.D. Winefordner, Appl. Spectroscopy 20, 223 (1966).

44. E.E. Whiting, J. Quant. Spectr. Radiative Transfer 8, 1379 (1968).